

4500

MOCVD growth and doping studies of III/V
semiconductors

Paul Hageman

MOCVD growth and doping studies of III/V semiconductors

CIP-GEGEVENS KONINKLIJKE BIBLIOTHEEK,
DEN HAAG

Hageman, Paulus Robertus

MOCVD growth and doping studies of III/V semiconductors / Paulus Robertus Hageman. -

[S.l.: s.n.].-Ill.

Thesis Nijmegen. - With ref. - With summary in Dutch.

ISBN 90-9005929-6

Subject headings: MOCVD / GaAs / AlGaAs

MOCVD growth and doping studies of III/V semiconductors

een wetenschappelijke proeve op het gebied
van de Natuurwetenschappen

Proefschrift

ter verkrijging van de graad van doctor
aan de Katholieke Universiteit te Nijmegen,
volgens besluit van het College van Decanen
in het openbaar te verdedigen op
maandag 19 april 1993
des namiddags te 1.30 uur precies

door

Paulus Robertus Hageman

geboren op 23 november 1961
te Doetinchem

Promotor: Prof. Dr. L.J. Giling

Voor Jeannette

The work described in this thesis is part of the research program of the "Nederlandse Maatschappij voor Energie en Milieu B.V." (NOVEM).

Voorwoord

Het leuke van experimenteel werk is, tenminste op onze afdeling, dat je samenwerkt met veel verschillende mensen om het doel te bereiken wat je voor ogen staat. Deze samenwerking beperkt zich gelukkig niet tot de afdeling alleen maar strekt zich uit over de gehele faculteit.

Als ik mensen ga bedanken voor hun hulp en meedenken loop ik het grote risico om iemand te vergeten. Om dit te voorkomen bedank ik hierbij iedereen die ik, ondanks mijn goede wil en tot mijn grote spijt, vergeten mocht zijn.

John Giling ben ik dankbaar voor het scheppen van de zeer ruime mogelijkheden om mijn onderzoek te verrichten en zijn inzet en enthousiasme voor mijn werk.

Harry bedank ik voor zijn grote hulp en raadgevingen op reactor-gebied en het verduidelijken van de CDA standpunten t.a.v. de mestproblematiek in Oost-Brabant en in het bijzonder in Mill. Piet ben ik dankbaar voor zijn hulp op allerlei terrein, maar specifiek voor de door hem gegeven samenhang tussen zelf-gemaakte kozijnen en het tracé van de Betuwe-lijn. Van de optische kwaliteiten van Stef heb ik veelvuldig (mis)bruik gemaakt. Onvermeld mogen niet zijn kwaliteiten als statische, kopsterke "target"-spits blijven in de traditie van Ray Clark. De samenwerking met Gerard heeft niet alleen nieuw leven in de zonnecelgroep geblazen maar ook, mede dankzij zijn smeuge ooggetuigeverslagen van de lotgevallen van de "gezellige jongens", zijn de koffiepauzes naar eredivisie niveau getild.

Dankzij Mart en zijn fenomenale kennis heb ik mijn experimenten theoretisch kunnen onderbouwen en bovendien mijn topografische kennis van Frankrijk kunnen vergroten. De vruchtbare samenwerking met Andre heb ik zeer gewaardeerd. Vooral mag ik Joost en Wouter niet vergeten te bedanken voor al het vuile werk dat zij voor mij hebben opgeknapt en Joost voor de gezellige uurtjes training. In dit rijtje moet ook Xiao niet vergeten worden die als mijn "leermeester" mij de kneepjes van het vak bijbracht.

Zonder mijn collega's Frank, Hans, Thijs, Michel (afdelingskampioen rendierwerpen), John, Roeland, Paul, Li en Jeannette zou het niet zo aangenaam zijn geweest op de afdeling als dat het geweest is. Jacky moet apart vernoemd worden om haar getoonde geduld en onverstoorbaarheid.

De algemene en technische diensten van de faculteit zijn mij erg tot steun geweest, in het bijzonder Willy van de werkplaats, Jos de glasblazer en Ferry die zelfs mij kon laten werken met een draaibank. Zeker mag niet vergeten worden de huishoudelijke dienst die telkens weer mijn rotzooi opruimde en Ko

voor het perfect laten functioneren van mijn grootste troost in bange dagen, de koffieautomaat.

Zeker niet op de laatste plaats wil ik mijn schoonmoeder bedanken voor haar "technische" adviezen en aanmoedigingen in de tijden van "Wackelcontact, Herr Hageman" en in langdurige periodes van vochtoverlast.

Contents

1	Introduction	1
1.1	Metalorganic Chemical Vapour Deposition	3
1.2	The MOCVD reactor	4
1.3	Physical and chemical aspects of the MOCVD process	6
1.4	Outline of this thesis	10
	References	11
2	Temperature dependence of silicon doping of GaAs by SiH_4 and Si_2H_6 in atmospheric pressure metalorganic chemical vapour deposition	13
2.1	Introduction	14
2.2	Experimental procedure	14
2.3	Results and discussion	15
2.3.1	SiH_4 doping	17
2.3.2	Si_2H_6 doping	20
2.3.3	Si_2H_6 doping in small cells	22
2.4	Conclusions	23
	Acknowledgments	23
	References	23
3	Si-doping of MOCVD GaAs: A closer analysis of the incorporation process	25
3.1	Introduction	27
3.2	Experimental procedure	27
3.3	Results and discussion	29
3.3.1	Electrical evaluations	29
3.3.2	Silicon precipitation	38
3.3.3	Rate limiting step of the silicon incorporation process	43
3.4	Conclusions	45

Acknowledgments	46
References	46
4 Pressure and temperature dependence of Silicon doping of GaAs using Si₂H₆ in Metalorganic Chemical Vapour Deposition	49
4.1 Introduction	51
4.2 Experimental procedure	51
4.3 Results	52
4.3.1 Growth and characterization of undoped GaAs	52
4.3.2 Disilane doping of GaAs	55
4.4 Discussion	59
4.4.1 Disilane doping of GaAs at 1000 mbar	62
4.5 Conclusions	63
Acknowledgments	64
References	64
5 Pressure and temperature dependence of Zn incorporation in MOCVD grown GaAs and AlGaAs using diethylzinc as precursor	67
5.1 Introduction	69
5.2 Experimental procedure	70
5.3 Results and discussion	71
5.3.1 The effect of the input mole fraction DEZn on the hole concentration	71
5.3.2 Hall mobilities	74
5.3.3 The effect of growth temperature on the hole concentration	75
5.3.4 Model	77
5.3.5 Depletion effects	81
5.4 Conclusions	83
Acknowledgments	84
References	84
6 Improvement of LPMOCVD grown GaAs heteroface solar cells: theory and practical implications.	87
6.1 Introduction	88
6.2 Solar cell construction	89
6.3 Theory	92
6.4 Characterization and results	96

6.5	Conclusions	104
	References	105
7	InGaP, a promising material for tandem solar cells	107
7.1	Introduction	108
7.2	Experimental procedure	109
7.2.1	MOCVD growth and characterization	109
7.2.2	Solar cell processing and efficiency measurement	109
7.3	Results and discussion	110
7.3.1	Lattice matching	110
7.3.2	Growth rate and incorporation coefficient	112
7.3.3	Photoelectrical quality	114
7.3.4	Electrical characterization and doping	115
7.3.5	Solar cell characteristics	116
7.4	Conclusions	116
	Acknowledgments	117
	References	117
8	Optical and electrical quality of InGaP grown on GaAs with Low Pressure Metalorganic Vapour Deposition	119
8.1	Introduction	120
8.2	Experimental procedure	121
8.3	Results and discussion	123
8.3.1	Influence of the growth temperature on the solid composition and growth rate of InGaP	123
8.3.2	The effect of the V/III ratio and the total gas flow on the growth rate and solid composition	128
8.3.3	Electrical and optical quality of the InGaP layers	128
8.3.4	Ordering of the InGaP epilayers	134
8.3.5	Morphology	135
8.3.6	Defects	136
8.4	Conclusions	137
	Acknowledgements	138
	References	138
	Summary	143
	Samenvatting	147

Curriculum Vitae	151
-------------------------	------------

Chapter 1

Introduction

Although today silicon is the most widely used semiconductor, the first transistors were made of germanium [1,2]. This was just after the second world war. In the mid-fifties the silicon-based bipolar transistor was for the first time presented. Nowadays, all integrated circuits (IC's) are based on the, in 1959 introduced, silicon-based planar transistor [3]. An incredible amount of research spent on this type of devices, has resulted in the impressive achievements of the micro-electronic industry to day.

However, the so-called III/V semiconductors are becoming more and more popular as a basis for high speed electronic devices and opto-electronic components. These III/V compounds like GaAs, $\text{Al}_x\text{Ga}_{1-x}\text{As}$, InP and $\text{In}_x\text{Ga}_{1-x}\text{As}_{1-y}\text{P}_y$, have some definite advantages over silicon. As is illustrated in fig. 1.1, the bandgap of these materials can be chosen as desired between 0.18 and 2.42 eV. On top of this, a considerable part of the III/V materials are direct semiconductors, in contrast to silicon, which make them very suitable as material for opto-electronic compounds like high efficiency solar cells, lasers and light-emitting diodes. Also, due to their superior material properties, all kind of devices have been developed, like the high-electron mobility transistor and the field-effect transistor, which operate at higher speed than their counterparts based on silicon.

Most of the devices, and certainly the opto-electronic ones, are made of several semiconductor layers, which differ in thickness, dopant element, doping level and composition. Among the growth techniques which are capable to meet these demands, Molecular Beam Epitaxy (MBE) and Metalorganic Chemical Vapour Deposition (MOCVD) are the most suitable for a wide range of materials. With these two techniques it is possible for reproducibly making material of good quality with all kind of different doping levels and with very sharp interfaces (even monolayer sharp) between separate layers. Nowadays, MOCVD reactors are developed [10] which are capable to grow on a large number of wafers in one run, with great repeatability and accuracy from wafer to wafer and run to run. So, the MOCVD method has a not only a great potential towards the production of devices but has already proven to be capable to produce, for instance solid state lasers and solar cells, in large numbers.

In this thesis the growth and doping of GaAs, $\text{Al}_x\text{Ga}_{1-x}\text{As}$ and $\text{In}_{1-x}\text{Ga}_x\text{P}$ has been investigated. The doping process of the epitaxial layers with silane (SiH_4) and disilane (Si_2H_6) is described in chapters 2, 3 and 4. Diethylzinc (DEZn) has been used to grow p-type layers as is given in chapter 5. These investigations have been used to grow a solar cell of 20.5 % efficiency (chapter 6). The last two chapters (7 and 8) deal with the alloy $\text{In}_{1-x}\text{Ga}_x\text{P}$, lattice

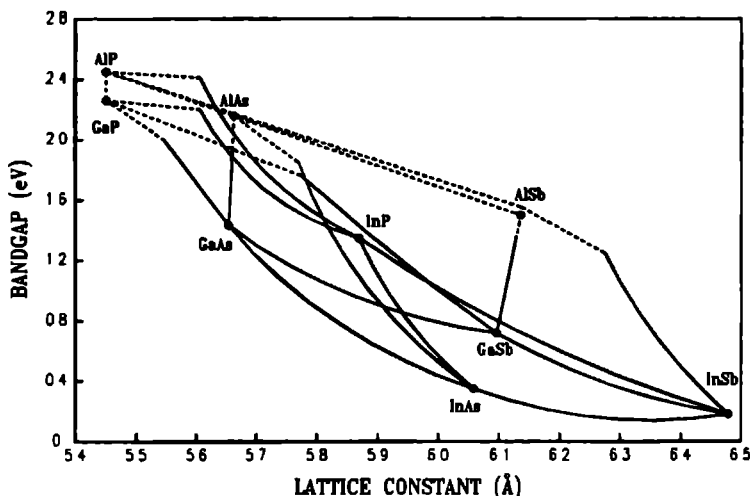


Figure 1.1 Bandgap (eV) versus the lattice constant (Å) for the major III/V compounds. The lines represent the possible alloys between two binary compounds. The solid lines indicate the direct bandgap combinations and the dashed lines the indirect bandgap materials.

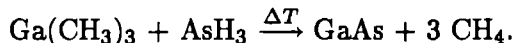
matched to GaAs. This material can be used as high bandgap material instead of $\text{Al}_{0.38}\text{Ga}_{0.62}\text{As}$. Although, it certainly has advantages over AlGaAs, control over the composition and crystallographic structure is not as straightforward as this semiconductor possesses atomic ordering or disordering on the group III lattice depending on the growth conditions and substrate orientations. This behaviour is responsible for typical optical and electrical properties [4].

This chapter will give a short introduction of the MOCVD growth technique and briefly describe the different aspects related to the physical and chemical processes. Some examples are given to illustrate the capability of the MOCVD process.

1.1 Metalorganic Chemical Vapour Deposition

The first publication on MOCVD was in 1968 by H.M. Manasevit [5]. He used the vapour of metalorganic compounds to grow semiconductor material. In this publication he described the growth of GaAs by transporting the metalorganic compound trimethylgallium (TMG, $\text{Ga}(\text{CH}_3)_3$) in combination with

arsine (AsH_3) with the use of a carrier gas to a heated surface. The overall chemical reaction of this process can be formulated as:



After the first growth of GaAs, it was demonstrated that with this MOCVD growth technique the complete range of III/V compounds could be grown, viz. GaP (with TMG and PH_3), ternary materials like GaAsP and AlGaAs (with the use of trimethylaluminum (TMA)) and the complete range of indium containing compounds like InP, GaInAs, GaInP and InAsP with the use of trimethylindium (TMI) [6]. Not only III/V semiconductors, but also II/VI materials can be grown with this method [6,7] as well as high-temperature superconductors [9] and compounds like GaN and AlN. The great flexibility in compounds which can be grown with MOCVD and the already mentioned capability for mass production, have brought MOCVD to maturity. However, still a lot of research is necessary to understand all the details of the chemical processes during growth.

1.2 The MOCVD reactor

All MOCVD reactors are build according to the same principles. A schematic drawing off the reactor used for the main part of this thesis, is given in fig. 1.2. Like all reactors it consists of a gas handling system, the actual reactor cell and a low pressure system with a cracking furnace or a scrubber (to remove the toxic part of the waste gasses) connected it. Hydrogen is used as carrier gas purified by a Pd diffusion cell.

The gas handling system takes care of the transport and dosimetry of the gasses into the reactor. The group V species, PH_3 and AsH_3 , are stored in cylinders. A diluted mixture of nitrogen and Si_2H_6 is used as n-type dopant and also stored in a cylinder. The group III species are all metalorganic compounds and stored as liquids or solids (trimethylindium) in stainless steel bubblers. The gas handling system is equipped with valves, flowmeters and pressure controllers to make it possible to transport the correct amounts of growth and doping species into the reactor. A vent-run system (manifold) is incorporated to allow for fast switching of the gasses between run lines (growth) or vent lines (exhaust). Most modern reactors are fully computerized, so that the automatic handling of valves, flow and pressure controllers, as

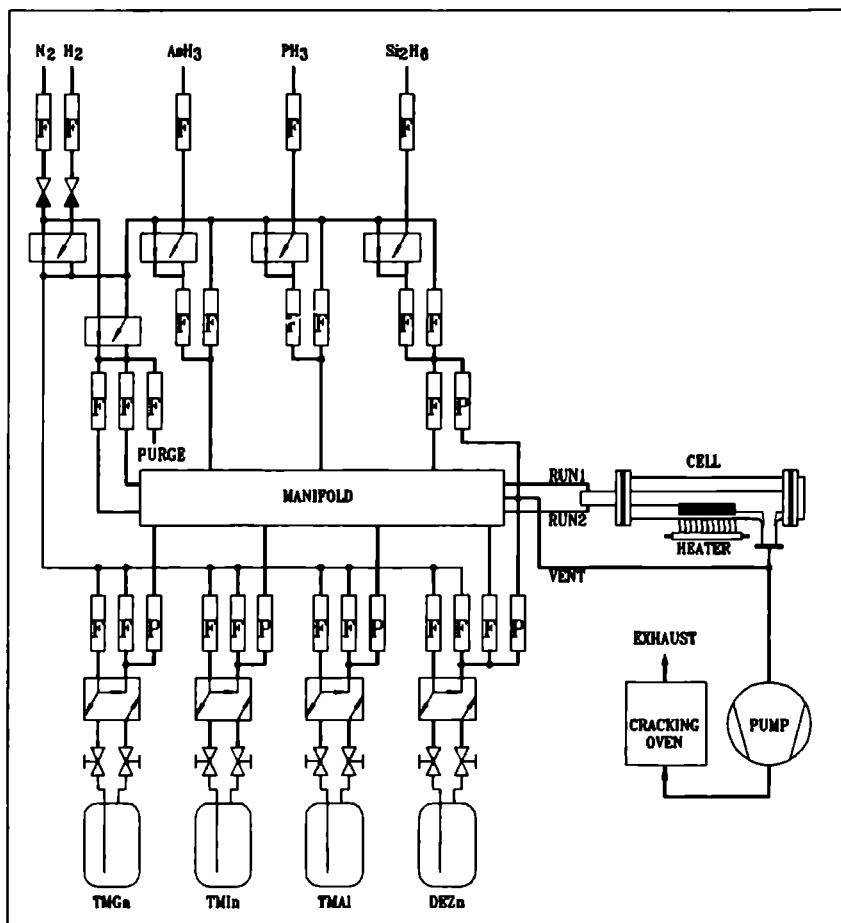


Figure 1.2 Schematic drawing of the low pressure MOCVD reactor used for the experiments in this thesis.

well as the temperature and pressure in the reactor cell, is possible. This automatization increases the controllability and safety of the process.

The main difference between the various types of MOCVD reactors is the reactor cell itself. Numerous designs have been developed, every one with its own advantages and disadvantages. We can distinguish between horizontal and vertical reactors, "T"-type reactors, barrel reactors, inverted horizontal reactors, chimney reactors etc. [11]. From all these different reactors types, versions operating at atmospheric or reduced pressure exists, some of them can even be equipped with a rotating susceptor to improve the uniformity over the substrate.

The exhaust of the reactors is, in the case of a low pressure reactor, connected to a vacuum pump with a pressure regulating system. Independent of the reactor (low or atmospheric pressure), in all cases a proper treatment of the waste gasses should be provided. This is one of the critical points of the MOCVD process. The, until now widely used hydrides (arsine and phosphine) are so toxic, that they can not be dumped untreated into the environment. All kind of gas scrubbers are available to remove the toxic part of the waste gasses. Also, a lot of investigation is spent to search for alternatives for the hydrides, like the alkyl derivatives of arsine and phosphine. Because of the use of the very toxic gasses and the explosive nature of the hydrogen carrier gas, the gas handling system should be very leak tight and robust. Always a proper safety system has to be incorporated into the reactor. After years of research this is no longer a problem.

1.3 Physical and chemical aspects of the MOCVD process

The MOCVD growth process can be divided in a physical part and a chemical part. The physical part concerns the behaviour of the gas flow, i.e. the convective and diffusional transport in the reactor. The chemical processes which occur in the gas phase and on the growing surface together with knowledge about the phase diagram of the III/V compounds and thermodynamic equilibriums (heterogeneous and homogeneous) determine the chemical part of the MOCVD process. This section will describe some of the physical and chemical aspects of the MOCVD process.

The growth of high quality material and the mass production with MOCVD requires controllability to a very high degree over the process. A

factor which fully determines the growth results and its controllability is the behaviour of the gas flow in the reactor cell. This flow should preferably be laminar and stable to avoid hard or impossible control over the gas flow as occurs when thermal convective conditions are present in the cell.

Research on horizontal reactors has resulted in knowledge on the flow behaviour in the cell. Due to this, boundary conditions could be defined, so one can determine at forehand if the gas flow is laminar or turbulent. A Reynolds number (dimensionless) can be calculated for the situation inside the reactor. The value of this number determines if the flow is laminar or turbulent. In the case of thermal convection in the reactor, another dimensionless number, the Rayleigh number, is defined. Also in this situation the value of this number is a criterion whether convection takes place or not. For a proper design of reactor cells one has to consider both criteria [12]. To avoid memory cells in the reactor, caused by return flows in horizontal reactors, the ratio of the dimensionless Grasshof and Reynolds numbers (Gr/Re) is a good criterion [13]. To fulfil these demands, the reactor cell should be low and the aspect ratio (width/height of the cell) should be larger than ≈ 4 .

In general, lowering the pressure or increasing the flow rates, will diminish convective instabilities and return flows. Duchemin [14] was the first to demonstrate the benefits of a low pressure reactor. In addition, the cell should be designed in a proper way, i.e. it should be streamlined in order to avoid vortex formation. Dead spaces in the cell should be minimized in order to diminish the memory effect and to increase the possible sharpness of the interfaces.

Control over the gasflow results in good controllability of the growth process and sharp interfaces. This last aspect is demonstrated in fig. 1.3, in which a photoluminescence spectrum at 4.2 K is given for a triple quantum-well. This structure consists of three GaAs wells with well widths of 54 , 26 and 11 Å, sandwiched between $Al_{0.25}Ga_{0.75}As$ barriers. The FWHM of the quantum well peaks indicate that the interfaces are rather sharp.

The chemistry in the MOCVD process is very complicated. Depending on the type of material grown, a lot of different species are present in the gas phase consisting of the actual growth components (group V and group III precursors) and of the compounds used for the doping of the epilayers. All these components, together with the carrier gas, are at high temperatures in the reactor cell. They form the reactive gas mixture from which the III/V epilayer is grown.

The decomposition behaviour of the different group III and group V precursors have been investigated in great detail. When concentrating on GaAs it is found that the decomposition is an activated process which takes place

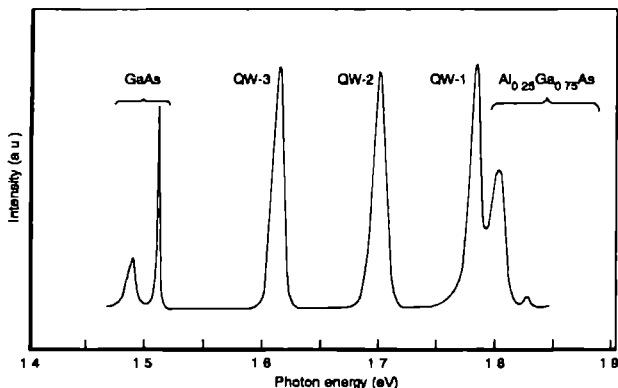


Figure 1.3 PL spectrum at 4.2 K of a triple quantum-well ($\text{Al}_{0.25}\text{Ga}_{0.75}\text{As}/\text{GaAs}/\text{Al}_{0.25}\text{Ga}_{0.75}\text{As}$) as grown in the reactor indicated in fig. 1.2.

in the gas phase. Depending on the experimental conditions, the presence of arsine and GaAs, the thermal stability of TMG varies. This chapter will not deal with this matter in great detail, but it is now believed that the decomposition of TMG proceeds step like. The rate limiting step in this decomposition is thought to be the removal of the first methyl group [11]. Not only the complicated decomposition reactions of the precursors in hydrogen, but also their reaction with traces of water and oxygen in the carrier gas should be considered. This particular is the case when AlGaAs is grown because of the great sensitivity of aluminum towards these compounds [15, 16].

Although a lot of possible reactions exist, it is proven that GaAs and other III/V compounds can be grown at various combinations of group III and V species, i.e. not only with TMG and AsH_3 , but also with triethylgallium, trimethylarsine, tertiarybutylarsine and elemental arsenic at different ratios of the group V and group III species. Also, the growth temperature can vary over a reasonably range for the growth of GaAs. Reep et al. [17] performed an extensive study on the temperature behaviour of the GaAs growth. It was shown that three temperature regions exist (see fig. 1.4). Below 600°C the growth is kinetically determined by decomposition of TMG in the gas-phase [18,19]. The growth rate increases in this region with increasing growth temperatures. The temperature region between the 600 and 800°C hardly shows any temperature dependence, because the growth is limited by the gas

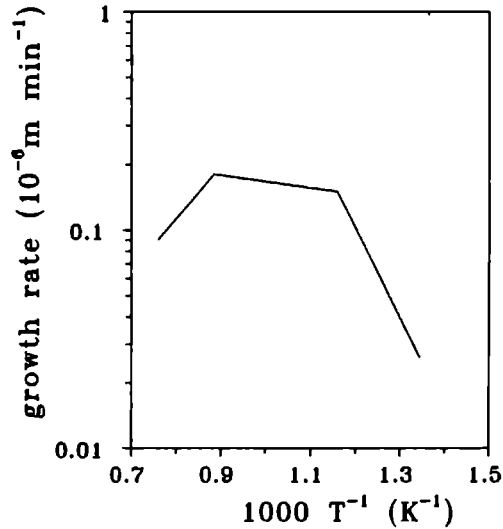


Figure 1.4 GaAs growth rate ($\mu m/min$) as a function of the inverse temperature (T^{-1}). Data points are from D.H Reep [17].

phase diffusion. Above $800^{\circ}C$ the growth rate decreases with increasing temperature. This points to the desorption of growth species from the growing surface. Fig. 1.4 is characteristic for the growth of III/V compounds and will get more attention further on this thesis.

Although MOCVD at a first sight seems to be a relative simple process, the physical and chemical aspects of the process are quite complicated and to a certain extent not yet completely understood. This lack of exact knowledge did not hamper the further development of MOCVD to a growth method by which excellent material and devices can be produced. An example of the excellent quality material which can be grown, is given in fig. 1.5. In this figure the photoluminescence (PL) spectrum at 4.2 K are given of an $Al_{0.34}Ga_{0.66}As/GaAs/Al_{0.34}Ga_{0.66}As$ double hetero structure. The GaAs part of this spectrum shows a low carbon content and very intensive and good resolved peaks in the excitonic region. The AlGaAs part of the PL spectrum only shows an excitonic peak and almost no donor acceptor transition, which is remarkable. The lifetimes of the minority charge carriers in this structure were, as measured by the Time-Related Single Photon Counting technique,

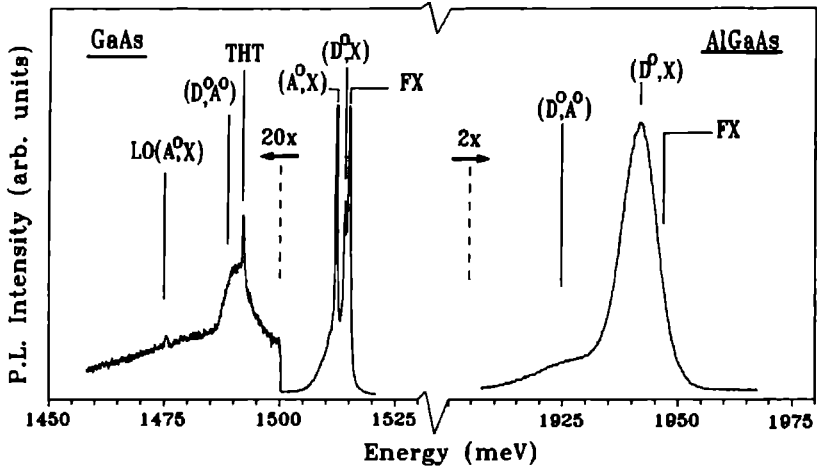


Figure 1.5 The 4.2 K PL spectra of a $\text{Al}_{0.34}\text{Ga}_{0.66}\text{As}/\text{GaAs}/\text{Al}_{0.34}\text{Ga}_{0.66}\text{As}$ double hetero structure; note the interruption in scale.

70 ns what again is indicative for good quality material.

1.4 Outline of this thesis

This thesis describes the growth and doping of GaAs, AlGaAs and InGaP. In chapters 2, 3 and 4 the doping processes of GaAs with silane and disilane are investigated in detail. These incorporation processes were studied as function of the total reactor pressure, temperature and input concentration. In addition, experiments were performed to study the depletion behaviour of the silicon incorporation ex silane. Also the dependence of this doping process on the substrate orientation is investigated. Based on the concept of the chemical boundary layer, a model is presented to describe the incorporation process of silicon from silane and disilane. It turned out that, except for a total pressure of 100 mbar, the doping of GaAs with silane or disilane are similar processes and determined by the same rate limiting step. In the case of disilane this rate limiting step changes with the total reactor pressure. As a result this doping process with disilane is temperature independent at 100 mbar reactor pressure

but shows a temperature dependence at 20 and 1000 mbar total pressure.

Chapter 5 deals with the zinc incorporation in GaAs and AlGaAs. Diethylzinc was used as zinc precursor to perform these p-doping experiments. In this chapter experiments are described for two different reactors, where temperature, pressure and concentration dependence on the zinc incorporation is studied. A model based on adsorption equilibrium is given to explain all results.

The obtained knowledge about the growth and doping processes (as described in chapter 2, 3, 4 and 5) has been used to develop and thereupon improve a GaAs/AlGaAs heteroface solar cell, which is described in chapter 6. As a result a GaAs solar cell has been made with an efficiency of 20.5 %. The development and improvement of the solar cell was based on theoretical and practical considerations with the aid of a simulation program.

Chapters 7 and 8 deal with a completely different III/V compound, i.e. InGaP. This semiconductor is grown lattice matched on GaAs. A thorough study of the growth and characterization of this material is presented. The growth is concentrated on the aspect of control of the composition of this III/V semiconductor. Special attention is paid to an interesting property of this material, viz. ordering on the group III sublattice. This ordering leads to unusual optical and electrical properties (hopping conduction at low temperatures).

References

- [1] J. Bardeen and W.H. Brattain, *Phys. Rev.* **74** (1948) 230.
- [2] W. Shockley, *Bell Syst. Techn. J.* **28** (1949) 435.
- [3] J.S. Kilby, *IEEE Trans. Electron Devices* **ED-23** (1976) 597.
- [4] F.A.J.M. Driessen, Thesis, Nijmegen (1993).
- [5] H.M. Manasevit, *J. Electrochem. Soc.* **116** (1968) 1725.
- [6] M.J. Ludowise, *J. Appl. Phys* **58** (1985) R31.
- [7] J.B. Mullin, S.J.C. Irvine and J. Tunnicliffe, *J. Crystal Growth* **68** (1984) 214.
- [8] B. Cockayne and P.J. Wright, *J. Crystal Growth* **68** (1984) 223.

- [9] T. Hirai and H. Yamane, *J. Crystal Growth* **107** (1991) 683.
- [10] P.M. Freijlink, *J. Crystal Growth* **93** (1988) 207.
- [11] M.R. Leys, *Chemtronics* **2** (1987) 155.
- [12] J. van de Ven, G.J.M. Rutten, M.J. Raaymakers and L.J. Giling, *J. Crystal Growth*, **76** (1986) 352.
- [13] E.P. Visser, C.R. Kleijn, C.A.M. Govers, C.J. Hoogendoorn and L.J. Giling, *J. Crystal Growth* **94** (1989) 929.
- [14] J.P. Duchemin, M. Bonnet, F. Koelsch and D. Huyghe, *J. Electrochem. Soc.* **126** (1979) 1134.
- [15] T.F. Kuech, D.J. Woford, E. Veuhoff, V. Deline, P.M. Mooney, R. Potemski and J. Bradley, *J. Appl. Phys.* **62** (1987) 632.
- [16] H. Terao and H. Sunakawa, *J. Crystal Growth* **68** (1984) 157.
- [17] D.H. Reep and S.K. Ghandi, *J. Electrochemical Soc.* **130** (1983) 675.
- [18] M. Suzuki and M. Sato, *J. Electrochem. Soc.* **132** (1985) 1684.
- [19] M. Suzuki and M. Sato, *J. Electrochem. Soc.* **134** (1987) 2552.

Temperature dependence of silicon doping of GaAs by SiH_4 and Si_2H_6 in atmospheric pressure metalorganic chemical vapour deposition

P.R. Hageman, X. Tang, M.H.J.M. de Croon
and L.J. Giling

Journal of Crystal Growth **98** (1989) 249

Abstract

The temperature dependence of silicon doping in the Metalorganic Chemical Vapour Deposition process has been investigated in the temperature range 550 °C to 800 °C using silane (SiH_4) and disilane (Si_2H_6). The experiments have been carried out at atmospheric H_2 - pressure in a long horizontal reactor. The silicon doping process with both silicon precursors appears to be strongly temperature dependent, with apparent activation energies, E_{act} , of 51.4 ± 5.8 kcal/mole (2.2 ± 0.3 eV) for silane and 45.5 ± 4 kcal/mole (2.0 ± 0.2 eV) for the doping process with disilane. A thorough analysis is given of the rate determining step in both cases based on the presence of a chemical boundary layer.

2.1 Introduction

The development of III/V devices requires well-defined doping profiles and high quality materials and interfaces. So, among other demands, there is a great need for suitable n- and p-type dopants. One of the most commonly used n-type dopants is silicon [1-4,7]. In principle there are two sources available for the silicon doping, viz. silane (SiH_4) and disilane (Si_2H_6).

In spite of the general applicability of silane as an n-type doping source (at least for Metalorganic Chemical Vapour Deposition (MOCVD) purposes) there is not much agreement upon the temperature dependence of the incorporation of silicon from silane in the literature. The apparent activation energies vary from 27 till 40 kcal/mole (1.2 - 1.8 eV) [1,5-8]. However, all these experiments are performed under different experimental conditions so that a comparison between these results is nearly impossible.

In contrast with silane (SiH_4), disilane (Si_2H_6) appears to be more suitable as a dopant source because of its claimed temperature independence [1]. When temperature gradients are present over the wafer and for certain reactor geometries (as will be shown later) it should be possible with disilane, at least in theory, to dope the epilayers more uniformly over larger areas than with silane.

2.2 Experimental procedure

In our experiments we have investigated the temperature dependence of the silicon incorporation in GaAs using silane and disilane. We have performed our experiments in a long horizontal reactor at atmospheric pressure [9]. This reactor allows flow- and temperature gradients to become fully developed. So it is in principle possible to calculate the temperature gradient and mass fluxes in our reactor.

We have used arsine (AsH_3) and trimethyl gallium (TMG) to accomplish the GaAs growth. All the epitaxial layers were grown on $(100) \xrightarrow{2^\circ} (110)$ GaAs substrates. The silane and disilane used were diluted gases of 100 ppm in hydrogen and in nitrogen respectively. We have utilized a partial pressure of silane of 4×10^{-8} atm and a partial pressure of disilane of 3.8×10^{-8} atm. Hydrogen was used as a carrier gas at 1 atm. The mean gas flow rate at the entrance of the reactor was about 7 cm/s. All the experiments were carried out under a V/III ratio of 20. The growth temperature was varied from 550 °C

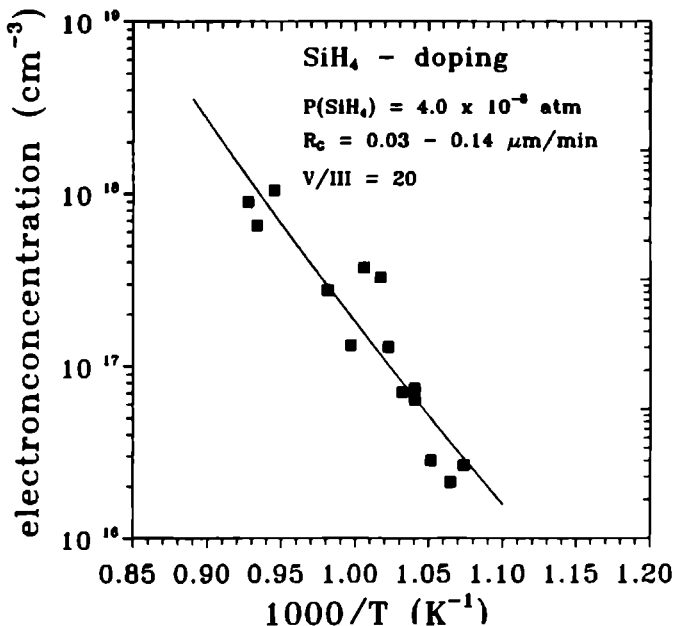


Figure 2.1 Silane (SiH₄) doping of GaAs ($P_{\text{SiH}_4} = 4 \times 10^{-8} \text{ atm}$) Dependence of the electron concentration (300 K, Hall-Van der Pauw) on the growth temperature. The solid line indicates the best fit. $P_{\text{H}_2} = 1 \text{ atm}$.

to 800 °C. The growth rate varied, depending on the position in the reactor and on the growth temperature, from 0.03 to 0.15 $\mu\text{m/min}$.

The temperature of the substrates was determined by a calibrated pyrometer. The electrical characterization was performed using Hall-Van der Pauw measurements and C-V measurements using a C-V profiler. All these electrical measurements were carried out at room temperature.

2.3 Results and discussion

In fig. 2.1 the results of the silane doping experiments are given. In this figure we have plotted the electron concentration as a function of the reciprocal temperature (range measured 550°C – 800°C). The electron concentration, and thus probably also the silicon incorporation, shows an Arrhenius type of

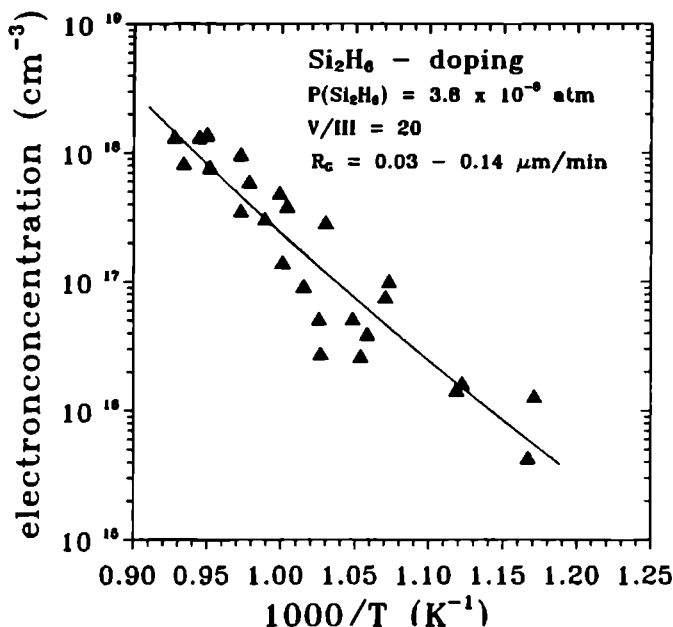


Figure 2.2 Disilane (Si_2H_6) doping of GaAs ($P_{\text{Si}_2\text{H}_6} = 3.8 \times 10^{-8}$ atm) Dependence of the electron concentration (300 K, Hall-Van der Pauw) on the growth temperature. The solid line indicates the best fit. $P_{\text{H}_2} = 1$ atm.

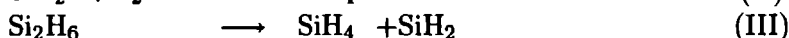
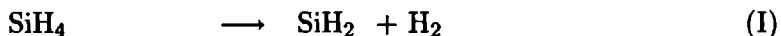
behaviour with an apparent activation energy, E_{act} , of 51.4 ± 5.8 kcal/mole (2.2 ± 0.3 eV). This value is significantly higher (about a factor 2) than those reported in literature [1,5,6].

The experiments with disilane have been performed over a wider temperature range, especially to lower temperatures. At the high temperature side, the experiments also cover the region where the growth rate itself falls off due to desorption of the Ga - growth species. In fig. 2.2 the results of the disilane doping experiments are plotted. Again the electron concentration (incorporated silicon) shows an Arrhenius type of behaviour with an apparent activation energy, E_{act} , of 45.5 ± 4 kcal/mole (2.0 ± 0.2 eV). This is an even more striking result than the one obtained by the silane doping considering the results of Kuech et al. [1] or of Shimazu et al. [8] who found that the doping with disilane is a thermally non activated process.

At first sight one would say that our doping experiments with silane and

disilane are in complete disagreement with the results one can find in the literature [1,5,6]. Still all results can be explained in a logical way -even the zero activation energy of Kuech and our value of 45.5 kcal/mole for the disilane process- when one takes into account the different conditions under which all these incorporation processes have been studied. In particular one has to consider the influence of the parameters: total pressure, partial pressure of hydrogen, length of the susceptor (i.e. boundary layer or not) and of course the trivial point of the type of reactor (vertical or horizontal). It is worthwhile to remember that we have performed our experiments in a regime of fully developed temperature and flow profiles in H₂ at atmospheric pressures, in contrast to the quoted authors where the experiments were performed in reactors where a physical boundary layer regime exists or at lower pressures [1,5,6]. This is basically the reason for the different results which have been obtained in the various studies.

In order to explain the results presented in fig. 2.1 and fig. 2.2 one has to consider the following reactions:



Gas phase decomposition of silane (I) and disilane (III) are highly activated reactions with an activation energy of about 50 kcal/mole [10]. The formation of silane from hydrogen and SiH₂ (II) is very fast and hardly activated. The result is, that at a H₂ pressure of 1 bar, the equilibrium concentration of SiH₂ is very low (fig. 2.3).

2.3.1 SiH₄ doping

Assuming that SiH₂ is the species that will adsorb on the growing surface and will be incorporated, one can imagine that the SiH₂ concentration will determine the silicon incorporation rate. We can exclude diffusion limitation of SiH₄ itself because in that case we would have found hardly any temperature dependence for this type of process.

In addition, in our experiments the doping concentration of silicon appears to be inversely proportional to the growth rate which also points to a kinetic limitation [11].

The decomposition of SiH₄ will take place in the chemical boundary layer which is in most cases a window in which a chemical reaction will occur [12].

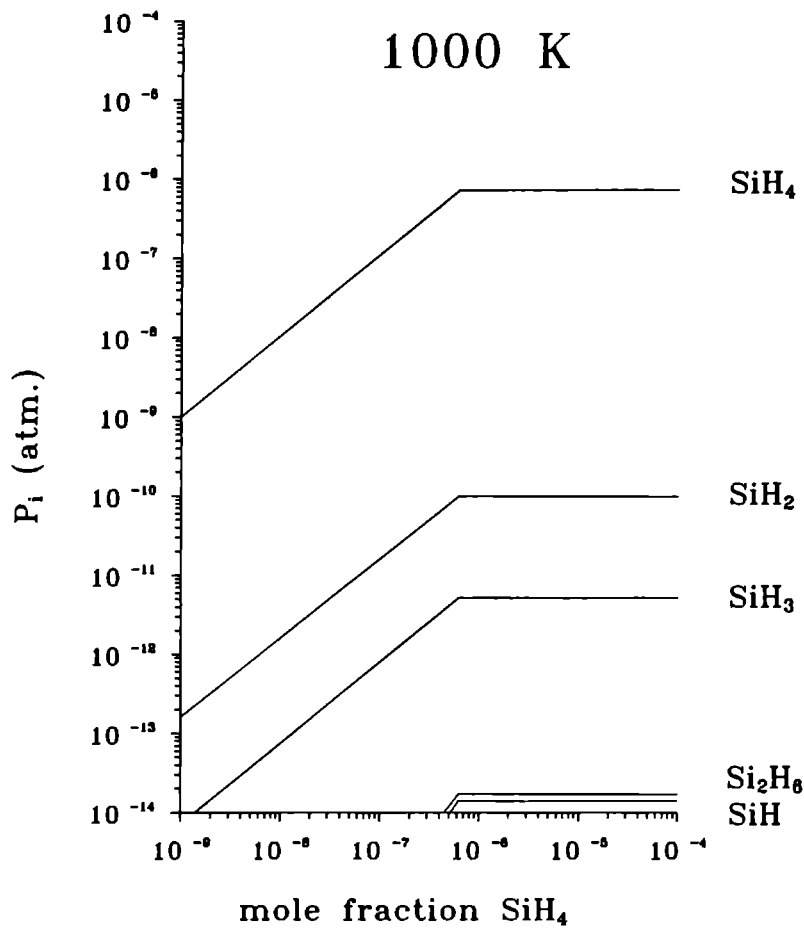


Figure 2.3 Equilibrium partial pressures of the most important silicon species as a function of the input concentration (molar fraction) of SiH_4 at 1000 K. $P_{\text{H}_2} = 1$ atm.

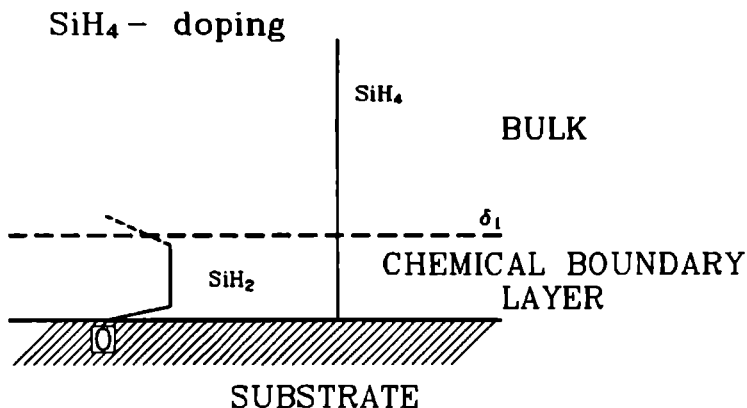


Figure 2.4 Sketched partial pressures profiles in the case of SiH₄ doping. Thermal diffusion effects are not taken into account. $P_{H_2} = 1$ atm. The figure is not on scale.

However, in this special case an equilibrium is present, so one can refer to this region as a chemical equilibrium zone. This zone, due to the high activation energy for the decomposition, is very thin [11]. From the results of the gasphase equilibrium calculations as given in fig. 2.3 [11] we may conclude that the SiH₂ concentration only will be a very small fraction of the SiH₄ concentration at that temperature (1000 K) and that virtually all silane will remain undecomposed. This also explains why there are no depletion effects as observed for this doping process [11].

From our experiments we must conclude that the doping with SiH₄ is determined by kinetics and not by diffusion. Most probably the gas phase decomposition of SiH₄ (I) will be the rate limiting step in the growth process, as this can explain the apparent activation energy observed in our experiments (fig. 2.1). The concentration profiles of SiH₄ and SiH₂ in and outside the chemical boundary layer are depicted in fig. 2.4. It is seen that inside the chemical boundary layer the silicon subsystem is in near equilibrium as the SiH₂ concentration is constant over the main part of this layer. The chemical decomposition of silane in the very thin layer close to the substrate, which is about 30 μm thick, followed by the diffusion of SiH₂ to the surface is responsible for the observed kinetic behaviour. This will be explained below.

2.3.2 Si₂H₆ doping

In the case of Si₂H₆ one has to consider in addition reactions (III) and (IV). Although the decomposition of Si₂H₆ (reaction III) has about the same activation energy as the decomposition of SiH₄ [10], the rate of reaction (III) is much higher than the rate of reaction (I) due to the high value of the pre-exponential factor [10], so that at all the growth temperatures used in this study nearly all the Si₂H₆ is decomposed into SiH₄ and SiH₂. At a H₂ pressure of 1 bar the total decomposition of Si₂H₆ occurs at the top of the chemical boundary layer.

The back reaction, i.e. the formation of Si₂H₆ from SiH₄ and SiH₂ (reaction IV), can be neglected because of the very low reaction rates due to the low concentration of silicon containing species as compared to the high hydrogen concentration in the reactor. So one can really say that at the growth temperatures all the Si₂H₆ is decomposed. The chemical situation for this case is depicted in fig. 2.5 in which the concentration profiles are sketched inside and outside the chemical boundary layer. The Si₂H₆ concentration declines from the input value to zero at the top of the chemical boundary layer. Here all Si₂H₆ is decomposed into SiH₂ and SiH₄. The diffusion length of the SiH₂ radical in H₂ is given by $\sqrt{\frac{D}{k_2 P_{H_2}}}$ where k_2 is the rate constant of the reaction of H₂ with SiH₂ (reaction II) and D is the diffusion coefficient of SiH₂ at the growth temperature. The value of this diffusion length is much smaller than the width of the chemical boundary layer and is in the order of 30 μm [10]. Inside the boundary layer virtually all SiH₂ has reacted with H₂ to SiH₄, only a very minor fraction of SiH₂, as determined by the $\text{SiH}_4 \rightleftharpoons \text{SiH}_2 + \text{H}_2$ equilibrium (fig. 2.3), will be present in a constant concentration over the main part of the chemical boundary layer. Close to the surface the SiH₂ concentration falls off to zero again because of the incorporation in the GaAs lattice. The SiH₄ concentration is almost constant over the boundary layer, at least for positions beyond the entrance region.

The observed kinetic behaviour can be attributed in the first place to the chemistry coupled to diffusion in the very small region of 30 μm inside the gas phase, i.e. the decomposition of SiH₄ to SiH₂ coupled to diffusion of SiH₂ to the surface, which as rate limiting step leads to the incorporation rate r_d :

$$r_d = k_1 [\text{SiH}_4] \sqrt{\frac{D}{k_2 P_{H_2}}},$$

which can be written as:

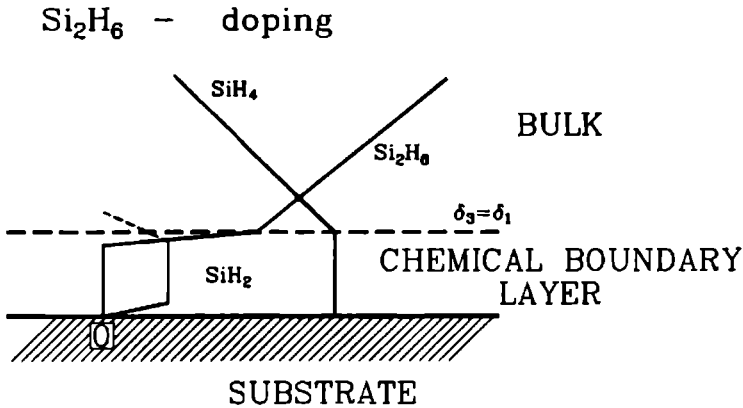


Figure 2.5 Sketched partial pressures profiles in the case of Si₂H₆ doping. Thermal diffusion effects are not taken into account. $P_{H_2} = 1$ atm. The figure is not on scale.

$$r_d = \frac{D}{\sqrt{\frac{D}{k_2 P_{H_2}}}} \frac{k_1}{k_2} \frac{[SiH_4]}{P_{H_2}} = \frac{D}{\delta} \frac{k_1}{k_2} \frac{[SiH_4]}{P_{H_2}} = \frac{D}{\delta} [SiH_2],$$

where k_1 is the reaction constant of the decomposition of SiH₄ [12]. This relation clearly reveals that diffusion of the SiH₂ molecule is responsible for the rate limiting step. The activation energy is determined by the product $k_1 \sqrt{\frac{D}{k_2}}$. As the temperature dependence of the factor $\sqrt{\frac{D}{k_2}}$ is about zero, the final activation energy is determined by k_1 i.e. the decomposition of silane.

In the second place the adsorption process itself can be rate limiting. The rate r_a for this process is given by:

$$r_a = k_{ads.} K \frac{[SiH_4]}{P_{H_2}} \Theta^*,$$

where K is the equilibrium constant for the silane decomposition and Θ^* is the number of free adsorption sites. Here the Arrhenius energy is determined by the temperature dependence of the product $k_{ads.} K$. As the activation energy

for the adsorption process will be about zero, the enthalpy, ΔH , for the silane decomposition will determine the kinetic process. As $\Delta H \approx E_{\text{act}}$ (reaction II) no distinction can be made at this point between these two processes. A calculation of the magnitude of the rate of adsorption, with data from [10] and [13], clearly reveals that this process is at least one order of magnitude faster than the decomposition in the gas phase however. So the conclusion is that actually the formation of SiH_2 radicals followed by their diffusion to the surface is the rate limiting step in this case.

From both studies presented above, i.e. the doping of GaAs by SiH_4 and Si_2H_6 , the same step appeared to be rate limiting viz. the production of SiH_2 radicals close to the substrate followed by their diffusion to the surface. Consequently, in both cases the same activation energy should be observed, viz. about 50 kcal/mole, being the activation energy for the decomposition of silane.

The observed values of 51.4 ± 5.8 kcal/mole and 45 ± 4 kcal/mole for the decomposition of silane and disilane respectively, deserve a closer analysis, especially because these values also include the temperature dependence of the growth rate itself. It will be shown in a subsequent paper [14] that when the proper corrections are taken into account both corrected values come close to the theoretical value. Also, in this coming paper a thorough analysis will be given for the pressure dependence of the activation energy.

2.3.3 Si_2H_6 doping in small cells

The total decomposition of Si_2H_6 at the top of the chemical boundary layer results in a relatively high concentration of SiH_2 radicals, which -when they are produced close enough to the crystal surface i.e. within a distance smaller than their diffusion lengths- will give rise to a very high efficiency of the dopant incorporation process. This is the case for studies performed at 0.03 to 1 bar H_2 - pressure on small susceptors which have a thin physical boundary layer for flow and temperature. Also is in this situation the incorporation seemingly temperature independent because the reaction is already for 100% completed at relatively low temperatures due to the high value of the pre-exponential factor for this decomposition reaction (note that the actual activation energy for the decomposition of Si_2H_6 is about as large as that of the decomposition of SiH_4 [10]). When the SiH_2 radicals are not produced from Si_2H_6 within reaching length of the crystal surface quite a different situation is created, because now the very fast reaction of SiH_2 with H_2 will take place (this de-

termines the actual diffusion length) resulting in the formation of SiH₄. This situation is predicted to take place in reactors where the flow and temperature profiles are fully developed together with high H₂ - pressures.

2.4 Conclusions

Concluding we can say that doping with SiH₄ is a kinetically determined process and for growing larger and uniform layers one has to be able to control the temperature within a few degrees. The doping with Si₂H₆ at 1 bar hydrogen pressure is a similar process and will cause the same troubles.

Acknowledgments

The authors would like to thank Mr. M. Hilbers for performing the C-V and Hall measurements.

This work was performed as a part of the research program of the "Stichting voor de Technische Wetenschappen" (S.T.W.) with financial support from the "Nederlandse Organisatie voor Wetenschappelijk Onderzoek" (N.W.O.) and as a part of E.C. contract EN3S-0078-NL.

References

- [1] T.F. Kuech, E. Veuhoff and B.S. Meyerson, J.Crystal Growth **68** (1984) 48.
- [2] S. Field and S.K. Ghandhi, J. Crystal Growth **74** (1986) 543.
- [3] M. Druminski, H.-D. Wolf and K.-H. Zschauer, J.Crystal Growth **57** (1982) 318.
- [4] E. Veuhoff, T.F. Kuech and B.S. Meyerson, J. Electrochem. Soc. **132** (1985) 1958.
- [5] S.J. Bass, J.Crystal Growth **47** (1979) 613.
- [6] J.P. Duchemin, M. Bonnet, F. Koelsch and D. Huyghe, J. Electrochem. Soc. **126** (1979) 1134.

- [7] H.K. Moffat, T.F. Kuech, K.F. Jensen and P.-J. Wang, *J.Crystal Growth* **93** (1988) 594.
- [8] M. Shimazu, K. Kamon, K. Kimura, M. Mashita, M. Mihara and M. Ishii, *J.Crystal Growth* **83** (1987) 327.
- [9] J. van de Ven, G.J.M. Rutten, M.J. Raaymakers and L.J. Giling, *J.Crystal Growth* **76** (1986) 352.
- [10] H.K. Moffat and K.F. Jensen, *J. Electrochem. Soc.* **135** (1988) 459.
- [11] X. Tang, H.G.M. Lochs, P.R. Hageman, M.H.J.M. de Croon and L.J. Giling, *J. Crystal Growth* **98** (1989) 827.
- [12] M.H.J.M. de Croon and L.J. Giling, *J. Electrochem. Soc.* **137** (1990) 3606.
- [13] M.E. Coltrin, R.J. Kee and J.A. Miller, *J. Electrochem. Soc.* **135** (1986) 1206.
- [14] M.H.J.M. de Croon and L.J. Giling, *Progr. Crystal Growth Characterization* **19** (1989) 125.

Si-doping of MOCVD GaAs: A closer analysis of the incorporation process

X. Tang, H.G.M. Lochs, P.R. Hageman, M.H.J.M. de Croon, L.J. Giling and A.J. Bons¹

Journal of Crystal Growth **98** (1989) 827

Abstract

Doping studies have been carried out as a function of silane input fraction over the entire dopant range of silicon in GaAs. In the lower dopant region, where the incorporation varies linearly with the silane input mole fraction, the compensation ratio N_A^-/N_D^+ appears to have a constant value of 0.3. In this region the incorporation is also orientation dependent. For SiH_4 input mole fractions higher than 1×10^{-6} the electron concentration does not change noticeably, however the compensation ratio rises from 0.3 to 0.7. Simultaneously precipitates are observed in the grown layer. From gas phase equilibrium calculations such silicon precipitation is predicted to take place at these higher input pressures of SiH_4 . As regards the incorporation rate of Si itself, analysis of the doping results reveals that, when corrections are made for differences in GaAs growth rate and small differences in growth temperature, a constant deposition of silicon along the MOCVD reactor is obtained. The absence of

¹Laboratory for Metallurgy, Technical University Delft, The Netherlands.

depletion effects and the observed temperature dependence imply that the limiting step for the Si incorporation is the decomposition of the SiH_4 which happens very close to the hot surface of the GaAs substrate.

3.1 Introduction

Metalorganic chemical vapour deposition (MOCVD) now has become a standard and versatile technique with a proved capability to grow many sophisticated structures such as superlattices, lasers and tandem solar cells. For most device applications, a good control of the doping process is necessary, including control of doping level, uniformity and doping profile. Up to now, no single dopant seems to be able to fulfill all the requirements such as wide doping range, easy control of uniformity, easy to handle, negligible memory effect, low diffusion coefficient and so on. As an n-type dopant, silicon is widely used for GaAs. For a long time, silane (SiH_4) has been used as the doping source. One of the dominant problems inherent with this dopant is a strong temperature dependence which makes uniform doping difficult for reactors where the temperature differs over the susceptor. When silane is replaced by disilane (Si_2H_6), the incorporation process appeared to be independent of growth temperature [1,2]. However, recent analysis has revealed that actually disilane should make no difference when compared with silane, except when lower pressures are used or when the flow and temperature profiles of the incoming gas are undeveloped [3,4]. Another well recognized effect is the compensation which can occur with silicon. In literature, for low and moderate Si concentrations, this problem is more or less ignored and it is assumed that silicon is incorporated as a donor [5,6]. In the present report, the compensation effect is studied over the entire dopant range. Another subject which has not received much attention is the formation of Si precipitates in the GaAs lattice what occurs at the highest doping levels. This effect has been studied using interference-contrast microscopy, photoluminescence and transmission electron microscopy (TEM), assisted by thermodynamic calculations.

In our long horizontal MOCVD reactor, which enables us to grow with well established flow and temperature profiles, it should in principle also be possible to reveal more about the details of the Si incorporation. Therefore the study is elaborated by examining the Si incorporation on various crystallographic orientations.

3.2 Experimental procedure

The doping experiments were carried out at atmospheric pressure with the use of trimethylgallium (TMG) and arsine (AsH_3) as source materials while 100 ppm silane (SiH_4) in H_2 was employed as dopant source. A horizontal re-

actor is used with a rectangular cross-section. The reactor is resistance heated at the bottom and water cooled on the top so that a known temperature profile is established. A long entrance length is used to ensure stabilization of both temperature and velocity profiles of the incoming gas mixture (for details, see ref.[7]). The arsine was passed through a molecular sieve before mixing with the carrier gas (H_2) in order to minimize the moisture level [8]. The ratio between AsH_3 and TMG (V/III ratio) was 20. The growth temperature was measured at the GaAs substrate surface with a calibrated optical pyrometer. It was kept constant at $700 \pm 5^\circ C$ for all the present MOCVD experiments except during the temperature series which was used to determine the activation energy of the Si incorporation. The GaAs substrates, obtained from MCP (UK), were Cr-doped semi-insulating, horizontal Bridgman grown and chemo-mechanically polished on one face. Typical etch pit densities were below $5000/cm^2$. The substrate orientations were $(100) \xrightarrow{2^\circ} (110)$, (110) , $(111)Ga$, $(111)As$, $(100) \xrightarrow{4^\circ} (110)$, and (100) . The $(100) \xrightarrow{2^\circ} (110)$ substrate is widely used because it is known to give the best morphology. Also in our experiments this orientation was mainly used. The other orientations (110) , $(111)Ga$, and $(111)As$ have been employed in order to study the orientation dependence of the Si incorporation process. However it appeared that under our experimental conditions, the growth on the exact $(111)As$ substrate always resulted in a rough surface with correspondingly unreliable Hall mobilities. Therefore these results had to be discarded. The orientations $(100) \xrightarrow{4^\circ} (110)$ specifically have been used for studying the Si precipitation.

The morphology after growth was observed with an interference-contrast microscope. The thickness of the grown layer was measured by cleaving and staining. The electrical characterization was performed by Hall-Van der Pauw measurements using a clover-leaf-configuration. Photoluminescence (PL) measurements were done at 5 K with an Ar^+ -laser (514.5 nm) and a double-monochromator fitted with an S1-photomultiplier. TEM measurements were performed to examine the precipitates in the epitaxial layers. All TEM samples have been thinned by mechanical polishing followed by ion beam milling using Ar^+ ions. The samples were studied in a Philips EM400T TEM operating at 120 kV.

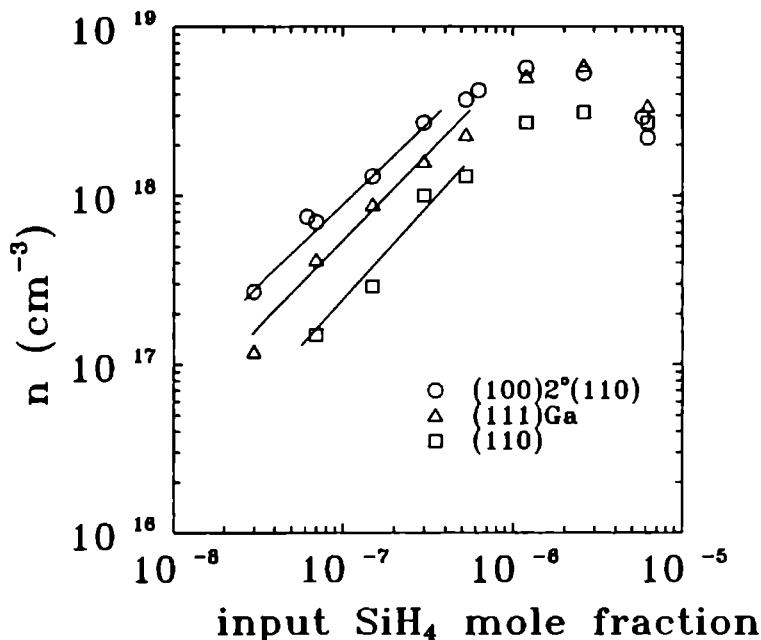


Figure 3.1 Net carrier concentration $n = N_D^+ - N_A^-$ versus the input mole fraction of silane for three different substrate orientations
 $T_G = 700\text{ }^\circ\text{C}$, $V/\text{III} = 20$

3.3 Results and discussion

3.3.1 Electrical evaluations

In fig. 3.1 the net carrier concentrations $n = N_D^+ - N_A^-$ as a function of the input mole fraction of SiH_4 are given for three substrate orientations, viz. $(100)^{2^\circ}(110)$ and the exact orientations $(111)\text{Ga}$ and the (110) . Below a silane mole fraction of 10^{-6} , a linear relationship is found for all three substrate orientations. Above this value saturation of the carrier concentration occurs. This is in accordance with literature [9-11]. As is evident from fig. 3.1 the difference in incorporation on the various substrate orientations is especially clear in the lower dopant regions. The efficiency of the incorporation increases in the order $(100)^{2^\circ}(110) > (111)\text{Ga} > (110)$.

This is in agreement with the results of Veuhoff et al.[2] on the Si-doping studies of the (111)As, (100) and (111)Ga orientations. Veuhoff et al. explained the difference on the (111)Ga and (111)As surfaces by assuming that on an ideal (111)Ga surface all the dangling bonds are empty, whereas on the (111)As surface each arsenic surface atom possesses a dangling bond filled with a pair of electrons. Because of this difference, adsorption of SiH_x ($x \leq 3$) radicals should be favoured on the (111)As surface. No explanation was given in that study for the behaviour of the (100) surface. A similar trend is also found by Nakanisi [12] in intentionally undoped GaAs grown by MOCVD where the background impurity concentration for five used orientations increases in the order $(311)\text{B} > (100) > (111)\text{A} > (311)\text{A} > (110)$. Nakanisi did not give an explanation for the incorporation differences however. A few orientation dependent studies have been made on Si-doped GaAs grown by MBE [13-15]. In these studies the observed differences on A ((211)A, (311)A, (511)A, (711)A) and B ((211)B, (311)B, (511)B, (711)B) polar faces were explained by the assumption of the coexistence of a single- and double-dangling bonds from the (111) faces and the (100) face respectively where the bonding between the adatom and the substrate is stronger at the double-dangling bond site than that at the single-dangling bond site. With this assumption they could explain the tendency of the A and B polar faces to be doped as p-type and n-type respectively.

The linear relation between carrier concentration and the silane input concentration, as observed in the lower dopant region, points to a first order reaction as the rate limiting step. The most likely process is subsurface trapping of the incorporated dopant, thereby breaking the exchange between adsorbed dopant atoms and neutral donors in the solid. This will occur whenever the vertical growth rate (G) is faster than the diffusing rate of subsurface Si_{Ga} to the surface (D), the actual condition being $G > D/b$ where b is of the order of the lattice constant. This automatically means that the ionization of the dopant cannot reflect itself in the slope of the curve. It must be remembered that when a full equilibrium for the dopant system is present, a slope 1/2 in the figure would be expected. Instead of subsurface trapping, trapping of the adsorbed dopant atoms by the moving steps can be the limiting factor. That step trapping at least partially is active is illustrated in fig. 3.2 where a comparison is given of the Si incorporation on (100) orientations with respectively 0° , 2° and 4° of misorientation. Although on the exact (100) surface two-dimensional nucleation is possible, which will introduce extra steps on the surface, we can still assume that the number of steps will increase with an increase in the degree of misorientation. When the growth rate is the same

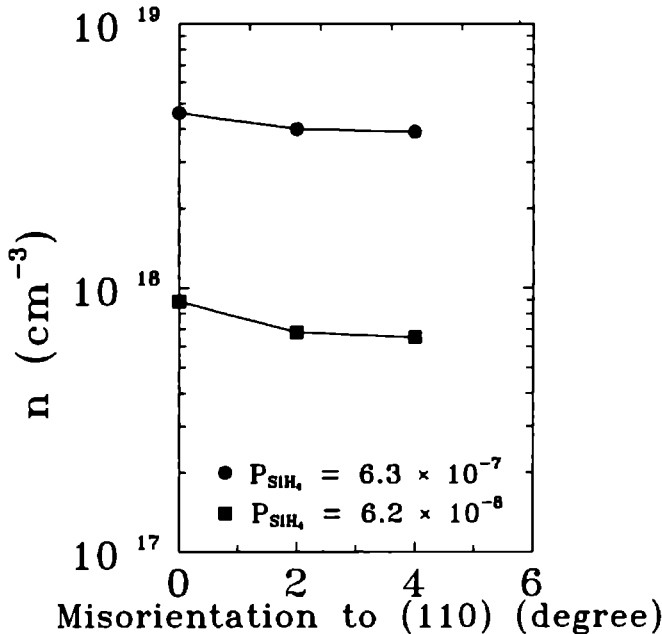


Figure 3.2 Net carrier concentration $n = N_D^+ - N_A^-$ versus the degree of misorientation of the (100) surface towards (110). $T_G = 700^\circ\text{C}$, $V/III = 20$.

for all these three orientations, which is found experimentally, the step velocity should decrease with an increase in misorientation. As a consequence the effect of step trapping will be more effective for samples that are less misoriented, as is observed (fig. 3.2). It must be remarked here that also the total amount of incorporated silicon (i.e. $Si_{Ga} + Si_{As}$) shows the same dependence on misorientation so that the effect as given in fig. 3.2 is not influenced by a possible change in compensation.

The room temperature Hall mobilities as a function of carrier concentration are given in fig. 3.3. No difference is found between the layers grown on the $(100)^{2^\circ}(110)$ and $(111)Ga$ orientations. However, above carrier concentrations of $3 \times 10^{18} \text{ cm}^{-3}$, the mobility values clearly diverge from the theoretical $N_A^-/N_D^+ = 0.3$ curve. The layers grown on the (110) orientation have overall lower mobility values as compared with the layers grown on the other two

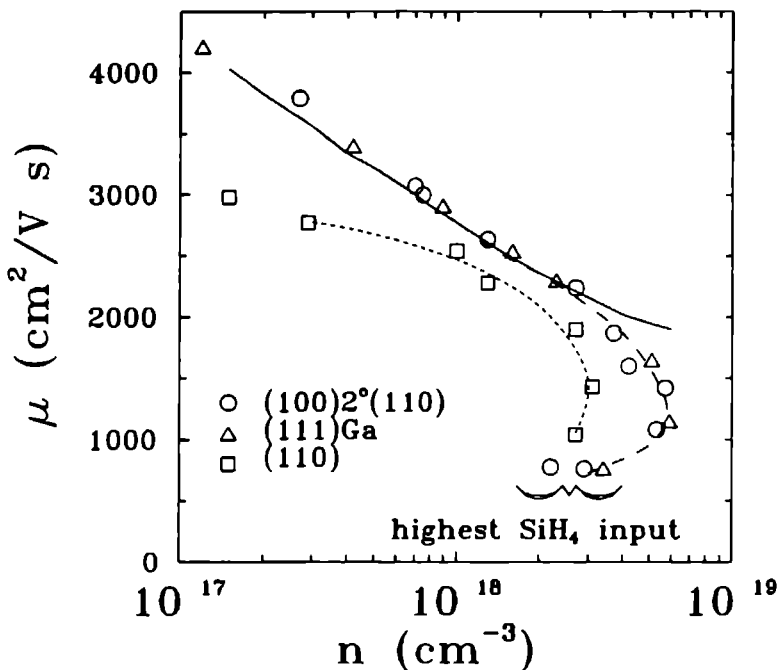


Figure 3.3 Hall mobility at room temperature versus the carrier concentration n for three different substrate orientations. The solid line gives the theoretical mobility at a compensation ratio $N_A^-/N_D^+ = 0.3$. $T_G = 700^\circ\text{C}$, $V/\text{III} = 20$.

orientations.

As Si is a group IV element, a Si atom may be incorporated at a Ga site which gives rise to a donor, or be incorporated at an As site which gives rise to an acceptor, so that this amphoteric behavior leads to compensation. The compensation ratio which is defined as N_A^-/N_D^+ can be calculated from the measurements of carrier concentration and mobility [16,17]. It should be pointed out that the calculations in refs. [16,17] are based on dilute solid solutions so that our calculated values above a carrier concentration of $3 \times 10^{18} \text{ cm}^{-3}$ should be treated with some care. The calculated results of N_A^-/N_D^+ are given in fig. 3.4.

For SiH_4 mole fractions below 3×10^{-7} , the compensation ratio has a nearly

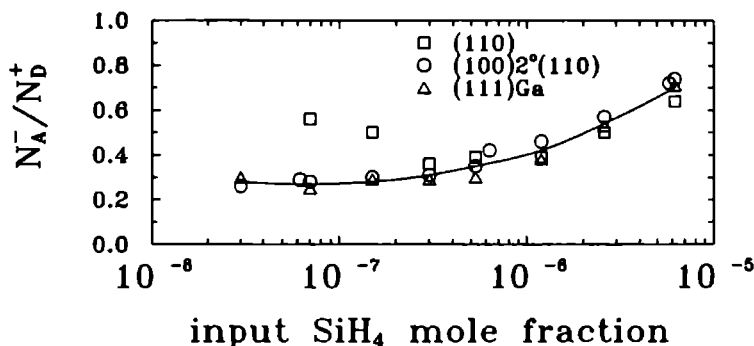


Figure 3.4 Compensation ratio N_A^-/N_D^+ versus silane input mole fraction for three different substrate orientations. The line in the figure is a guide to the eye.

constant value of 0.3 for the $(100)^{2^\circ}(110)$ and $(111)\text{Ga}$ orientations. For the (110) orientation, however, the compensation ratio starts at a value 0.6 for low P_{SiH_4} , decreasing to the value 0.3 for $P_{\text{SiH}_4} \approx 3 \times 10^{-7}$. The rather high overall compensation is in contrast with other reports where the compensation ratio is found to be very low [18] or assumed to be zero [5,6]. We have checked whether the high Si_{As} concentration could be due to a low effective V/III ratio during growth. This possibility exists in our reactor, because, despite the high V/III ratio used in our experiments, during growth an arsenic deposit is formed at the cooled top wall of the reactor thereby lowering the effective V/III ratio. Removal of the top cooling, whereby also the arsenic deposition was avoided, resulted in the same compensation ratios, however.

For carrier concentrations larger than $3 \times 10^{18} \text{ cm}^{-3}$ ($P_{\text{SiH}_4} > 10^{-6}$) all compensation ratios rise from the value 0.3 to 0.7 at $P_{\text{SiH}_4} = 6 \times 10^{-6}$. This means that at higher silicon concentrations more Si atoms are incorporated at As-sites.

The relatively high compensation of 0.3 found in this study in the lower dopant regions may be due to a difference in growth conditions. We are growing layers in the region where the gas flow and the temperature profiles are fully developed and stabilized, whereas most experiments which are mentioned in literature have been performed with a very short susceptor which is placed in the region where both gas flow and temperature profiles still have to develop. The consequences are that in our reactor surface equilibrium processes can

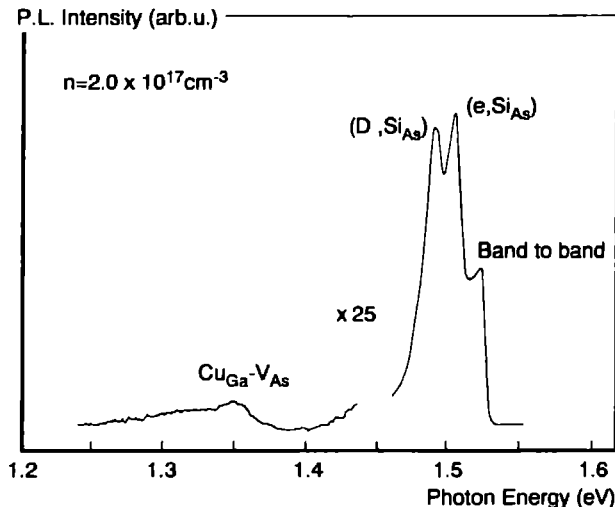


Figure 3.5 Low temperature (5 K) PL spectrum for a $(100)^{2^{\circ}}(110)$ sample with a carrier concentration $n = 2 \times 10^{17} \text{ cm}^{-3}$.

get a chance to adjust, this in contrast to the short cells where kinetics will prevail. The existence of silicon on As-sites could be proved by the presence of a Si_{As} -peaks in photoluminescence spectra. Our PL spectra clearly reveal (e, A^0) and (D^0, A^0) transitions, in which Si_{As} as an acceptor is involved, when n is larger than $2 \times 10^{17} \text{ cm}^{-3}$ (fig. 3.5). Below this value the Si_{As} peak may still be present, but is difficult to resolve due to the overlap with a C_{As} peak.

The fact that Si acts as an acceptor in GaAs is not a new phenomenon. Under LPE conditions, it is known that even p-type GaAs can be obtained by adding Si to the Ga melt [19]. Also under MBE conditions, p-type GaAs can be grown on certain substrate orientations [13,14]. A detailed analysis of the compensation effect based on a step incorporation mechanism has been given in a separate paper [20].

The total carrier concentration $(N_{\text{D}}^{+} + N_{\text{A}}^{-})$ can be calculated based on the net carrier concentration and the mobility values. The calculated $N_{\text{D}}^{+} + N_{\text{A}}^{-}$ value is equal to the total number of incorporated Si atoms if the Si atoms are exclusively incorporated at lattice sites and completely ionized. This is not

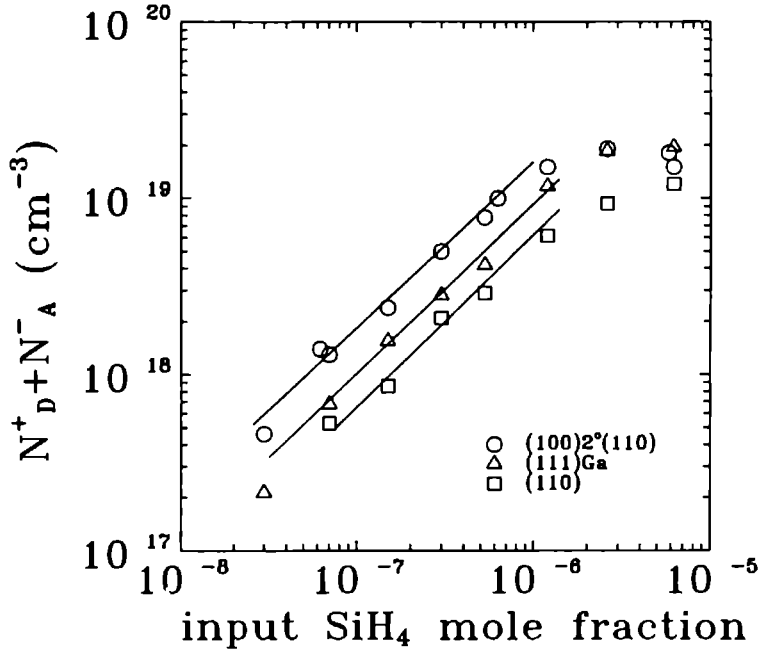


Figure 3.6 Total carrier concentration $N_D^+ + N_A^-$ versus the input mole fraction of silane for three different substrate orientations. $T_G = 700^\circ\text{C}$, $V/\text{III} = 20$.

true when certain Si complexes, e.g. $[\text{Si}_{\text{Ga}}-\text{V}_{\text{Ga}}]$, are formed as is characterized by infrared local vibrational mode (LVM) absorption [21]. However this $[\text{Si}_{\text{Ga}}-\text{V}_{\text{Ga}}]$ complex was not observed for a sample doped up to $1 \times 10^{18} \text{ cm}^{-3}$ so our assumption is quite probable.

In fig. 3.6 the $N_D^+ + N_A^-$ values are given versus the input of silane for the three orientations. They again show the earlier observed systematic trend $(100)2^\circ(110) > (111)\text{Ga} > (110)$, despite the difference in mobilities found for these orientations. The GaAs growth rate was found to be constant for all the orientations studied, so that its influence on the Si incorporation can be excluded.

The difference in the total amount of Si found in various substrate ori-

entations must originate from processes such as diffusion in the gas phase, adsorption-desorption over the surface and diffusion of the adsorbed species on the surface. The selective incorporation of Si on an arsenic or a gallium position can only take place during the incorporation at a step or a kink site. Incorporation means that double or triple bonds are formed so that desorption is unlikely once the silicon atom is arrived at the step or kink site. Because all orientations receive the same silicon flux in the form of SiH_2 radicals (viz. those radicals which are produced in the chemical boundary layer within its diffusion length from the substrate [3]), all surfaces in principle could have the same coverage of silicon species.

The differences in incorporation rates as observed in our experiments, indicate that the difference in the sticking coefficient or the difference in desorption must play a role. In other words, a quasi equilibrium must be present at these surfaces. In principle, the origin of the difference in adsorption-desorption can be found in the absolute value for the bond strength of the SiH_2 radical with the adsorption sites on the (100), (111)Ga and (110) surfaces. Under MOCVD conditions the (100) surface is arsenic stabilized, where all arsenic atoms form dimers with each other in a $\sigma - \pi$ configuration. No extra AsH_3 adsorption will be possible on this arsenic stabilized surface. Adsorption of the electronically incomplete shell species SiH_2 on an arsenic atom is favoured, however, because the electron shell becomes completely filled in this process. The (111)Ga surface on the other hand is electronically poor because only single dangling bonds are present on the surface. Now the arsenic rich conditions do not lead to an arsenic stabilized surface, but only result in adsorption of AsH_3 .

So the great difference with the (100) surface is that the AsH_3 molecules on the (111)Ga surface do not form dimers, i.e. do not form an intrinsic part of the lattice. Adsorption of SiH_2 on the (111)Ga surface will occur at the gallium sites which are left free. Because of the electron deficiency of the Ga atoms, a completely filled adsorption bond will be formed between SiH_2 and Ga. Because of the electron deficiency, combined with the electropositive character of Ga with respect to arsenic, the Si-Ga bond strength will be smaller than the Si-As bond strength. The consequence is that desorption of SiH_2 on a (111)Ga surface is somewhat larger than on a (100) surface in the As-stabilized configuration. Because the step incorporation chances for both surfaces are alike, as well as the diffusion possibilities over the surface, the total incorporation rate is mainly determined by the silicon coverage on these surfaces. One can say that these adsorbed silicon species form the supply source to the steps. The consequence is that the silicon incorporation rate on

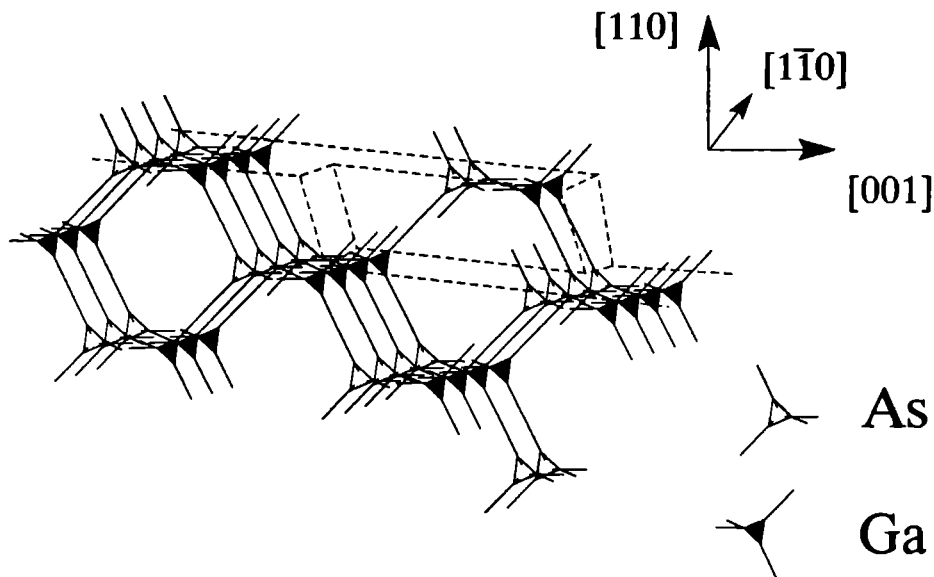


Figure 3.7 Side-view of a (110) surface showing the [001] steps and a kink site. The periodic bond chains are lying along the channels in the $[1\bar{1}0]$ direction.

(100) is larger than on (111)Ga. This will be discussed in more detail in a forthcoming paper [20].

The still smaller incorporation rate on (110) has to be explained by the zipper like growth along the channels in the $[1\bar{1}0]$ directions, where the periodic bond chains are lying [22,23] (fig. 3.7). Not only steric hindrance now plays an important role as to what diminishes the sticking coefficient, but also the difference in diffusion behaviour which is almost restricted to a linear motion along the channel line only.

The above discussion, although difficult to quantify, gives the trend for the incorporation of Si on the various orientations, viz. $(100) > (111)\text{Ga} > (110)$, as is found experimentally.

3.3.2 Silicon precipitation

For carrier concentrations higher than $3 \times 10^{18} \text{ cm}^{-3}$ saturation occurs for all the substrate orientations studied (fig. 3.1). The saturation point corresponds to a silane input mole fraction of about 1×10^{-6} .

When the silicon concentration in GaAs is increased, the solubility limit of Si in GaAs can be exceeded. The solubility of Si in solid GaAs has been determined to reach a maximum of 4 at. % ($\approx 1.6 \times 10^{21} \text{ cm}^{-3}$) at the eutectic temperature of 1130 °C [24]. However more precise data which cover the lower temperature region used for MOCVD (550 - 750 °C) are lacking, so no prediction can be given when precipitation will occur at these temperatures.

One can proceed in another way by calculating the chemical composition of the Si-Ga-As-H-C system using the existing data base of chemical equilibrium constants. For the growth temperature of 1000 K of GaAs by MOCVD, equilibrium calculations have been performed as a function of the input mole fraction of silane [25].

For input values of SiH_4 larger than 1×10^{-6} thermodynamics predict the formation of solid silicon (fig. 3.8). Above this value the partial pressures of all gaseous silicon species are fixed, because all the additional silicon which is introduced into the system will be transferred into solid silicon. The theoretically calculated value of input silane mole fraction of 1×10^{-6} where silicon nucleation will occur, favourable coincides with the observed tendency for electrical saturation (fig. 3.1). It must be understood that differences will exist between the incorporation behaviour, which is a kinetic process, and the theoretically predicted equilibrium situation. When precipitation is predicted, it will only occur in practice when the silicon atoms in the bulk of the crystal have time enough to find each other (large diffusion coefficients at the given temperature together with low growth rates). When the growth temperature is low enough, as in MBE systems, the individual silicon atoms may simply be trapped in the grown layers and never will have a chance to come to equilibrium because of the small diffusion coefficient in the bulk.

Such a system will be supersaturated and will show a large domain of electrical activity as indeed has been observed. In MOCVD the temperatures are higher and consequently the silicon atoms will have more chance to meet each other during the growth process. This promotes clustering and consequently a smaller electric active region is to be expected. This is also found experimentally [26,27].

The Si-nucleation has been confirmed indirectly by photoluminescence experiments. By looking at the band-to-band recombination peak in the PL

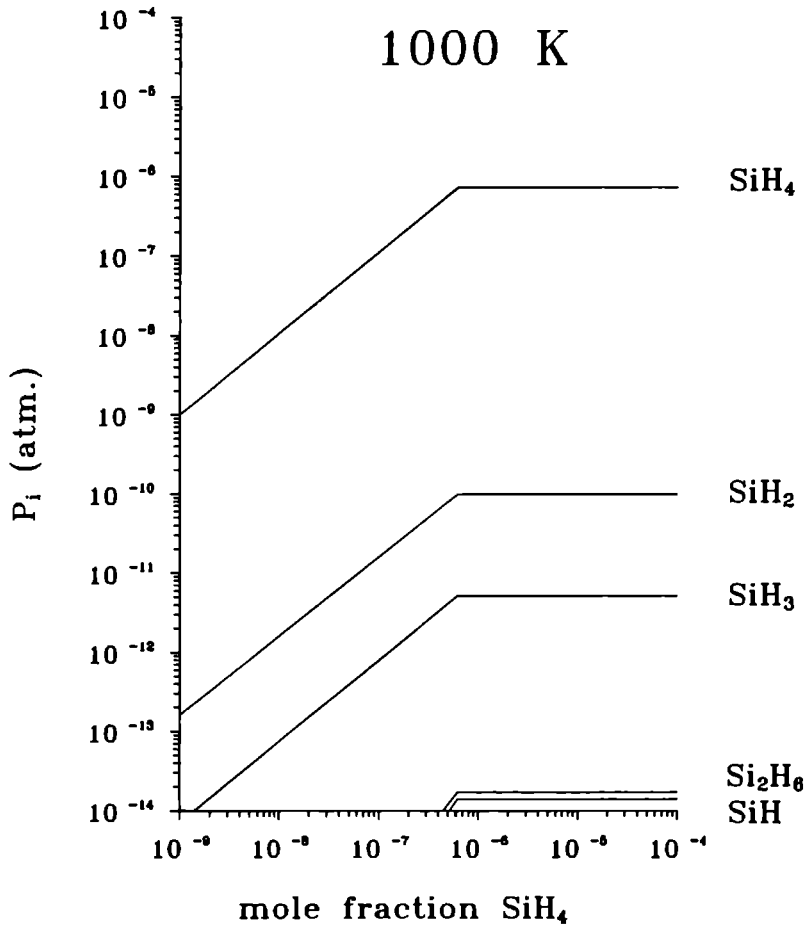


Figure 3.8 Gas phase partial pressures of silicon compounds as a function of the input mole fraction of silane as calculated from thermodynamic equilibrium constants. The system contains TMG, AsH_3 , and SiH_4 in H_2 at 1 atm total pressure and at a temperature of 1000 K. All the non-silicon containing species have been omitted in this figure. The horizontal parts in the curves are due to the formation of solid silicon which fixes the pressures.

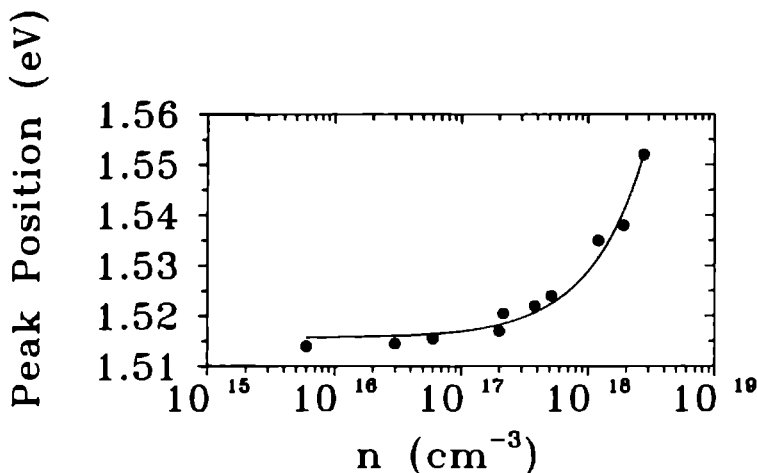


Figure 3.9 PL peak position of the band to band recombination of silicon doped GaAs (at 5 K) versus room temperature net carrier concentration.

spectra, it is found that when the carrier concentration is above a certain value, which in our case is approximately $1 \times 10^{17} \text{ cm}^{-3}$, the peak position starts to shift to higher energies (fig. 3.9). This phenomenon is caused by the filling of the conduction band [28]. The peak energy keeps increasing when more Si is incorporated at lattice sites. This result is also found by Druminski et al. [6]. An interesting point from their study is that when the total Si concentration is higher than $1 \times 10^{19} \text{ cm}^{-3}$, the PL peak position is fixed. We were unable to confirm these results because the samples with the highest Si content showed no photoluminescence signal at all. The results of Druminski et al. show that the excess Si atoms are no longer electrically active as donors or acceptors. This phenomenon has been explained [6] by the formation of precipitates of Si or some other kind of electrically inactive complex. Up to now no direct proof has been given of precipitate formation of Si in MOCVD GaAs.

There are some additional techniques which might be able to give information on precipitate formation, viz. SIMS, wet chemical etching, morphological study of the epitaxial layers and TEM. The SIMS technique is only suited to measure the total Si concentration, it can not discriminate whether the Si

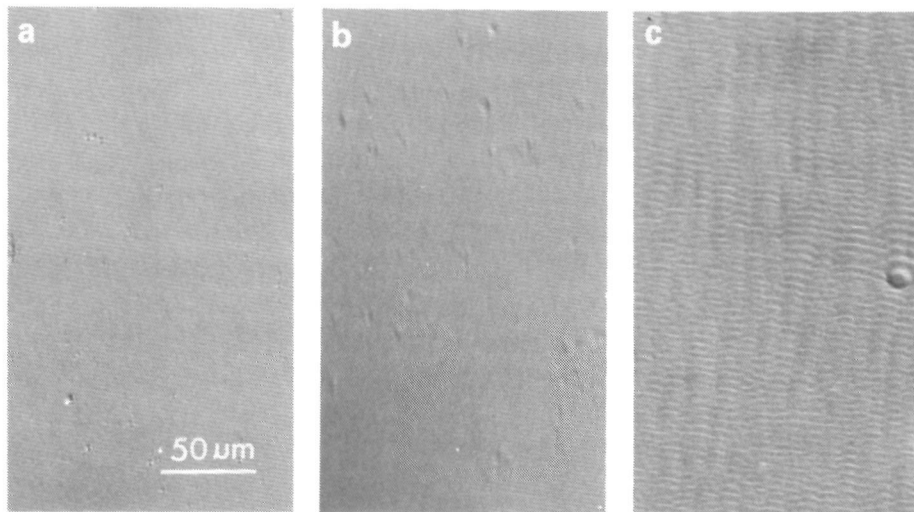


Figure 3.10. Surface morphologies of epitaxial layers as obtained by interference microscopy for three (100) (mis-)oriented samples. The silane input mole fraction in each case was 5.8×10^{-6} . (a) $(100)^{4^\circ} \rightarrow (110)$, (b) $(100)^{2^\circ} \rightarrow (110)$, (c) exact (100). At lower silane input values all surfaces are smooth.

atoms are incorporated at the Ga or As lattice sites or incorporated as precipitates. Also the wet chemical etching technique DSL (defect selective etching with light), which has proved to be so powerful for defect revealing [29], fails because at these high carrier concentrations the etch rate under illumination is simply zero, probably due to the high recombination rate of the created hole-electron pairs. In principle observation of the surface morphology should give valuable results. In order to study this more precisely, an additional series of samples has been grown with SiH_4 input mole fractions around the critical value 1×10^{-6} , viz. 6.2×10^{-8} , 6.3×10^{-7} and 5.8×10^{-6} , respectively. The GaAs substrates used had three different orientations, (100), $(100)^{2^\circ} \rightarrow (110)$, and $(100)^{4^\circ} \rightarrow (110)$. The morphology appeared to be similar for all the samples grown with the two lower Si input concentrations. For the highest Si input concentration, the morphology of the exact (100) samples shows a difference as compared with the misoriented (100) samples (fig.3.10). The surfaces in figures 3.10(a) and 3.10(b) are flat, whereas fig.3.10(c) shows a wavy surface

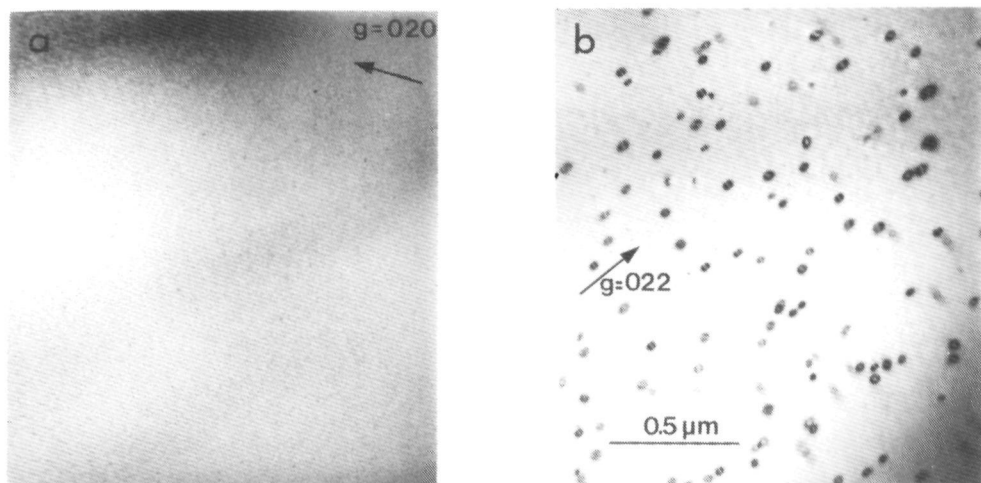


Figure 3.11 TEM micrographs of two Si-doped samples. (a) silane mole fraction 6.2×10^{-8} and (b) silane mole fraction 5.8×10^{-6} . The small granular contrast in the background is caused by surface damage due to ion-beam thinning.

consisting of macrosteps. In our opinion, the observed macrostep formation has to be explained as a result of step blocking by precipitates or clusters of adsorbed impurities.

Crystal growth is taking place by step propagation on the surface. The steps or the kink sites along a step provide favourite places for species to incorporate. According to the theory of Cabrera and Vermileya [30], a step which moves along an atomically smooth terrace will be stopped by a pair of impurities that are less than $2\rho_c$ apart from each other (ρ_c is the critical radius) and will squeeze itself between pairs of impurities when they are more than $2\rho_c$ apart. When a step is stopped by impurities, a macrostep has to be formed to overcome the impurities. This is true for immobile impurities. In case the adsorbed impurity atoms are still mobile and can diffuse over the surface, the moving step is able to drive the impurity atoms in front of the step. The larger the terrace is - as is the case for exact (100) - the higher the impurity density can become. Because of this condensation effect the critical distance between two impurities will be reached first at the exact orientation.

This explains the difference in morphology between exact and misoriented (100) samples. The phenomenon of macrostep formation is often observed in solution grown crystals [31].

The most direct proof of the presence of precipitates has come from our TEM studies of these samples. Defects indeed have been observed in the samples grown with the highest silane input (fig. 3.11). These defects are identified as dislocation loops, interpreted as interstitial dislocation loops due to the Si-doping. Similar observations have been reported in studies of heavily Si-doped Bridgman-grown GaAs [32] and annealed Si-implanted GaAs [33]. The dislocation loop densities have been measured to be approximately $3 \times 10^{13} \text{ cm}^{-3}$.

From the above we conclude that indeed precipitates are formed which cause the formation of macrosteps as well as the observed dislocation loops by TEM. It proves that Si-nucleation starts between a SiH_4 input mole fraction of 6.3×10^{-7} and 5.8×10^{-6} . This is consistent with the thermodynamic analysis which predicts a critical SiH_4 input mole fraction of 1×10^{-6} for the formation of solid silicon. These silicon precipitates will not give a contribution to the free carrier concentration but will decrease the electron mobility as is shown in fig. 3.3.

3.3.3 Rate limiting step of the silicon incorporation process

It is known from previous studies [7] that the growth of GaAs by MOCVD at high temperature is limited by the diffusion of TMG through the gas phase. As a consequence gas phase depletion is known to occur, especially for long deposition lengths without a tilt of the susceptor. This depletion phenomenon can be calculated with a rather high precision [7,34]. In this study the depletion of gallium containing gaseous species from the gas phase is demonstrated by the exponential decrease in growth rate as given in fig. 3.12(a).

Also if the silicon incorporation process would be dominated by gas phase diffusion, a similar depletion behaviour has to be expected for the Si doping as well. However, when the Si incorporation is corrected for the difference in growth rate and a small difference in growth temperature over the susceptor, there appears to be no depletion at all (fig. 3.12(b)). The corrections are based on the observations (i) that the Si incorporation rate is inversely proportional to the GaAs growth rate, which is also reported by other authors [9,35,36], and (ii) that the Si incorporation rate from silane is a strong function of the

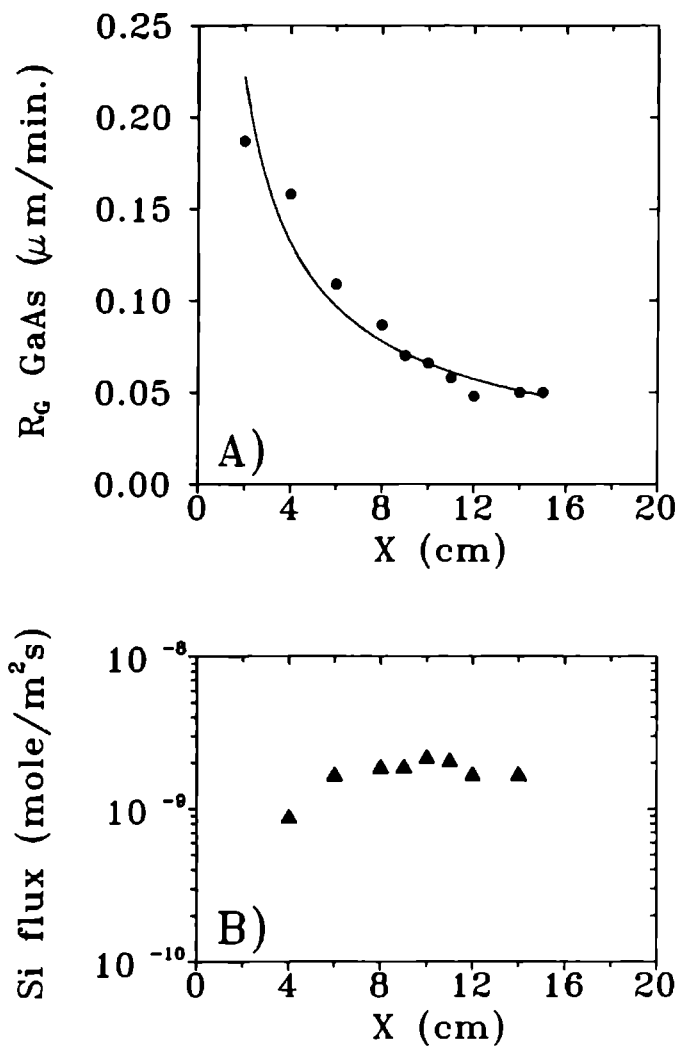


Figure 3.12 (a) Growth rate of GaAs as a function of the axial position x in the reactor, showing the exponential depletion effect; (b) Silicon flux ($\text{mole}/\text{m}^2\text{s}$) to the surface as a function of the axial position x . The flow and temperature profiles are fully developed for $x \geq 6$ cm.

growth temperature [1,9,36]:

$$N_{\text{Si}} \propto \exp(-E_a/RT), \quad (3.1)$$

where E_a is the activation energy for the incorporation process.

In a separate paper we have reported on the Si incorporation rate as function of the growth temperature [3], the activation energy for this process is found to be 47 kcal/mole. This high value corresponds to the activation energy $E_a(k_+)$ of the decomposition reaction of silane according to



The product SiH_2 is believed to adsorb on the GaAs surface and to be responsible for the incorporation of Si. Due to the high activation energy this decomposition reaction will only occur in appreciable quantities at the highest gas temperatures, i.e. close to the crystal surface in the chemical boundary layer [3]. Because the activation energy $E_a(k_-)$ for the back reaction is very small ($E_a(k_-) \ll E_a(k_+)$), the diffusion length of the SiH_2 radicals in the hydrogen carrier gas of 1 bar is extremely small viz. about 30 μm [3], so only those SiH_2 molecules that are created very close to the hot susceptor i.e. in the lowest part of the chemical boundary layer can be incorporated. SiH_2 molecules that are created away from the susceptor will react with H_2 and form SiH_4 again. This phenomenon explains the nearly constant Si concentration in the bulk gas phase and the absence of depletion. So for the doping of GaAs with Si using silane, the decomposition of SiH_4 into SiH_2 very close to the surface followed by diffusion of SiH_2 towards the crystal surface is the rate limiting step for the incorporation process, although the growth process itself is diffusion limited.

3.4 Conclusions

Doping studies have been carried out as a function of silane input fraction over the entire dopant range of silicon in GaAs. It is found that up to a carrier concentration of $3 \times 10^{18} \text{ cm}^{-3}$, the silicon incorporation varies linearly with the silane input concentration. The efficiency of the incorporation increases in the order $(100) \xrightarrow{2^\circ} (110) > (111)\text{Ga} > (110)$. This trend can be explained by the relative bond strengths between SiH_2 species and the various oriented surfaces, i.e. the difference in free enthalpy of adsorption (ΔG_{ads}^0). This implies that a

certain degree of dopant adsorption-desorption equilibrium is present at these surfaces. Additionally for the (110) face the size effect of the SiH₂ molecules has to be taken into account.

All the Si-doped layers grown are found to be compensated. For the (100)^{2°}→(110) and (111)Ga orientations, the compensation ratio has a value of about 0.3 for doping up to $3 \times 10^{18} \text{ cm}^{-3}$ and increases above this value to 0.7. The (110) orientation always shows a higher compensation ratio.

For carrier concentrations larger than $3 \times 10^{18} \text{ cm}^{-3}$ ($P_{\text{SiH}_4} > 10^{-6}$), precipitates in the crystal are formed due to Si nucleation in the matrix. This is in agreement with equilibrium calculations of the system Si-Ga-As-H-C.

The rate limiting step for the Si incorporation is concluded to be the decomposition of SiH₄ into SiH₂ and H₂ followed by diffusion of SiH₂ to the surface. This process happens very close to the hot substrate because of the very small free diffusion length of the SiH₂ radical in 1 bar H₂.

Acknowledgments

This work was performed as a part of the research program of the "Stichting voor de Technische Wetenschappen" (STW) with financial support from the "Nederlandse Organisatie voor Wetenschappelijk Onderzoek" (NWO).

References

- [1] T.F. Kuech, E. Veuhoff and B.S. Meyerson, *J. Crystal Growth* **68** (1984) 48.
- [2] E. Veuhoff, T.F. Kuech and B.S. Meyerson, *J. Electrochem. Soc.* **132** (1985) 1958.
- [3] P.R. Hageman, X. Tang, M.H.J.M. de Croon and L.J. Giling, *J. Crystal Growth* **98** (1989) 249.
- [4] M. Shimazu, K. Kamon, K. Kimura, M. Mashii, M. Mihara and M. Ishii, *J. Crystal Growth* **83** (1987) 327.
- [5] R. Azoulay, L. Dugrand, D. Ankri and E.V.K. Rao, *J. Crystal Growth* **68** (1984) 453.

- [6] M. Druminski, H.-D. Wolf, K.-H. Zschauer and K. Wittmaack, *J. Crystal Growth* **57** (1982) 318.
- [7] J. van de Ven, G.M.J. Rutten, M.J. Raaijmakers and L.J. Giling, *J. Crystal Growth* **76** (1986) 352.
- [8] L.M. Fraas, J.A. Cape, P.S. McLeod and L.D. Partain, *J. Vac. Sci. Technol.* **B3** (1985) 921.
- [9] S.J. Bass, *J. Crystal Growth* **47** (1979) 613.
- [10] K. Okamoto, S. Onozawa and T. Imai, *J. Appl. Phys.* **56** (1984) 2993.
- [11] N. Bottka, R.S. Sillmon and W.F. Tseng, *J. Crystal Growth* **68** (1984) 54.
- [12] T. Nakanisi, *J. Crystal Growth* **68** (1984) 282.
- [13] S.S. Bose, B. Lee, M.H. Kim, G.E. Stillman and W.I. Wang, *J. Appl. Phys.* **63** (1988) 743.
- [14] W.I. Wang, *Surf. Sci.* **174** (1986) 31.
- [15] S. Subbanna, H. Kroemer and J.L. Merz, *J. Appl. Phys.* **59** (1986) 488.
- [16] W. Walukiewicz, L. Lagowski, L. Jastrzebski, M. Lichtensteiger and H.C. Gatos, *J. Appl. Phys.* **50** (1979) 899.
- [17] W. Walukiewicz, J. Lagowski and H.C. Gatos, *J. Appl. Phys.* **53** (1982) 769.
- [18] R. Venkatasubramanian, K. Patel and S.K. Ghandhi, *J. Crystal Growth* **94** (1989) 34.
- [19] F.E. Rostzoczy, *J. Electrochem. Soc.* **17** (1968) 516.
- [20] X. Tang, J. te Nijenhuis, Y. Li and L.J. Giling, *J. Crystal Growth* **107** (1991) 263.
- [21] J. Maguire, R. Murray, R. C. Newman, R.B. Beall and J.J. Harris, *Appl. Phys. Letters* **50** (1987) 516.
- [22] L.J. Giling and W.J.P. van Enckevort, *Surf. Sci.* **161** (1985) 567.
- [23] W.J.P. van Enckevort and L.J. Giling, *J. Crystal Growth* **45** (1978) 90.

- [24] L.A. Borisova and N.A. Valisheva, *Izv. Akad. Nauk. SSSR Neorgan. Mater.* **10** (1974) 1083.
- [25] L.C. Keizer, X. Tang, R.Z.C. van Meerten and L.J. Giling, *J. Crystal Growth* **102** (1990) 667.
- [26] M. Heiblum, W.I. Wang, L.E. Osterling and V. Deline, *J. Appl. Phys.* **54** (1983) 6751.
- [27] R. Sacks and H. Shen, *Appl. Phys. Letters* **47** (1985) 374.
- [28] D.M. Szijsd, P. Porro, A. Majerfeld and S. Lagomarsino, *J. Appl. Phys.* **68** (1990) 2367.
- [29] J.L. Weyher and J. van de Ven, *J. Crystal Growth* **78** (1986) 191.
- [30] N. Cabrera and D.A. Vermileya, *Growth and Perfection of Crystals*, (Wiley, New York, 1958) p. 393.
- [31] J.P. van der Eerden and H. Muller-Krumbhaar, *Phys. Rev. Letters* **57** (1986) 2431.
- [32] D.B. Darby, P.D. Augustus, G.R. Booker and D.J. Stirland, *J. Microscopy* **118** (1980) 343.
- [33] C.P. Stewart, R. T. Blunt, G.R. Booker and I.R. Sanders, *Physica* **116B** (1983) 635.
- [34] H. Moffat and K.F. Jensen, *J. Crystal Growth* **77** (1986) 108.
- [35] R.J. Field and S.K. Ghandhi, *J. Crystal Growth* **74** (1986) 543.
- [36] J.P. Duchemin, M. Bonnet, F. Koelsch and D. Huyghe, *J. Electrochem. Soc.* **126** (1979) 1134.

Pressure and temperature dependence of Silicon doping of GaAs using Si_2H_6 in Metalorganic Chemical Vapour Deposition

P.R. Hageman, M.H.J.M. de Croon ¹, J.N.H. Reek and
L.J. Giling

Journal of Crystal Growth **116** (1992) 169

Abstract

The doping of GaAs with disilane in a metal organic chemical vapour deposition (MOCVD) process has been investigated at various input concentrations of disilane, total pressures and temperatures. The carrier concentration is linearly dependent on the input concentration of disilane. The temperature dependence of the incorporation process of silicon using disilane as a precursor changes as the total pressure varies. At a total pressure of 100 mbar the process is temperature independent in contrast to the behaviour at total pressures of 20 and 1000 mbar. So the doping process with disilane appears to

¹Technical University of Eindhoven, Lab. voor Chemische Technologie, p.o. box 513, Eindhoven

depend on the total pressure. Using the concept of chemical boundary layers the results are explained in terms of the different rate determining steps in the doping process as a function of different total pressures.

4.1 Introduction

Metalorganic chemical vapour deposition (MOCVD) has become one of the most important growth techniques of III/V semiconductor materials. Many different devices can be manufactured employing MOCVD. Most of these device structures consist of one or more n-type layers. In MOCVD only a few number of elements are used for n-type doping of III/V semiconductor layers, viz. Te, S, Se and Si. Among these elements silicon can be employed for low ($n \approx 1 \times 10^{15} \text{ cm}^{-3}$) and high doping levels (up to $n \approx 1 \times 10^{18} \text{ cm}^{-3}$), without exceptionally high compensation levels [1]. Moreover it is possible to obtain abrupt doping profiles with silicon as a dopant because of its lack of memory effects [2], its low diffusion coefficient in GaAs and its low elemental vapour pressure [3].

In the early days only silane was used as dopant source for silicon in MOCVD [4,5]. The major disadvantage of silane is its temperature dependence of the incorporation process in GaAs [5-11] and other III/V materials. This effect can be as large as a 2% change in carrier concentration for a variation of 1°C for a growth temperature of 650°C [12]. Therefore it is very difficult to obtain uniform doping profiles over a wafer if temperature gradients are present, even if they are small. Disilane as an alternative silicon dopant source for the doping of III/V semiconductors was proposed by Kuech et al.[13]. It appeared that disilane does not lead to a temperature dependence of the incorporation process. It also has a higher doping efficiency than silane, at least in the temperature and pressure regimes used [12-16]. However, more detailed studies of this process reveal that doping of GaAs with disilane also can be temperature dependent when different growth conditions are employed [8,9,14,17].

In an earlier paper [9] we presented an analysis of the incorporation of silicon from disilane in GaAs at a total reactor pressure of 1 bar based on the concept of the chemical boundary layer [18,19]. This new study will treat the analysis in more detail and at various total reactor pressures in combination with new experimental data on the pressure and temperature dependence of the doping of GaAs with disilane.

4.2 Experimental procedure

In our experiments we investigated the temperature and pressure dependence of silicon incorporation in GaAs using disilane as a dopant. The study was

carried out in a commercial, computer controlled MOCVD reactor [20] using trimethylgallium (TMG) and arsine (AsH_3) as source materials. As a dopant precursor, 100 ppm disilane (Si_2H_6) in N_2 was used. Hydrogen, purified by a Pd-diffusion cell, was used as carrier gas at a flowrate of 7 slm. The pressure of the reactor is adjustable between 20 and 100 mbar, however it is also possible to perform experiments at atmospheric pressure. The reactor cell has a rectangular cross-section and is heated by infra-red radiation.

All experiments were carried out with a ratio of AsH_3 and TMG (V/III ratio) of 125. The growth temperature, determined by a thermocouple placed in the susceptor close to the substrate, varied between 550° and 800°C . Disilane was added to the reactor in mole fractions from 1×10^{-10} to 4×10^{-7} . The GaAs growth rate varied, depending on the growth temperature and pressure in the reactor, from 1.4 to $2.3 \mu\text{m}/\text{hour}$.

The GaAs substrates were all semi-insulating and chemo-mechanically polished on one side. All substrates used in this study were $(100)^{2^\circ}(110)$ oriented. The thickness of the grown layers was obtained by cleaving and staining, using an interference-contrast microscope or, if necessary, a scanning electron microscope (SEM). The samples were electrically characterized by Hall-Van der Pauw measurements performed at room temperature.

The material quality of the grown (undoped) epilayers was investigated by photoluminescence measurements. These measurements were performed at 4.5 K, with the sample in He exchange gas. Optical excitation was provided by the 2.41 eV (514.5 nm) line from an Ar^+ laser with an excitation density of $5.3 \text{ W}/\text{cm}^2$. The luminescence was dispersed by a double monochromator fitted to a cooled photomultiplier tube with a S1 response.

4.3 Results

4.3.1 Growth and characterization of undoped GaAs

The growth rate of undoped GaAs is plotted versus the reciprocal temperature for three growth pressures (20, 100 and 1000 mbar) in fig. 4.1. From this figure it appears that the growth rate of GaAs is almost independent of the temperature at a pressure of 100 mbar. One has to conclude that at this pressure and in this temperature range ($600 - 700^\circ\text{C}$) the growth of GaAs is a diffusion limited process [21-23].

At the other total pressures (20 and 1000 mbar, fig. 4.1) the growth rate is only weakly dependent of the growth temperature. However, trends are

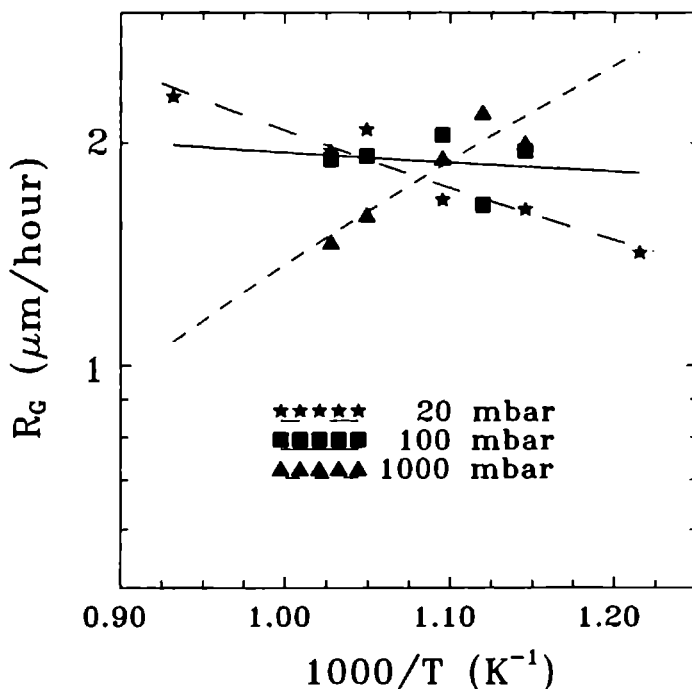


Figure 4.1 Semi log plot of the growth rate of GaAs in $\mu\text{m}/\text{hour}$ versus $1000/T (\text{K}^{-1})$ at total pressures of 20, 100 and 1000 mbar.

still clear. At 20 mbar the apparent activation energy, E_{act} , for the growth process is now about 4 kcal/mole in the same temperature region. This points to the fact that the growth of GaAs at these conditions is determined by diffusion of the growth species to the substrate, coupled to the decomposition of trimethylgallium (TMG) [23,24]. The change of the apparent activation energy when going to lower pressures is caused by the lower residence times of the reactants in the reactor and lower collision frequencies compared to the situation at 100 mbar so that the kinetic control over the growth rate increases at this lower pressure [25]. At atmospheric pressure the E_{act} of the growth process is -4 kcal/mole, so the growth process of GaAs seems to be determined by diffusion of the growth species to the substrate but now coupled to the high temperature desorption of the growth species from the substrate [21-23]. However, this result is not really reliable because of the influence

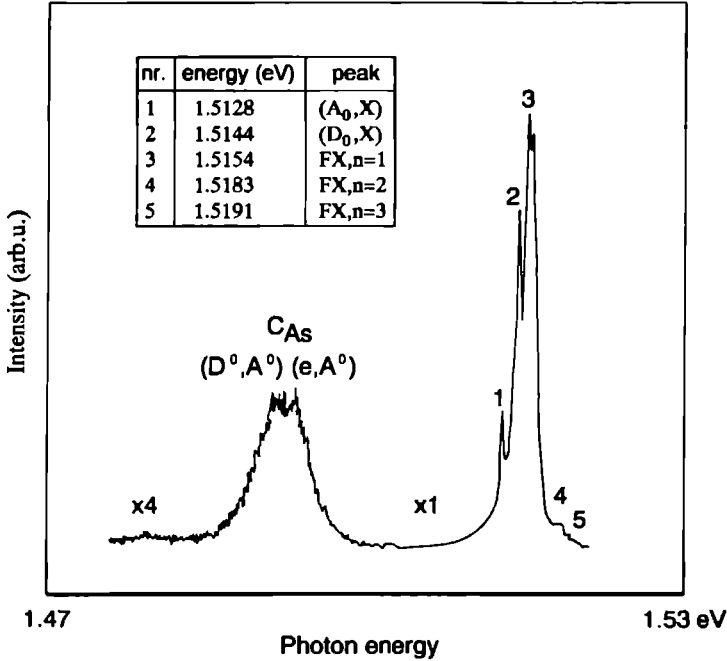


Figure 4.2 Photoluminescence spectrum at 4 K of undoped GaAs grown at 640 °C with a V/III ratio of 125 at 20 mbar.

of non developed flow profiles in the reactor at this pressure which will be discussed in section 4.4.3. So altering the total pressure (in this temperature region) at which the experiments are performed influences the rate determining step in the GaAs growth process.

In fig. 4.2 a photoluminescence (PL) spectrum is shown for an undoped GaAs sample grown at 20 mbar and at a temperature of 640 °C. This PL spectrum reveals the good quality and the low background doping level of the undoped GaAs epilayers. The well resolved and highly intense peak in the excitonic region, as compared to the also well resolved carbon acceptor peak, is an indication for a relative low carbon content and for a low residual impurity concentration of the sample. The largest peak in the excitonic region is the free excitonic transition peak and not a bound excitonic transition peak. This is a strong indication for a very low impurity content in the epilayer. A third indication for the good quality of the sample is the fact that higher excited states (n=2 and n=3) from the free exciton peak are visible. Electrical char-

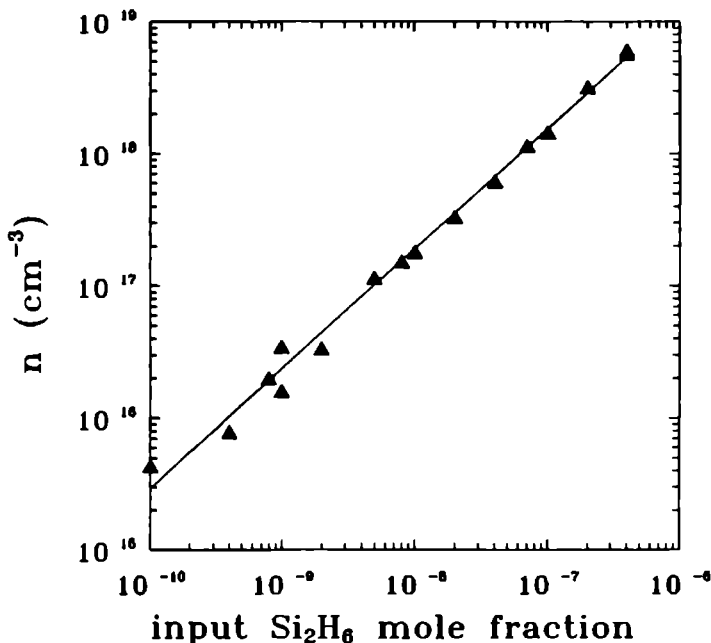


Figure 4.3 Free carrier concentration n (cm^{-3}) (in GaAs) plotted versus the input mole fraction of disilane. The growth was performed at 640°C with a V/III ratio of 125 at 20 mbar.

acterization of these undoped layers was not possible because even epilayers up to $11\ \mu\text{m}$ thicknesses were fully depleted.

4.3.2 Disilane doping of GaAs

Figure 4.3. shows the free carrier concentration n ($= N_D^+ - N_A^-$) in GaAs:Si versus the input mole fraction Si_2H_6 for a growth pressure of 20 mbar as determined by room temperature Hall-Van der Pauw measurements. In this series of experiments the growth temperature ($T = 640^\circ\text{C}$), the TMG and AsH_3 partial pressures and the total pressure in the reactor (20 mbar) were kept constant.

In this log-log plot the carrier concentration increases linearly with respect to the disilane input mole fraction with a slope of 0.95. Saturation of the

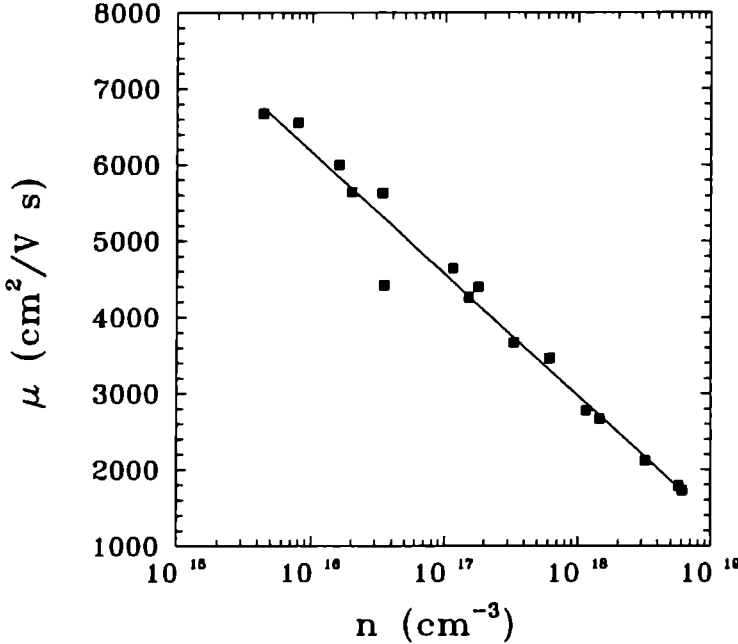


Figure 4.4 Mobility μ (cm^2/Vs) plotted versus the free carrier concentration n (cm^{-3}) for GaAs grown at at 640 °C with an V/III ratio of 125 at 20 mbar.

carrier concentration is a common and undesired phenomenon in silicon doping of GaAs using SiH_4 and Si_2H_6 [1,7,11,12,14,16,26,27]. However, no saturation is observed in the carrier concentration as a function of the input mole fraction Si_2H_6 in our measurements up till $n = 6.1 \times 10^{18} \text{ cm}^{-3}$. Similar experiments at 100 and 1000 mbar have not been performed.

In fig. 4.4 the corresponding room temperature mobilities (μ) are plotted as a function of the free carrier concentration. As is visualized in this semi log plot the mobility is linearly dependent of the carrier concentration and no deviation from this linear dependence is observed. With the known values of the free carrier concentration and the mobilities a compensation ratio Θ , defined as (N_A^-/N_D^+) , can be determined using the tables of Walukiewicz et al.[28].

The obtained values of Θ versus the free carrier concentration are plotted in

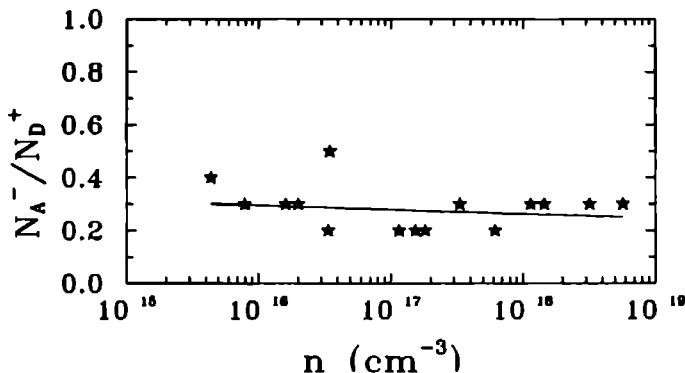


Figure 4.5 Compensation ratio N_A^- / N_D^+ (Θ) of GaAs grown at 640 °C with an V/III ratio of 125 at 20 mbar doped with disilane plotted versus the free carrier concentration n (cm^{-3}).

fig. 4.5. A nearly constant value of about 0.3 is observed for Θ for all measured values of the free carrier concentration, demonstrating that no extra compensation occurs at the higher silicon concentrations. It is remarkable that the compensation ratio remains 0.3, a normal value for relatively low doping levels. However, we obtained this value even at the highest carrier concentrations. In literature one finds values of Θ as high as 0.7 at these doping levels [27].

In fig. 4.6 the silicon deposition rate R_{Si} is plotted as a function of the reciprocal temperature at various total reactor pressures. This deposition rate is defined as:

$$R_{\text{Si}} = \frac{N_{\text{Si}} \times M_{\text{GaAs}} \times R_{\text{GaAs}}}{N_{\text{Av}} \times \rho_{\text{GaAs}}} \text{ (mole/m}^2 \text{ sec)}, \quad (4.1)$$

in which N_{Si} equals the total incorporated silicon concentration (cm^{-3}), M_{GaAs} the molecular weight of GaAs, R_{GaAs} the growth rate of GaAs in $\text{mole/m}^2\text{s}$, N_{Av} is Avogadro's constant and ρ_{GaAs} is the density of GaAs.

Using the free carrier concentration as determined by Hall-Van der Pauw measurements and the corresponding compensation ratio, one can derive the following relation between the free carrier concentration and the incorporated silicon concentration [28]:

$$N_{\text{Si}} = \left(\frac{1 + \Theta}{1 - \Theta} \right) \times n, \quad (4.2)$$

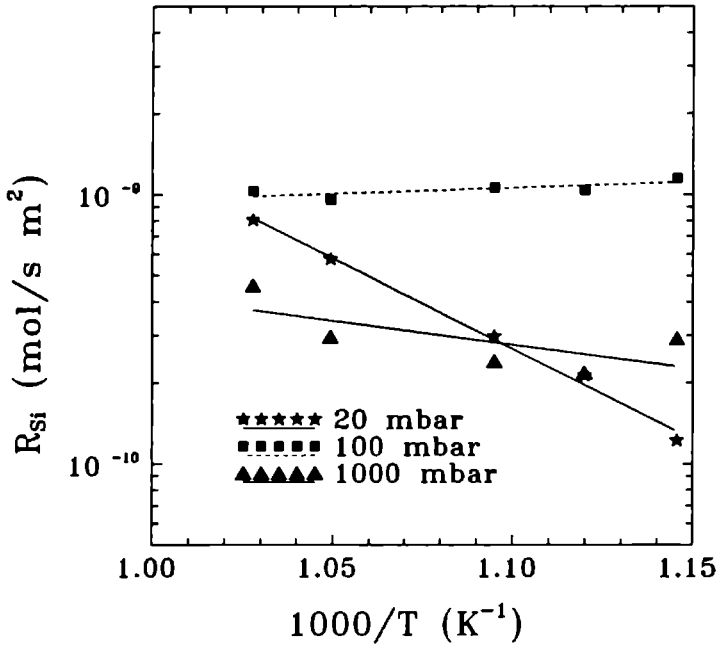


Figure 4.6 Deposition rate of silicon R_{Si} in mole/s m² as function of $1000/T$ (K⁻¹) for 3 different total pressures using $\Theta = 0.3$.

in which n is the free carrier concentration (Hall-Van der Pauw) and Θ is the compensation ratio. In our experiments Θ has nearly a constant value of 0.3. So eq. 4.1 becomes now:

$$R_{Si} = \frac{1.86 n \times M_{GaAs} \times R_{GaAs}}{N_{Av} \times \rho_{GaAs}} \text{ (mole/m}^2 \text{ s)}. \quad (4.3)$$

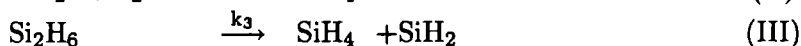
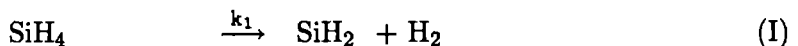
Using the silicon deposition rate R_{Si} (eq.4.3) in stead of the normally used quantity n (free carrier concentration) has the advantage of making the silicon incorporation process independent of the GaAs growth process. So, in this manner the determined activation energy (calculated from fig. 4.6) more likely is the activation energy of the doping process alone and is not masked by the combination of the doping process and the deposition of GaAs.

Figure 4.6 shows that at a total pressure in the reactor of 20 mbar the silicon doping process of GaAs using Si_2H_6 as a dopant source has an Arrhenius

type of behaviour with an apparent activation energy, E_{act} , of 32 kcal/mole. In contrast to this a nearly temperature independent behaviour is observed for a total pressure of 100 mbar ($E_{\text{act}} = -2$ kcal/mole). At a pressure of 1000 mbar however, the process again is temperature dependent with an E_{act} of 9.5 kcal/mole. Note however that the same value for the compensation ratio ($=0.3$) as for the situation at 20 mbar has been used for the calculation of the positions of the experimental points in this figure. Experimentally it appears that at these higher pressures the compensation ratio differs only slightly from the situation at 20 mbar. In the log-log plot of fig. 4.6 this variation is hardly noticable.

4.4 Discussion

For the doping of GaAs with Si_2H_6 as a dopant source, one has to consider the following chemical equations:



Beforehand one can state that the decomposition of SiH_4 (reaction I) and of Si_2H_6 (reaction III) are highly activated reactions with activation energies of about 50 kcal/mole [29,30]. Although both decomposition reactions have about the same activation energy, reaction III is much faster than reaction I because of a higher pre-exponential factor in the rate equation [29,30].

For the discussion of the experimental results we assume that the completely saturated molecules SiH_4 and Si_2H_6 have a sticking coefficient of about zero at the GaAs surface, as these molecules can only adsorb physically at the surface, whereas the radical SiH_2 has a sticking coefficient of about 1. Due to the strong Si-As and Si-Ga bonds desorption of SiH_2 from the growth surface is unlikely to happen in the temperature range of the experiments. This implies that silylene is the species that will be incorporated and not silane or disilane. The rate of reaction IV is negligible under almost every growth condition because of the very low concentration of the silicon containing species (e.g. SiH_2 and SiH_4) in the gas mixture. Although in this way the system has

been simplified, it is still very complicated to derive the exact rate equation for the incorporation of silicon in GaAs using Si_2H_6 as a precursor. But a qualitative description, which will satisfy for explaining the results of most growth experiments, will be given below.

Using the concept of the chemical boundary layer [18,19] we can calculate for reaction I,II and III the thicknesses of their respective chemical boundary layers δ_1, δ_2 and δ_3 , using the following equation [18,19,24]:

$$\delta \approx \frac{(1 + \beta) \left(\frac{T_S}{T_0} \right)^{1+\beta}}{\left(\frac{T_S}{T_0} \right)^{1+\beta} - 1} \frac{R_G T_S}{E_{\text{act},i}} \delta_T, \quad (4.4)$$

in which T_S is the susceptor temperature, T_0 is the temperature of the top of the reactor, β equals the temperature dependence of the thermal conductivity of the carrier gas (≈ 0.7), R_G is the gas constant, δ_T is the width of the temperature boundary layer which is in our case the height of the reactor (3 cm) and $E_{\text{act},i}$ (kcal/mole) is the activation energy of the particular reaction. This equation can be simplified to:

$$\delta \approx \frac{4}{E_{\text{act},i}} \delta_T \quad (\text{kcal/mole}). \quad (4.5)$$

The simplification (4.5) is only valid at a susceptor temperature of about 1000 K and a reasonably high E_{act} [18].

Due to the fact that the activation energy of reaction I and II are about equal it is obvious from equation (4.2) that $\delta_1 = \delta_3$ (about 2.5 mm). Reaction II has a very low activation energy of about 3.5 kcal/mole [29] which leads to such a great value of δ_2 that this safely can be set equal to the height of the reactor. The deposition rate of silicon (R_{Si}) consists of a kinetically determined (R_K) and a diffusionally (R_D) determined part. Depending on the conditions (e.g. pressure, temperature, type of carrier gas etc.) one of these fluxes will dominate. In an approximated form the deposition rate of silicon, in this example ex Si_2H_6 , can be expressed as:

$$\frac{1}{R_{\text{Si}}} = \frac{1}{R_D} + \frac{1}{R_K}. \quad (4.6)$$

Here R_D equals the completely diffusionally limited deposition rate of silicon through the bulk of the gas phase, $R_D = \frac{D}{h} C_0$, while R_K is the completely

kinetically controlled deposition rate in the boundary layer, $R_K = k\delta C_0$. In the expressions D stands for the binary diffusion constant, h for the height of the reactor, C_0 for the input concentration and δ for the thickness of the chemical boundary layer. This leads to the following expression for the silicon deposition rate:

$$R_{Si} = \frac{kC_0\delta D/h}{D/h + k\delta} \quad (4.7)$$

Here we have used already the concept of the chemical boundary layer, which implies that we have to divide the reactor into two parts, i.e. the chemical boundary layer itself and the bulk of the gas phase. A N_{CVD} number can be introduced for both the chemical boundary layer and the bulk gas phase². This dimensionless number is defined as the ratio between the chemical reaction flux and the diffusional flux, i.e. it determines the relative magnitude of both parallel fluxes mentioned in eq. 4.6.

Now we can calculate N_{CVD} for the case of doping with Si_2H_6 . From calculations of the diffusional flux of Si_2H_6 through the bulk gas phase ($\frac{D}{h}C_0$) coupled to the decomposition in the boundary layer ($kC_0\delta$) (at a temperature of about 1000 K and at a total pressure in the reactor of 100 mbar), using the known values of D_{300} and k_{1000} [29, 30], it follows that under these conditions the N_{CVD} number, $\frac{k_{1000}\delta}{D_{300}/h}$, is larger than 1. This points to the fact that the decomposition of disilane is fully controlled by diffusion from the bulk gas phase. Thus the doping process at 100 mbar total pressure will be completely limited by the diffusion of Si_2H_6 through the bulk of the gas phase. This favourably coincides with the results of the performed experiments and also with literature data [8,9,12-14].

When we calculate the N_{CVD} number for the chemical boundary layer for the decomposition of Si_2H_6 and the diffusion of Si_2H_6 through this layer, we arrive at a value in the order of 1. For this case $N_{CVD} = \frac{k_{1000}\delta C_0}{C_0 D_{1000}/\delta} = \frac{k_{1000}\delta^2}{D_{1000}}$. This implies that Si_2H_6 decomposition and diffusion in the boundary layer at this pressure are equally important, so that the decomposition takes place about everywhere in the boundary layer with the same reaction rate. This decomposition leads to the production of the radical species SiH_2 . It is possible to calculate the amount of SiH_2 produced in the boundary layer which will be able to reach the growing surface. Because of the fast reaction II the diffusion length of the SiH_2 species is given by [24] :

²Instead of this N_{CVD} number sometimes a Nusselt number has been used. This dimensionless number is defined as the ratio between the diffusional flux and the chemical reaction flux. A more correct name for this number is Damköhler II.

$$\sqrt{\frac{D_{\text{SiH}_2}}{k_2 P_{\text{H}_2}}}, \quad (4.8)$$

in which D_{SiH_2} is the binary diffusion constant of SiH_2 in H_2 and k_2 is the reaction constant of the reaction of SiH_2 with H_2 (reaction II), both at 1000K. For a total pressure of 100 mbar and a temperature of about 1000 K this length is calculated to be about 3 mm which is larger than the width of the boundary layer δ_3 meaning that most of the SiH_2 produced in this layer will actually reach the growing surface and will be incorporated.

At the relative low pressure of 20 mbar the diffusional fluxes will strongly increase compared to the situation at 100 mbar total pressure because of the inverse pressure dependence of the binary diffusion constants. At the same time, the decomposition rate constant will decrease because of its total pressure dependence [30]. The calculated N_{CVD} numbers in bulk and chemical boundary layer now appear to be both of order 1. So the production of SiH_2 species in this case will be determined both by diffusion and kinetics. This coincides with the results given in fig. 4.6 and also with literature data [14]. The value of the experimentally determined apparent activation energy of 32 kcal/mole can be compared to the theoretical one as obtained from equation 4.7 using $D = D_0 \left(\frac{T}{T_0}\right)^{1.7}$ and $k = AT^\beta \exp(-E_{\text{act}}/RT)$ with $E_{\text{act}} = 51$ kcal/mole [30]. This exercise yields a value of 38 kcal/mole which is equal to the measured value of 32 kcal/mole within the uncertainty limits of the experiments.

4.4.1 Disilane doping of GaAs at 1000 mbar

In this situation the total pressure is ten times as high as in the case of the situation of 100 mbar. This leads to smaller binary diffusion constants and higher decomposition rate constants [31] and thus to N_{CVD} numbers which are larger than one both in the bulk and in the chemical boundary layer. One may deduce from this that at the top of the chemical boundary layer all Si_2H_6 will be decomposed into SiH_4 and SiH_2 and that this reaction is completely bulk gas phase diffusion limited.

Due to the fact that the total pressure is a factor ten higher than the situation at 100 mbar, the concentration H_2 is also ten times larger. This has considerable influence on reaction II, i.e. it causes a large increase of the production of SiH_4 . A consequence is that the diffusion length of SiH_2 (equation 4.8) becomes smaller than the width of the chemical boundary layer

δ_3 . So inside this layer all SiH₂ will, in practice, have reacted to SiH₄, except for the fraction that is determined by the SiH₄ \rightleftharpoons SiH₂ + H₂ equilibrium. This fraction will be very low due to the high concentration of H₂.

Because of this equilibrium the silane concentration will remain almost constant in the boundary layer. So at 1000 mbar doping with Si₂H₆ effectively appears to be doping with SiH₄. Therefore an activation energy of about 40 - 50 kcal/mole is to be expected. In a reactor with fully developed flow and temperature profiles we indeed found an activation energy of 45 kcal/mole [9]. However, the results presented in this paper give an activation energy of only 9.5 kcal/mole. The large difference between these two values can be explained by taking into account the flow profiles at 1000 mbar in this reactor, which is built for low pressures. Calculations reveal that, at 1000 mbar, in this relatively high cell (3 cm) memory cells and spiral rolls are present due to the high Grasshoff (≈ 2100) and Raleigh numbers (≈ 3000) [32], whereas fully developed laminar flows are present at 100 and 20 mbar in the same reactor. As the theory of chemical boundary layer only works well in fully developed flow profiles, as was shown in an earlier paper [9], we can only rely on the experimental results obtained in this work at 20 and 100 mbar. For atmospheric pressure data we refer to the data obtained in our earlier work [9].

The combined result is that the kinetics of the doping process of Si₂H₆ strongly depends on the total pressure and that consequently the apparent activation energy changes according to the step that determines the silicon deposition rate.

4.5 Conclusions

The doping of GaAs using disilane as a doping source was studied at different temperatures and total pressures. The incorporation of silicon from Si₂H₆ in GaAs is almost linearly dependent on the input concentration of disilane in the range from 4×10^{15} up to 6.1×10^{18} cm⁻³. No extra compensation due to the amphoteric behaviour of silicon in GaAs is observed, even not in the samples with the highest silicon concentrations. By applying different total pressures we investigated the pressure dependence of the doping process. At 100 mbar no temperature effect is found. The doping process is completely bulk gas phase diffusion controlled with an activation energy of -2 kcal/mole. This is in contrast to the experiments at 20 and 1000 mbar where activation

energies of 32 kcal/mole and 45 kcal/mole are measured. At the lowest total pressure the decomposition of Si_2H_6 almost completely determines the silicon deposition process with a small contribution of bulk diffusion. At 1000 mbar the decomposition of SiH_4 instead of Si_2H_6 determines the silicon incorporation process.

So in conclusion Si_2H_6 is a good n-type dopant which can be used in a wide doping range, from 10^{15} till 10^{19} cm^{-3} , without exceptionally high compensation ratio's. To avoid differences in doping levels due to temperature gradients over the wafer one should grow at total pressures of about 100 mbar.

Acknowledgments

The authors are greatly indebted to S.M. Olsthoorn for performing and discussing the photoluminescence measurements and G. Bauhuis for performing the electrical characterization of the samples.

This work was financed by NOVEM, project No. 41.220-003.1.

References

- [1] R. Venkatasubramanian, K. Patel and S.K. Gandhi, *J. Crystal Growth* **94** (1989) 34.
- [2] J.S. Roberts, N.J. Mason and M. Robertson, *J. Crystal Growth* **68** (1984) 422.
- [3] R. Sankaran, *J. Crystal Growth* **50** (1980) 859.
- [4] J.-P. Hallais, *Acta Electronica* **21** (1978) 129.
- [5] S.J. Bass, *J. Crystal Growth* **47** (1979) 613.
- [6] A.M. Beers and J. Bloem, *Appl. Phys. Letters* **41** (1982) 153.
- [7] E. Veuhoff, T.F. Kuech and B.S. Meyerson, *J. Electrochem. Soc.* **132** (1985) 1958.
- [8] H.K. Moffat, T.F. Kuech, K.F. Jensen and P.-J. Wang, *J. Crystal Growth* **93** (1988) 594.

- [9] P.R. Hageman, X. Tang, M.H.J.M. de Croon and L.J. Giling, *J. Crystal Growth* **98** (1989) 249.
- [10] J.P. Duchemin, M. Bonnet, F. Koelsch and D. Huyghe, *J. Electrochem. Soc.* **126** (1979) 1134.
- [11] M. Druminski, H.-D. Wolf and K.-H. Zschauer, *J. Crystal Growth* **57** (1982) 318.
- [12] T.F. Kuech, E. Veuhoff and B.S. Meyerson, *J. Crystal Growth* **68** (1984) 48.
- [13] T.F. Kuech, B.S. Meyerson and E. Veuhoff, *Appl. Phys. Letters* **44** (1984) 986.
- [14] M. Shimazu, K. Kamon, K. Kimura, M. Mashita, M. Mihara and M. Ishii, *J. Crystal Growth* **83** (1987) 327.
- [15] H. Sakaguchi, R. Suzuki and T. Meguro, *J. Crystal Growth* **93** (1988) 602.
- [16] N. Furuhashi, K. Kakimoto, M. Yoshida and T. Kamejima, *J. Appl. Phys.* **64** (1988) 4692.
- [17] T.F. Kuech, M.A. Tischler, P. Potemski, F. Cardone and G. Scilla, *J. Crystal Growth* **98** (1989) 174.
- [18] M.H.J.M. de Croon and L.J. Giling, *J. Electrochem. Soc.* **137** (1990) 2867.
- [19] M.H.J.M. de Croon and L.J. Giling, *J. Electrochem. Soc.* **137** (1990) 3606.
- [20] D. Schmitz, G. Strauch, J. Knauf, H. Jürgensen and M. Heyen, *J. Crystal Growth* **93** (1988) 312.
- [21] W.G.J.H.M. van Sark, M.H.J.M. de Croon, G. Janssen and L.J. Giling, *Semicond. Sci. Technol.* **5** (1990) 36.
- [22] W.G.J.H.M. van Sark, M.H.J.M. de Croon, G. Janssen and L.J. Giling, *Semicond. Sci. Technol.* **5** (1990) 291.
- [23] D.H. Reep and S.K. Gandhi, *J. Electrochem. Soc.* **130** (1983) 675.

- [24] M.H.J.M. de Croon and L.J. Giling, *Prog. Crystal Growth and Charact.* **19** (1989) 125.
- [25] M. Tirtowidjo and R. Pollard, *J. Crystal Growth* **98** (1989) 420.
- [26] T. Lideikis and G. Treideris, *J. Crystal Growth* **96** (1989) 790.
- [27] X. Tang, H.G.M. Lochs, P.R. Hageman, M.H.J.M. de Croon, L.J. Giling and A.J. Bons, *J. Crystal Growth* **98** (1989) 827.
- [28] W. Walukiewicz, L. Lagowski, L. Jastrebski, M. Lichtensteiger and H.C. Gatos, *J. Appl. Phys.* **50** (1979) 899.
- [29] H.K. Moffat and K.F. Jensen, *J. Electrochem. Soc.* **135** (1988) 459.
- [30] K.F. Roenigk, K.F. Jensen and R.W. Carr, *J. Phys. Chem.* **91** (1987) 5732.
- [31] K.F. Roenigk, PhD Thesis, University of Minnesota (1987).
- [32] E.P. Visser, C.R. Kleijn, C.A.M. Govers, C.J. Hoogendoorn and L.J. Giling, *J. Crystal Growth* **94** (1989) 929.

Pressure and temperature dependence of Zn incorporation in MOCVD grown GaAs and AlGaAs using diethylzinc as precursor

P.R. Hageman, M.H.J.M. de Croon¹, X. Tang ² and L.J. Giling

in press: Journal of Crystal Growth

Abstract

Zinc doping of MOCVD grown GaAs and AlGaAs using diethylzinc (DEZn) as precursor has been studied as a function of the zinc input mole fraction, growth temperature, aluminium fraction of the AlGaAs alloy and total reactor pressure. The experiments have been performed in two different reactors which differ in pressure and temperature distributions. We have found that the zinc incorporation follows a linear behaviour in a log-log plot of hole concentration versus zinc input mole fraction with a slope of 1 and that

¹Laboratorium voor Chemische Technologie, Eindhoven University of Technology, P.O. box 513, 5600 MB Eindhoven, The Netherlands

²AMTC-Advanced Semiconductor Materials International, Rembrandtlaan 2A, 3723 BJ Bilthoven, The Netherlands.

the incorporation of zinc is independent of the fraction Al in $\text{Al}_x\text{Ga}_{1-x}\text{As}$ up to $x=0.45$. The zinc incorporation decreased with increasing growth temperature following an Arrhenius type of behaviour for both GaAs and AlGaAs. This temperature behaviour did not change when the reactor pressure was lowered. All experimental results can be explained satisfactorily by a model which takes into account that the incorporation of zinc is precluded by an adsorption-desorption equilibrium of zinc at the step of the growing crystal.

5.1 Introduction

Metalorganic chemical vapour deposition (MOCVD) nowadays is an important technique for growing III/V semiconductor materials. Making devices requires multi-layer structures which consist of doped and undoped layers. As a p-type dopant the elements Zn [1-4], Mg [5-7], Be [8,9], Cd [10] and C [11-13] have been employed in MOCVD. Among these elements zinc is the one most widely used in MOCVD for GaAs and AlGaAs.

Although the diffusion coefficient of zinc in these III/V semiconductors is rather high [14-16] -sometimes causing problems in obtaining sharp doping profiles- zinc is preferred by most users because the zinc precursors can be handled very easily, its doping range is wide ($10^{16} - 10^{20} \text{ cm}^{-3}$) and high doping levels can be easily obtained. This last point is especially important for opto-electronic devices where heavily doped layers are necessary for making low resistance ohmic contacts to the devices. The problems connected with the adsorption of the zinc precursors on the tubing of the reactor (memory effect) can easily be avoided nowadays by using low pressure pipe-lines up to the zinc source [17].

Two precursors are frequently used in MOCVD for zinc doping, i.e. diethylzinc (DEZn) and dimethylzinc (DMZn). The latter has a vapour pressure higher than that of trimethylgallium (TMG) and therefore the doping process is difficult to control with DMZn. DEZn has a vapour pressure much lower than that of TMG and is therefore preferred in the MOCVD process.

In literature, a considerable number of studies on zinc doping of GaAs have been published [1-4,12,17-24], in contrast to the relatively small amount of work on the p-type doping of AlGaAs with zinc [25]. When the hole concentration is plotted versus the input mole fraction DEZn on a log-log plot, in most cases a linear relation has been reported [1,2,19-21] although non-linear relations have been obtained also [2,21,22]. However, the slope of the linear relations in the log-log plot is not constant, but varies between 0.4 and 1.4.

In contrast with the previous point, there is much more agreement regarding the temperature dependence of the zinc doping using DEZn. In general it is found that the hole concentration decreases with increasing growth temperatures [1,3,21,26]. However, the "apparent activation energy" varies between -48 kcal/mole (-2.1 eV) and -76 kcal/mole (-3.3 eV) where the minus sign indicates that no activation energy is involved, but that the reaction is exothermic. This temperature behaviour is explained in the literature by taking into account the temperature dependence of the zinc evaporation from the crystal

surface [2-4] or by considering the concentration of gallium vacancies as a function of temperature [27].

In this paper we present experimental results on the zinc doping of GaAs and $\text{Al}_x\text{Ga}_{1-x}\text{As}$ (up to $x = 0.45$) as a function of growth temperature, input mole fraction precursor and total reactor pressure using DEZn. Also data on the depletion effects of the zinc incorporation will be given and discussed. These results are obtained in two different reactors which differ mainly in their temperature distribution and total pressure. Since the results are identical to each other, it implies that they are reactor independent in contrast to the large spread in results published in literature. The discussion of the results will lead to a model which describes the doping of GaAs as a function of temperature, total reactor pressure and position on the susceptor.

5.2 Experimental procedure

The experiments were carried out in two different reactors. The first MOCVD reactor (hereafter referred to as reactor I) was operated at atmospheric pressure [28] and was equipped with a horizontal reactor cell with a rectangular cross section. The cell is resistance heated at the bottom and water cooled at the top. This reactor allows flow profiles and temperature gradients to become fully developed. So in principle it is possible to calculate the temperature gradient and mass fluxes in this reactor.

The second reactor (hereafter referred to as reactor II) is a commercially available computer controlled MOCVD reactor [29]. The reactor can be operated at low pressures, is infra-red heated and the horizontal reactor cell, which actually is a liner in a cylindrical cell, has a rectangular cross section. The top of the cell is not cooled controllably, which implies that only the bottom temperature of the cell is known and that the temperature of the top of the cell is floating. In addition the cell is too short to allow for fully developed flow and temperature profiles at higher pressures.

The experiments in reactor I were performed with a V/III ratio (ratio between the amounts of arsine and the group III components) of 20 and constant P_{TMG} and P_{AsH_3} at growth temperatures ranging from 680 °C to 750 °C. The mean gas flow rate in the reactor was about 7 cm/s. The growth rate varied between 0.08 and 0.3 $\mu\text{m}/\text{min}$ depending on the position in the reactor and on the growth temperature.

In reactor II the V/III ratio was kept constant at 125 with constant P_{TMG}

and P_{AsH_3} . The growth temperature was varied between 600 °C and 700 °C. The experiments were all carried out at a total reactor pressure of 20 mbar (i.e. a mean gas velocity of 228 cm/s) except when a specific reactor pressure is mentioned. The growth rate varied depending on the position in the reactor and the growth temperature between 0.025 and 0.035 $\mu\text{m}/\text{min}$.

In both reactors the growth was performed using arsine (AsH_3), trimethyl gallium (TMG) and trimethyl aluminium (TMA). Hydrogen, purified by a Pd-diffusion cell, was used as a carrier gas. The precursor for the zinc doping was in both cases diethylzinc (DEZn). The GaAs substrates were all $(100) \xrightarrow{2^\circ} (110)$ oriented, semi-insulating and chemo-mechanically polished on one side. The thicknesses of the grown layers were measured by cleaving and staining, using an interference-contrast microscope or, if necessary, a scanning electron microscope (SEM). The samples were electrically characterized by Hall-Van der Pauw measurements performed at room temperature using a clover leaf configuration or with C-V measurements using a conventional C-V profiler.

5.3 Results and discussion

At all growth conditions and in both reactors all the grown epilayers possessed mirror-like surfaces. This specular morphology was independent of the input mole fraction of DEZn, the growth temperature and the aluminium fraction of the AlGaAs epilayers. In the following sections the influence of these parameters on the incorporation of zinc will be discussed, while the electrical quality of the grown epilayers will be compared with theoretical values. Finally a special experiment has been performed to examine and explain the depletion effect of the zinc incorporation in reactor I.

5.3.1 The effect of the input mole fraction DEZn on the hole concentration

GaAs

The hole concentration as a function of the input mole fraction DEZn in GaAs is plotted in fig. 5.1 for both reactors. No saturation effect is observed in this figure, which is in agreement with literature [3].

For reactor I two series of experiments were performed at the same growth conditions ($V/\text{III} = 20$ and $P_{\text{reactor}} = 1\text{atm.}$, same P_{TMG}) except for the

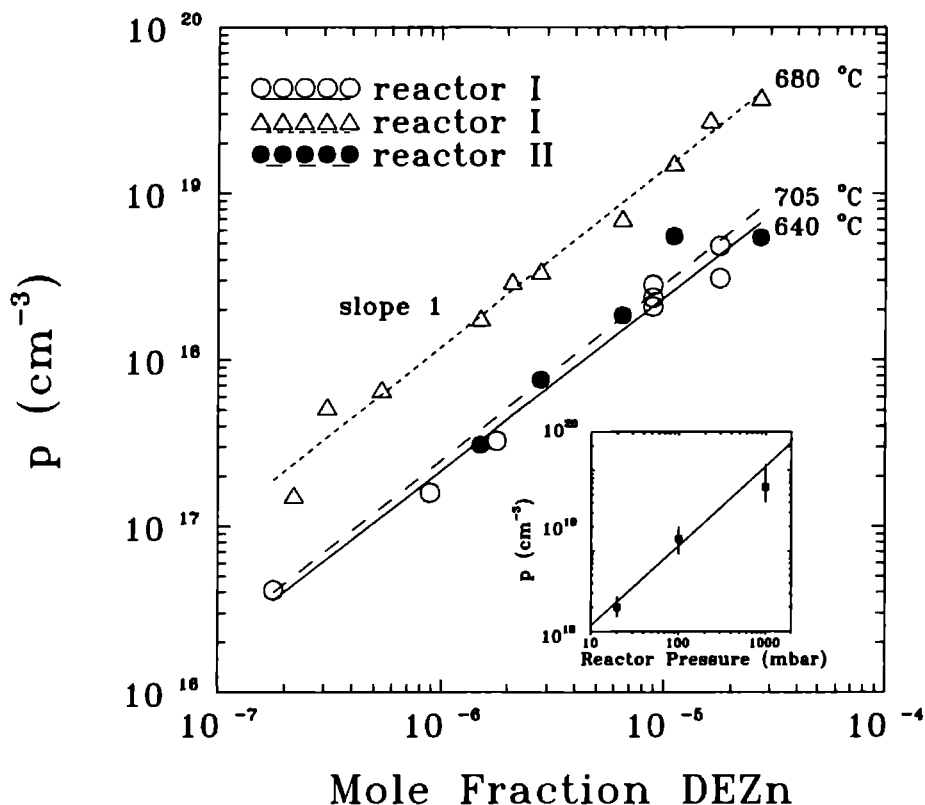


Figure 5.1 Log-log plot of the hole concentration (cm^{-3}) versus the input mole fraction DEZn for GaAs:

(○): reactor I, $T=705\text{ }^{\circ}\text{C}$, $P_{\text{tot}}=1\text{ bar}$, $V/\text{III}=20$;

(△): reactor I, $T=680\text{ }^{\circ}\text{C}$, $P_{\text{tot}}=1\text{ bar}$, $V/\text{III}=20$;

(●): reactor II, $T=640\text{ }^{\circ}\text{C}$, $P_{\text{tot}}=20\text{ mbar}$, $V/\text{III}=125$.

The inset is a log-log plot of the hole concentration (cm^{-3}) versus the reactor pressure (mbar) as obtained in reactor II at $640\text{ }^{\circ}\text{C}$ and 10^{-5} DEZn.

growth temperatures which were 680 and 705 °C respectively. In fig. 5.1 these data points are shown in a log-log plot. In this plot the hole concentration is linearly dependent on the input mole fraction DEZn with a slope of 1. The difference in concentration between these two sets of experiments is solely caused by the difference in growth temperature as will be discussed further on in this paper.

In fig. 5.1 data points are also given from experiments performed in reactor II at 640 °C, with a V/III ratio of 125 at 20 mbar total reactor pressure. These data points also give a straight line with a slope of 1. The lower hole concentrations in this case are due to the trivial effect that at lower total pressures also all partial pressures are reduced. This effect was checked in reactor II for three pressures, viz. total pressures of 20, 100 and 1000 mbar keeping all other growth conditions the same. The results are plotted in the inset in fig. 5.1. From this log-log plot it follows that the hole concentration indeed increases linearly at higher total pressures with a slope quite close to 1, demonstrating that the effect indeed is due to the increase of the partial pressure of DEZn at increasing total reactor pressure.

From these experiments it follows that both at atmospheric and at low pressure the hole concentration increases linearly with increasing input mole fraction DEZn with slope 1.

AlGaAs

Similar growth and doping experiments were performed with $\text{Al}_x\text{Ga}_{1-x}\text{As}$ with x varying between 0 and 0.45. In reactor I (atmospheric pressure) $\text{Al}_{0.10}\text{Ga}_{0.90}\text{As}$ was grown at a temperature of 720 °C as a function of the input mole fraction DEZn. The electrical data were obtained with Hall-Van der Pauw measurements. The results are plotted in fig. 5.2. Again a linear relationship between the input mole fraction DEZn and the hole concentration is observed. The small deviation from the value 1 in the slopes of the lines in figs. 5.1 and 5.2 is entirely due to the uncertainties in layer thicknesses and hole concentrations.

At low pressure two sets of experiments were performed in reactor II. The first set was performed at 720 °C for $x_{\text{Al}} = 0.25$, while the second set was carried out at 710 °C for $x_{\text{Al}} = 0.45$. The electrical data were obtained with Hall-Van der Pauw and C-V measurements. These points give a straight line with a slope of 1 (fig. 5.2) for both Al fractions. The difference in hole concentration between the two sets of experiments of reactor II is completely

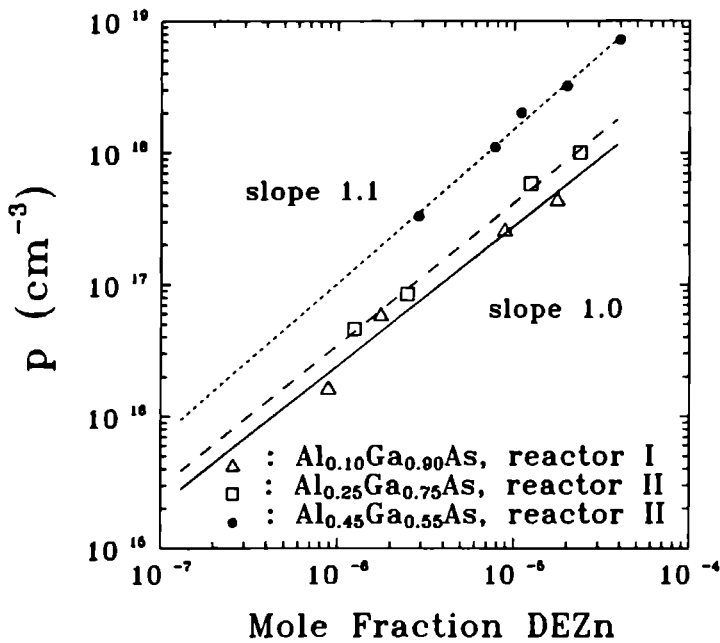


Figure 5.2 Log-log plot of the hole concentration (cm^{-3}) versus the input mole fraction DEZn for $\text{Al}_x\text{Ga}_{1-x}\text{As}$:

- (Δ): reactor I, $x=0.1$, $T=720^\circ\text{C}$, Hall data;
- (\square): reactor II, $x=0.25$, $T=720^\circ\text{C}$, Hall data;
- (\bullet): reactor II, $x=0.45$, $T=710^\circ\text{C}$, C-V data.

due to the 10°C difference in growth temperature. So it appears that the amount of aluminium has no direct influence on the zinc incorporation.

5.3.2 Hall mobilities

For all zinc doped samples the hole mobilities were measured at room temperature using the Hall-Van der Pauw technique. The values, as measured for GaAs and AlGaAs, are given in fig. 5.3 together with the theoretical values for uncompensated material. The mobility values are in reasonable agreement with the theoretical values [30], indicating that the quality of the grown

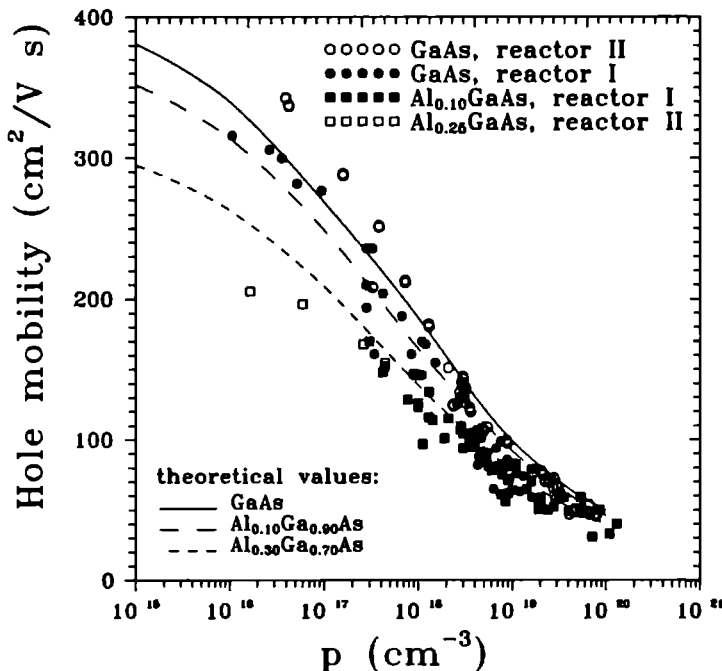


Figure 5.3 Semi-log plot of the hole mobility (cm²/ V s) versus the hole concentration (cm⁻³) for the different materials (GaAs, Al_{0.10}Ga_{0.90}As and Al_{0.25}Ga_{0.75}As) grown in the two different reactors. The lines (solid and dashed) in the figure represent the theoretical values for the different materials [30].

material is acceptable to good.

The samples of reactor II in general show somewhat higher mobilities as compared to the samples of reactor I. This is probably due to the low pressure system of reactor II (up to the metalorganic sources) what reduces contamination.

5.3.3 The effect of growth temperature on the hole concentration

In both reactors experiments were performed to investigate the influence of

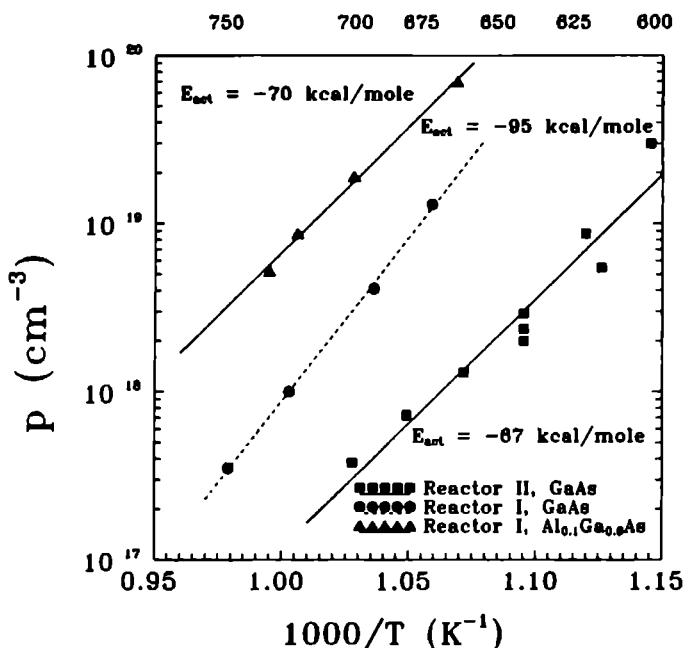


Figure 5.4 Semi-log plot of the hole concentration (cm^{-3}) versus the reciprocal temperature (K^{-1}) for GaAs and $\text{Al}_{0.10}\text{Ga}_{0.90}\text{As}$ grown in the two different reactors.

the growth temperature on the zinc incorporation. In these experiments the input mole fraction of DEZn and other growth parameters were kept constant, whereas the growth temperature was varied. The results are shown in fig. 5.4, in which the hole concentration is plotted as a function of reciprocal temperature (range measured 600 - 750 °C). For both reactors the zinc incorporation in GaAs and AlGaAs decreased for increasing temperature, as was already observed in figs. 5.1 and 5.3. The hole concentration shows an Arrhenius type of behaviour with a negative apparent activation energy (E_{act}) of -67 kcal/mole for GaAs grown in reactor II, an activation energy of -90 kcal/mole for GaAs grown in reactor I and of -70 kcal/mole for $\text{Al}_{0.10}\text{Ga}_{0.90}\text{As}$ grown in reactor I. From these negative values of the apparent activation energies of the doping with DEZn one can conclude that this E_{act} is not an activation energy only but incorporates also a ΔH from an adsorption equilibrium.

This temperature behaviour can not be attributed solely to the evaporation

zinc, as described in ref. [3,4], because the obtained values for the apparent activation energy of the zinc incorporation process are significantly higher than the value given for ΔH of the evaporation of zinc (≈ 48 kcal/mole) from the surface [2-4].

3.4 Model

In the discussion of the zinc incorporation mechanism we have to explain the experimental results as described earlier in this paper, i.e. the linear behaviour of the zinc incorporation as a function of the input mole fraction DEZn (fig. 5.1 and fig. 5.2), the dependence on the total reactor pressure (inset fig. 5.1) and a typical temperature dependence (fig. 5.4).

From equilibrium calculations [31] it is known that at the temperatures used in these experiments (600 - 700 °C) the most abundant zinc species is monoatomic zinc (Zn). As the partial pressure of Zn will be proportional to the input mole fraction of DEZn, we have:

$$P_{Zn} \propto P_{DEZn}. \quad (5.1)$$

In this section we will use the concentration ($[Zn] = \frac{P_{Zn}}{RT}$) instead of partial pressure. We will assume that there is a steady-state situation at the surface. Another assumption is that in a first approximation at the growth conditions used the (001) surface is almost free of adsorbed species [32].

At these conditions the zinc incorporation can be described by the rate of sorption, desorption and incorporation of the Zn species at the surface:

$$\underbrace{k_a C|_{y=0}}_{\text{adsorption}} - \underbrace{k_d \Theta_{Zn}}_{\text{desorption}} - \underbrace{\frac{N_s}{N_{Av}} \frac{\Theta_{Zn}}{\tau}}_{\text{incorporation}} = 0, \quad (5.2)$$

which:

- k_a = rate constant for adsorption of monoatomic zinc on GaAs or AlGaAs (cm s^{-1}),
- k_d = rate constant for desorption of monoatomic zinc from GaAs or AlGaAs ($\text{mole cm}^{-2} \text{ s}^{-1}$),
- $C|_{y=0}$ = concentration of monoatomic zinc in the gas phase at the height of the surface (mole cm^{-3}),
 $C|_{y=0} = (P_{DEZn}|_{y=0})/(RT_{y=0})$,
- Θ_{Zn} = Zn coverage of the surface (dimensionless),

- N_S = number of adsorption sites (cm^{-2}),
 N_{Av} = Avogadro's number (mole^{-1}),
 τ = time needed for the growth of 1 monolayer
 of III/V semiconductor (s).

Equation 5.2 is very general, i.e. it can also be used for the adsorption, desorption and incorporation taking place at a step instead of a process taking place at the surface. In this last case only the number of adsorption sites, N_S , and the time needed to incorporate the adsorbed species, τ , have to be redefined. It appears, however, that these two numbers fortunately decrease proportionally to each other. So the same expression will hold when the process takes place entirely at the step.

The time needed for the growth of 1 monolayer III/V semiconductor (τ), is given by:

$$\tau = \frac{d \rho_{\text{(III/V)}}}{M_{\text{(III/V)}} r_{\text{(III/V)}}}, \quad (5.3)$$

in which:

- d = thickness of 1 monolayer GaAs or AlGaAs (cm),
 $\rho_{\text{(III/V)}}$ = density of GaAs or AlGaAs (g cm^{-3}),
 $M_{\text{(III/V)}}$ = molecular weight of GaAs or AlGaAs (g mole^{-1}),
 $r_{\text{(III/V)}}$ = growth rate of GaAs or AlGaAs ($\text{mole cm}^{-2} \text{ s}^{-1}$).

From eq. 5.2 one can derive the zinc coverage of the surface:

$$\Theta_{\text{Zn}} = \frac{k_a C|_{y=0}}{k_d + \frac{N_S}{N_{Av}} \tau} = \frac{\frac{k_a}{k_d} C|_{y=0}}{1 + \frac{N_S}{N_{Av}} \frac{\tau}{k_d}}. \quad (5.4)$$

The deposition rate of zinc can be expressed as:

$$r_{\text{dep,Zn}} = \frac{N_S}{N_{Av}} \frac{\Theta_{\text{Zn}}}{\tau} \quad (\text{mole cm}^{-2} \text{ s}^{-1}). \quad (5.5)$$

With eq. 5.4 this results in:

$$r_{\text{dep,Zn}} = \frac{\frac{N_S}{N_{Av}} \frac{k_a}{k_d} \tau C|_{y=0}}{1 + \frac{N_S}{N_{Av}} \frac{\tau}{k_d}}. \quad (5.6)$$

For eq. 5.6 two extremes can be distinguished.

The first situation, case A, is valid when :

$$\frac{N_S}{N_{Av} \tau k_d} \ll 1, \text{ so } r_{\text{dep,Zn}} = \frac{N_S}{N_{Av}} \frac{k_a}{k_d \tau} C|_{y=0}. \quad (5.7)$$

Equation 5.7 can be written as follows:

$$\frac{N_S \Theta_{Zn}}{N_{Av} \tau} \ll k_d \Theta_{Zn},$$

so that it becomes clear that in case A the incorporation of zinc is much slower than the desorption of zinc from the step or from the GaAs surface. This implies that the Zn coverage, Θ_{Zn} , is determined by the adsorption-desorption equilibrium.

The second situation, case B, is valid when :

$$\frac{N_S}{N_{Av} \tau k_d} \gg 1, \text{ so } r_{\text{dep,Zn}} = k_a C|_{y=0}. \quad (5.8)$$

Case B (eq. 5.8) represents the situation at which every zinc species that arrives at the III/V surface will stick to the step and will be incorporated. However, this situation describes a pure kinetic adsorption reaction for which the activation energy of k_a will always exhibit a zero or a positive activation energy, i.e. the hole concentration will increase when the growth temperature is increased. This is in complete disagreement with the experimental results and with the literature data [1,3,21,26]. Therefore only case A will be worked out in more detail.

From a combination of eq. 5.3 and eq. 5.7 it follows that the expression for the deposition rate of zinc can be formulated as:

$$r_{\text{dep,Zn}} = \frac{N_S}{N_{Av}} \frac{k_a}{k_d} \frac{M_{(III/V)} r_{(III/V)}}{d \rho_{(III/V)}} C|_{y=0} \quad (\text{mole cm}^{-2} \text{ s}^{-1}). \quad (5.9)$$

The hole concentration (N_{Zn}), as measured with the Hall-Van der Pauw method, is defined as:

$$N_{Zn} = N_{Av} \frac{r_{\text{dep,Zn}}}{r_{(III/V)}} \frac{\rho_{(III/V)}}{M_{(III/V)}} \quad (\text{cm}^{-3}). \quad (5.10)$$

Here we have assumed that all the incorporated zinc has been built in on a substitutional site and is electrically active. This would not be true if the experiments were performed in the saturation range [3]. This is not the case in our experiments, see figs. 5.1 and 5.3.

Rewriting eq. 5.10 in combination with eq. 5.9 gives the simple general description for the hole concentration in GaAs and AlGaAs for the situation (case A) that the adsorption-desorption equilibrium of the zinc species on the GaAs (or AlGaAs) surface or step determines the zinc incorporation rate:

$$N_{\text{Zn}} = \frac{N_{\text{S}}}{d} \frac{k_{\text{a}}}{k_{\text{d}}} C|_{y=0}. \quad (5.11)$$

The following conclusions can be drawn from this equation. The first point to be mentioned is that the resulting hole concentration will depend linearly on the concentration of zinc species in the gas phase at the height of the surface ($C|_{y=0}$), i.e. it will also depend linearly on the concentration of zinc species in the bulk gas phase, and so is linearly dependent on the input mole fraction DEZn. This is consistent with the experimental results as presented in figs. 5.1 and 5.2. The second point is connected with the adsorption equilibrium constant $k_{\text{a}}/k_{\text{d}}$. In principle, this constant will be a function of the aluminium fraction in the $\text{Al}_{1-x}\text{Ga}_x\text{As}$ alloy because of its dependency on the heat of adsorption of Zn species. However, experimentally no dependence of this constant is observed with regard to the aluminium fraction.

The pressure dependence of the zinc incorporation (see inset of fig. 5.1) can now be explained also. In lowering the total reactor pressure, the partial pressure of DEZn is also lowered and with it the concentration of the zinc species at the surface ($C|_{y=0}$). This explains the lower zinc incorporation at the lower pressures as compared to that of the experiments performed at 1 atmosphere.

The temperature behaviour of zinc doping with DEZn is now easy to explain. It is entirely determined by the temperature behaviour of the ratio $\frac{k_{\text{a}}}{k_{\text{d}}}$, what is equal to the equilibrium constant K for the adsorption/desorption of Zn. This constant K can be expressed as $K = e^{\Delta S^0/R} e^{-\Delta H^0/RT}$ where ΔH^0 is determined by the heat of adsorption. The observed mean apparent activation energy (E_{act}) of the zinc incorporation, both for GaAs and AlGaAs, is -75 kcal/mole. According to the model this negative value for the activation energy corresponds entirely to the adsorption enthalpy for the process of adsorbing Zn-atoms on the surface or step of GaAs or AlGaAs.

The question remains whether this adsorption enthalpy is due to the adsorption on the surface or to the step. The observed value for the adsorption enthalpy of Zn on an As-stabilized GaAs surface seems to be quite high for a normal adsorption process where one bond is formed. The highest values found in the literature are -65.2 kcal/mole for an As-H bond and -56.5 kcal/mole for an As-C bond [32]. No specific values for the As-Zn bond could be found but

the As-Zn bond strength certainly is not that strong. However, when it is assumed that the adsorption of Zn takes place at a step, a double bond will be formed. For the desorption of Zn now two bonds have to be broken, which requires twice as much energy. This means that the value for a single Zn-As bond strength will be 37.5 kcal/mole what seems to be a quite acceptable value. Therefore to our opinion the observed temperature behaviour of the zinc incorporation is explained by the adsorption-desorption behaviour of zinc at the step of the growing crystals.

5.3.5 Depletion effects

Although in the literature no depletion effects have been reported for the incorporation of zinc, we did observe in the top-cooled atmospheric pressure reactor a significant depletion effect. In order to study this process in more detail, we performed some specific depletion experiments in reactor I. Due to the special design of this reactor [28] (long susceptor, top-cooled reactor cell, fully developed temperature and flow profiles), the growth of GaAs and AlGaAs in this reactor can be modelled rather easily and with reasonable precision [33-35]. It must be mentioned that when undoped (or silicon doped) GaAs or AlGaAs is grown in this reactor (I), only an arsenic deposit is found at the top of the reactor due to its relatively low temperature (300 K). But when the doping experiments with DEZn are performed, a deposit is found at the top of the reactor which is also due to the deposition of zinc. This deposition is responsible for the depletion of zinc. This effect is not observed in reactor II because, in this reactor, the top of the cell is not cooled and therefore the top of the reactor cell is much higher in temperature.

The samples for the investigation of the depletion effect of the zinc incorporation were grown under standard conditions. Experiments were performed for $\text{Al}_{0.10}\text{Ga}_{0.90}\text{As}$ and GaAs. The substrates were placed on the susceptor at positions from 2 to 18 cm away from the beginning of the susceptor (x-coordinate). The heating starts at the beginning of the susceptor at $x=0$.

In fig. 5.5 the hole concentration in a semi log plot is given versus the position on the susceptor for the two materials. It is evident from this figure that, in this top-cooled reactor, the zinc incorporation exhibits a depletion effect for both GaAs and $\text{Al}_{0.10}\text{Ga}_{0.90}\text{As}$. The depletion effect is, in both cases, about equally strong. In this figure theoretical fits are also shown, which will be discussed below.

The depletion will be modelled as follows. Because of the zinc deposition on

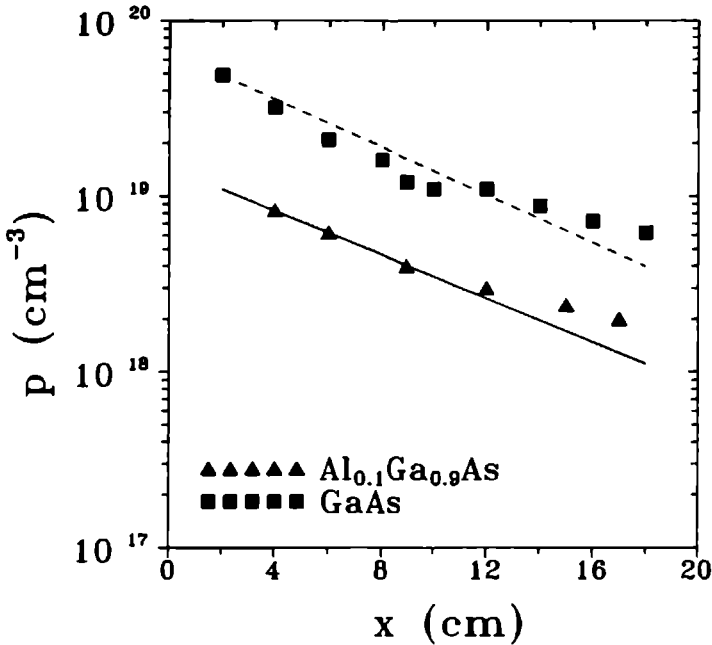


Figure 5.5 Semi-log plot of the hole concentration (cm^{-3}) versus the horizontal position (x-coordinate) on the susceptor of reactor I for GaAs and $\text{Al}_{0.1}\text{Ga}_{0.9}\text{As}$. The growth was performed at atmospheric pressure. The results are corrected for the temperature gradient present in this reactor. In the figure also the theoretical fits for N_{Zn} as obtained from eq.5.13 for GaAs (dashed line) and for $\text{Al}_{0.1}\text{Ga}_{0.9}\text{As}$ (solid line) are given.

the top of the cell at $y=h$ we take as a boundary condition for the calculation that the concentration of Zn in the reactor at the top of the cell is zero, so $C|_{y=h} = 0$ (h is the height of the reactor). This implies that all the Zn-species that arrive will completely stick at the cold part of the reactor (top). As without top cooling no zinc depletion is observed, we can conclude that only a very small amount of the input mole fraction DEZn is incorporated in the lattice. So the following boundary condition for the zinc concentration at the growing surface $\frac{dC}{dy}|_{y=0} = 0$ is used. Working along the lines described in ref. [28] one obtains for the concentration of zinc species at the surface:

$$C|_{y=0} = \frac{4 C_{Zn}}{\pi} \sum_{n=1}^{\infty} \frac{(-1)^{n-1}}{2n-1} \exp \left(-\frac{(2n-1)^2 \pi^2}{4} \frac{D_{Zn} x}{v h^2} \right), \quad (5.12)$$

in which:

- C_{Zn} = input concentration DEZn,
- D_{Zn} = binary diffusion coefficient of zinc species in H_2 ,
- x = horizontal coordinate in the reactor,
- v = mean gas velocity in the direction of the flow.

When this solution for $C|_{y=0}$ is substituted in eq. 5.11 one arrives at the following equation for the hole concentration:

$$N_{Zn} = \frac{k_a}{k_d} \frac{N_S}{d} \frac{4 C_{Zn}}{\pi} \sum_{n=1}^{\infty} \frac{(-1)^{n-1}}{2n-1} \exp \left(-\frac{(2n-1)^2 \pi^2}{4} \frac{D_{Zn} x}{v h^2} \right). \quad (5.13)$$

Based on eq. 5.13 two calculations have been performed for the zinc incorporation, where the diffusion constant of monoatomic zinc has been calculated according to ref. [36]. These calculations are presented in fig. 5.5. As one can see, the theoretical lines are in good agreement with the experimental results demonstrating that the observed depletion of Zn during the growth of GaAs is indeed caused by the deposition of zinc at the cooled top of the reactor. From the parameter fit, we obtained a value for $K = \frac{k_a}{k_d}$ of $\approx 3.2 \times 10^7$ mole cm^{-3} . This is a realistic value for K . We can check that by calculating the zinc coverage of the surface (Θ_{Zn}) at the used growth conditions with the aid of this K value. This results in a zinc coverage of about 2.3×10^{-3} under these experimental conditions, which corresponds well with the obtained hole concentrations.

5.4 Conclusions

Zinc doping experiments have been performed in two different reactors, one operating at atmospheric pressure and the other at low pressure. In contrast to the previous published results on the zinc incorporation rate, we have found that the results were reactor independent. From analysis of the results follows that the incorporation of zinc can be explained by an adsorption/desorption equilibrium at the step followed by incorporation in the the growing crystal. In

addition depletion experiments were performed which showed that a depletion of zinc can be induced when the top of the reactor is water-cooled.

Acknowledgments

The authors would like to thank S.W. Kortboyer and W.P.J.H. Jacobs for their assistance in growing some of the samples.

The authors are greatly indebted to G.J. Bauhuis for performing the electrical characterization of the samples.

This work was financed by NOVEM, project No. 41.220-003.1, and the "Stichting voor de Technische Wetenschappen" (STW) with financial support from the "Nederlandse Organisatie voor Wetenschappelijk Onderzoek" (NWO).

References

- [1] R.W. Glew, J. Crystal Growth **68** (1984) 44.
- [2] Y.K. Su, C.Y. Chang, T.S. Wu, Y.C. Chou and C.Y. Nee, J. Crystal Growth **67** (1984) 472.
- [3] K. Okamoto, H. Mawatari, K. Yamaguchi and A. Noguchi, J. Crystal Growth **98** (1989) 630.
- [4] S.Z. Sun, E.A. Armour, K. Zheng and C.F. Schaus, J. Crystal Growth **113** (1991) 103.
- [5] A.W. Nelson and L.D. Westbrook, J. Appl. Phys. **55** (1984) 3103.
- [6] A. Kozen, S. Nojima, J. Tenmyo and H. Asahi, J. Appl. Phys. **59** (1986) 1156.
- [7] C.R. Lewis, Electron. Lett. **18** (1982) 570.
- [8] N. Bottka, R.S. Stillman and W.F. Tseng, J. Crystal Growth **68** (1984) 54.
- [9] E. Kuphal, J. Appl. Phys. **50** (1979) 4146.
- [10] E.E. Wagner, D.E. Mars, G. Hom and G.B. Stringfellow, J. Appl. Phys. **51** (1980) 5434.

- [11] N.I. Buchan, T.F. Kuech, G. Scilla and F. Cardone, *J. Crystal Growth* **110** (1991) 405.
- [12] M.A. Tischler, R.M. Potemski, T.T. Kuech, F. Cardone, M.S. Goorsky and G. Scilla, *J. Crystal Growth* **107** (1991) 268.
- [13] M.C. Hanna, Z.H. Lu, E.W. Mao, T. McCormick, E.G. Oh, A. Majorfeld and D.M. Szmyd, *J. Crystal Growth* **107** (1991) 279.
- [14] A. Flat, A.G. Milnes and D.L. Feucht, *Solid State Electronics* **20** (1977) 1024.
- [15] B.I. Boltaks, T.D. Dzhaferov, Yu.P. Demakov and I.E. Maronchuk, *Soviet Phys.-Semicond.* **9** (1975) 545.
- [16] S. Reynolds, D.W. Vook and J.F. Gibbons, *J. Appl. Phys.* **63** (1988) 1052.
- [17] T.F. Kuech, P.-J. Wang, M.A. Tischler, R. Potemski, G.J. Scilla and F. Cardone, *J. Crystal Growth* **93** (1988) 624.
- [18] P. Enquist, J.A. Hutchby and T.J. de Lyon, *J. Appl. Phys.* **63** (1988) 4485.
- [19] G. Keil, M. le Metayer, A. Cuquel and D. le Pollotec, *Rev. Physique Appl.* **17** (1982) 405.
- [20] J.P. Hallais, *Acta Electron.* **21** (1978) 129.
- [21] V. Aebi, C.B. Cooper III, R.L. Moon and R.R. Saxena, *J. Crystal Growth* **55** (1981) 517.
- [22] H.M. Manasavit and A.C. Thorsen, *J. Electrochem. Soc.* **119** (1972) 99.
- [23] G. Vassilieff and B. Saint-Cricq, *J. Appl. Phys.* **54** (1983) 4581.
- [24] P.J. Wright, B. Cockayne, A.C. Jones and E.D. Orrell, *J. Crystal Growth* **91** (1988) 63.
- [25] T. Nakanisi, *J. Crystal Growth* **68** (1986) 282.
- [26] J. van de Ven, H.G. Schoot and L.J. Giling, *J. Appl. Phys.* **68** (1986) 1648.
- [27] C.Y. Chang, L.P. Chen and C.W. Wu, *J. Appl. Phys.* **61** (1987) 1860.

- [28] J. van de Ven, G.M.J. Rutten, M.J. Raaymakers and L.J. Giling, *J. Crystal Growth* **76** (1986) 352.
- [29] P.R. Hageman, M.H.J.M. de Croon, J.N.H. Reek and L.J. Giling, *J. Crystal Growth* **116** (1992) 169.
- [30] the calculations were performed using the PC-1D program from Iowa State University, Research Foundation Inc.
- [31] L.C. Keizer, X. Tang, R.Z.C. van Meerten and L.J. Giling, *J. Crystal Growth* **102** (1990) 667.
- [32] L.J. Giling and M.H.J.M. de Croon, *J. Crystal Growth* **107** (1991) 56.
- [33] W.G.J.H.M. van Sark, M.H.J.M. de Croon, G. Janssen and L.J. Giling, *Semicond. Sci. Technol.* **5** (1990) 16.
- [34] W.G.J.H.M. van Sark, M.H.J.M. de Croon, G. Janssen and L.J. Giling, *Semicond. Sci. Technol.* **5** (1990) 36.
- [35] W.G.J.H.M. van Sark, M.H.J.M. de Croon, G. Janssen and L.J. Giling, *Semicond. Sci. Technol.* **5** (1990) 291
- [36] R.H. Persy, C.H. Chiltan and S.D. Kirckpatrick, *Perry's Chemistry and Engineering Handbook*, 4th ed. (McGraw-Hill, New York, 1969)

Chapter 6

Improvement of LPMOCVD grown GaAs heteroface solar cells: theory and practical implications

6.1 Introduction

In 1985 a joint solar cell project was started in the Netherlands within the framework of the Dutch National Research Program Solar Energy (NOZ). Groups of the universities of Delft (TUE), Utrecht (RUU), Eindhoven (TUE) and Nijmegen (KUN) participated in this project. The long term aims of this program are a cheap amorphous silicon solar cell with reasonable efficiency and secondly high efficiency GaAs/AlGaAs solar cells [1].

Our group at the university of Nijmegen concentrates on the research of III/V solar cells. The first goal is to make reasonably good GaAs ($\eta \approx 20\%$) and AlGaAs ($\eta \approx 16\%$) cells. In the second place these two type of cells should be combined into a tandem solar cell which will boost the efficiency up to 30 %. Currently the III/V semiconductor InGaP, lattice matched to GaAs, is under investigation. The use of InGaP instead of AlGaAs in solar cells will certainly bring advantages because the photovoltaic quality of InGaP is better than that of AlGaAs [2-4].

To overcome the economical drawback of the expensive GaAs substrates for the solar cells mentioned above, a research program has been started in Nijmegen to grow GaAs and InGaP on silicon substrates. If the efficiency will be comparable, III/V solar cells grown on silicon substrates will be sooner economical beneficial than the cells grown on GaAs substrates. These silicon substrates bring additional advantages over GaAs substrates in increasing the strength of the cell construction.

The GaAs solar cells grown in our group reached an efficiency of about 18% [5]. These cells were grown in an atmospheric MOCVD reactor. In order to improve the efficiency to values of 20% and higher the properties of the materials (especially the minority carrier lifetimes) should be improved as well as the quality of the p/n-junction (this will result in a lowering of the saturation current of the diode and its ideality factor). In the specific case of the atmospheric reactor, which was already more than 9 years in use, it turned out that it was impossible to improve the material properties to the high standards needed. In order to be able to meet those high standards a new low pressure MOCVD reactor was installed. With this fully computerized machine, high quality material and interfaces could be grown. An inevitable consequence of using a totally different reactor was that quite a lot of time had to be spent to discover the optimal parameters for growing and doping (n- and p-type) GaAs and AlGaAs.

In this chapter the influence of different material properties on the effi-

ciency of the solar cells is investigated, both theoretically and in practice. The theoretical results are used for calculating the maximum obtainable efficiency of our basic cell (see fig. 6.1). In order to improve the cells the second step is to determine the material properties in practice. The results from these measurements are coupled back to the theoretical approach so that the influence of the measured material parameters on the efficiency of the cell can be calculated. Now a realistic maximum efficiency of our cells can be calculated. From measurements (i.e. I-V curves) of working solar cells in combination with the measured material parameters weak points in the design of the cells or in the growth method of the materials can be discovered and improved.

6.2 Solar cell construction

In order to obtain high solar cell efficiencies with this new low pressure MOCVD reactor, we have chosen a rather standard GaAs solar cell as starting point for our analysis and improvements. The construction of this basic solar cell, made in our laboratory, is shown in fig. 6.1. The various layers and materials will be discussed below.

The discussion of the solar cell construction starts with the *back contact*. This contact is a standard Ni/Au-Ge/Ni metal combination [6], e-beam evaporated onto the substrate in a separate high-vacuum machine. After the evaporation the contact is annealed at 450 °C in an inert atmosphere.

The next part in the cell construction is the *substrate* on which the cell is grown. GaAs wafers, silicon doped ($\approx 2 - 3 \times 10^{18} \text{ cm}^{-3}$) and (100) $\xrightarrow{2^\circ}$ (110) oriented, are used as substrates.

The first grown layer of the cell is the *buffer layer*. This layer is deposited in order to get a suitable and well defined surface on which the solar cell can be grown properly. The buffer layer is doped higher than the base on top of it in order to force the carriers, created in the base, into the proper direction, i.e. holes to the top of the cell and electrons to the bottom. This effect is called "back surface field". This layer can partly be replaced by $\text{Al}_x\text{Ga}_{1-x}\text{As}$ to enlarge the back surface field effect.

Going upwards the next layer is the *base* of the cell. In this section of the cell the infra-red part of the incoming light is absorbed. The minority carrier lifetime must be high enough in combination with good minority carrier drift mobilities to ensure a large enough diffusion length of the minority carriers. Only when the base meets these demands a maximum efficiency can

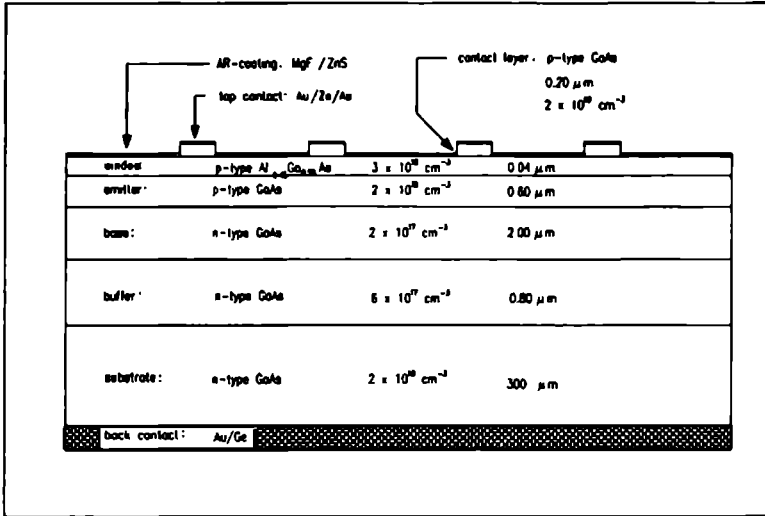


Figure 6.1 Schematic drawing of the basic GaAs solar cell.

be obtained.

The interface between the base and the emitter is the *p/n junction*. The p/n junction needs to be well defined, i.e. no highly compensated layer (due to diffusion or inter mixing of the different dopants during growth) should exist in the junction. Also the diode ideality factor should be as close to one as possible. Defects in the junction have to be avoided at any price because these defects lower the shunt resistance considerably, thereby limiting the efficiency to a large extent.

The *emitter* is the first layer of the cell in which photons are absorbed which attribute to the cell efficiency. The emitter used is relatively thin ($\approx 0.6 \mu\text{m}$) and highly doped ($p \approx 0.8 - 2 \times 10^{18} \text{ cm}^{-3}$). In this layer the high energy part of the incoming light will be completely absorbed. The generated electrons have to diffuse towards the junction in order to be completely separated from the holes. The quality of the material determines the chance that the electrons really reach the junction before recombining. The emitter is the most important part of the solar cell because it absorbs a large part of the incoming photons. In this way the quality of the material used for the emitter determines to a great extent the efficiency of the solar cell.

In order to diminish the high surface recombination at the emitter/air interface, a *window layer* is grown onto the emitter [7]. The window layer consist of the material AlGaAs with a reasonably high aluminum content ($x_{Al} = 0.45$). The interface recombination of the GaAs/AlGaAs interface is much lower than the emitter/air interface [8,9] which results in a considerable increase of the current.

The *cap layer* is a thin ($0.2 \mu\text{m}$) GaAs layer which is heavily doped ($\geq 1 \times 10^{19} \text{ cm}^{-3}$). This will enhance the formation of an ohmic topcontact on it. Due to the high doping level in this cap layer the specific contact resistance can be low. Additionally, the replacement of AlGaAs by GaAs also enhances the formation of a good contact because GaAs is less sensitive towards oxygen and humidity than AlGaAs. The reaction between (Al)GaAs and O_2 and H_2O results in a nonconductive oxide which increases the contact resistance. In the processing of the solar cell the caplayer is etched away everywhere, except under the topcontact, to prevent the unwanted adsorption of light in this GaAs layer.

The *topcontact* consists of the well known gold/zinc metallization [6] and is evaporated onto the cap layer of the cell using the e-beam equipment. Also this contact is annealed at 450°C for 5 minutes in an inert atmosphere.

The topcontact design has to provide an optimum between the losses due to shadowing of the cell by the contact and losses due to resistance (i.e. contactresistance, resistance in the caplayer and resistance of the contact metal). The actual topcontact has been designed following the lines described in [10], using conservative parameters for the contact resistance. The calculations resulted in a topcontact design which shadows about 4.5 % of the cell.

Because of the high reflectivity of the solar cell a considerable part of the incoming light is reflected and does not contribute to the energy conversion. An *anti-reflection coating* consists of material of a lower index of refraction and, if properly designed, can increase the amount of absorbed photons with about 30%. In the cell depicted in fig. 6.1, the anti-reflection coating is a three layer type, consisting of $\text{MgF}_2/\text{ZnS}/\text{MgF}_2$ (2/52/98 nm). For practical reasons sometimes a SiO ARC has been used. Due to this coating the short-circuit current increases with an average of 30%.

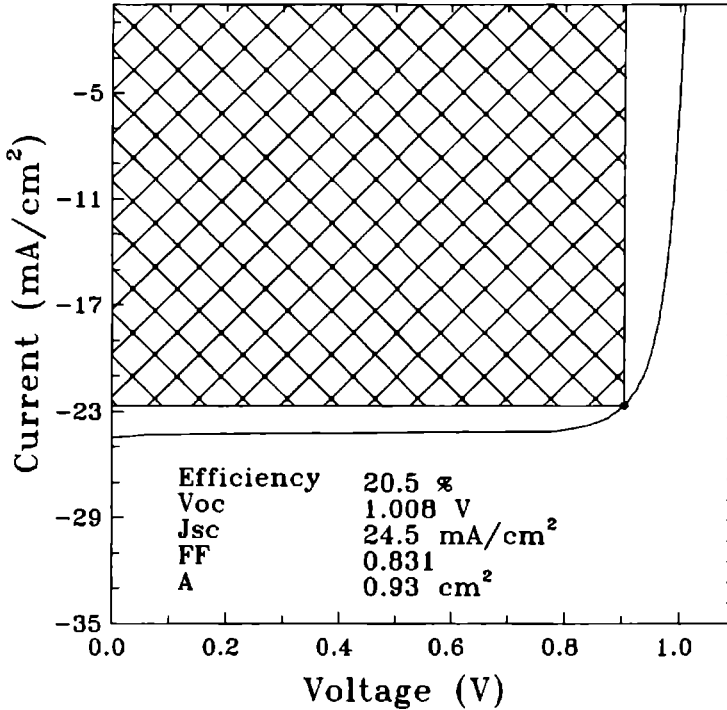


Figure 6.2 I-V curve of our record GaAs solar cell under AM1.5 illumination (1 sun). In the figure the short circuit current (I_{SC}), the open circuit voltage (V_{OC}), the voltage and current at the maximum power point (I_m and V_m resp.) are given. The hatched area in the figure is the maximum power rectangle.

6.3 Theory

In this section a theoretical analysis of the principles of the basic solar cell will be given. Coupled to this, a critical consideration of the appropriate formulas will give more insight in the solar cell performance.

In principle a solar cell is a diode, so its performance can be described by the well known Shockley equation [11]:

$$I = I_S \left\{ \exp \left(\frac{qV}{nkT} \right) - 1 \right\} - I_L, \quad (6.1)$$

in which I_S is the saturation current (mA), I_L is the light current (mA), T is the temperature (K), V is the potential difference across the junction (V), q is the elementary charge (C) and n is the diode ideality factor. When n equals 1 eq. 6.1 describes the ideal current-voltage characteristics of a diode, i.e. only diffusion and drift currents have to be taken into account. In case of GaAs also the recombination in the junction has to be considered. When this is the case the value of n is between 1 and 2. If n equals 2, the recombination current determines the current.

Another point which has to be included is the existence of a series resistance in the junction. This series resistance will lower the voltage drop across the depletion region and thereby it will lower the current. Equation 6.1 has to be modified to include this series resistance and becomes [11]:

$$I = I_S \left\{ \exp \frac{q(V - IR)}{nkT} - 1 \right\} - I_L, \quad (6.2)$$

in which R is the series resistance in the junction (Ω). From this equation one can easily see that for solar cell applications the series resistance must be as low as possible in order to obtain high efficiencies.

The power extracted from the cell is defined as:

$$P = I V. \quad (6.3)$$

The maximum obtainable power (P_m) is found by differentiating eq. 6.3 and equating to zero ($\frac{dP}{dV} = 0$).

In fig. 6.2 the I-V curve is given for our record GaAs solar cell. In this figure the short current (I_{SC}), i.e. the current at $V=0$, and the open circuit voltage (V_{OC}), i.e. the voltage across the cell at infinite load resistance, are depicted. Also the maximum power point is given and the so-called maximum power rectangle.

With eq. 6.1 and with the definition for the maximum power an expression for the dependence of V_m from I_S and I_L can be obtained. This relation is:

$$\exp(qV_m/nkT)(1 + (qV_m/nkT)) = \frac{I_L}{I_S} + 1. \quad (6.4)$$

From this relation it is obvious that if the saturation current (I_S) of the diode decreases, V_m and consequently P_m will increase. A higher light current (I_L) causes an enhancement of V_m and P_m .

The saturation current density can be calculated according to the following formula (given for $n=1$) [11]:

$$J_s = \frac{I_s}{A} = qN_C N_V \left[\frac{1}{N_A} \left(\frac{D_n}{\tau_n} \right)^{1/2} + \frac{1}{N_D} \left(\frac{D_p}{\tau_p} \right)^{1/2} \right] e^{-E_g/kT}, \quad (6.5)$$

where N_C is the effective density of states in the conduction band (cm^{-3}), N_V is the effective density of states in the valence band (cm^{-3}), N_A is the acceptor impurity density (cm^{-3}), N_D is the donor impurity density (cm^{-3}), D_n is the diffusion coefficient for electrons in p-type material (cm^2/s), D_p is the diffusion coefficient for holes in n-type material (cm^2/s), $\tau_{n,p}$ are the minority charge carrier lifetimes of electrons and holes respectively (s) and A is the device junction area (cm^2). The diffusion coefficients D_n and D_p are coupled to the mobility of the carriers through the Einstein relation [11]:

$$D_{p,n} = \left(\frac{kT\mu_{p,n}}{q} \right). \quad (6.6)$$

The diffusion length of the minority charge carriers is defined as:

$$L_{p,n} = \sqrt{D_{p,n} \tau_{p,n}}. \quad (6.7)$$

From eq. 6.5 one can conclude that the saturation current decreases (and with it the maximum power increases) with increasing minority charge carrier lifetimes. Also it follows from eq. 6.5 and eq. 6.6 that I_s decreases at increasing minority charge carrier mobility. So one can conclude from this that the minority charge carrier lifetime is an important material parameter in solar cells.

I_L has also to be considered because it is, beside the V_{OC} , one of the two output parameters of a solar cell. The light current is determined by the amount of carriers which are really collected after being generated in the cell. In fig. 6.3 a cross section of the p/n-junction is drawn with its depletion areas on both sides of the junction and the diffusion lengths of the electrons (L_n) and holes (L_p). Light enters the cell from the left as is symbolized by the arrows. Inside the depletion area ($x_p < x < x_n$) the collection efficiency of the, in this part of the cell generated, carriers is 1 (i.e. $C=1$) because of the presence of a high internal electrical field. Outside this depletion area the chance that a created electron or hole reaches the depletion area and will be swept across the junction and be separated can be described with $C_n = \exp\left(-\frac{(x-x_n)}{L_p}\right)$ and $C_p = \exp\left(-\frac{(x-x_p)}{L_n}\right)$ [12]. The total amount of separated carriers outside the depletion area is the product of the amount of created carriers and the

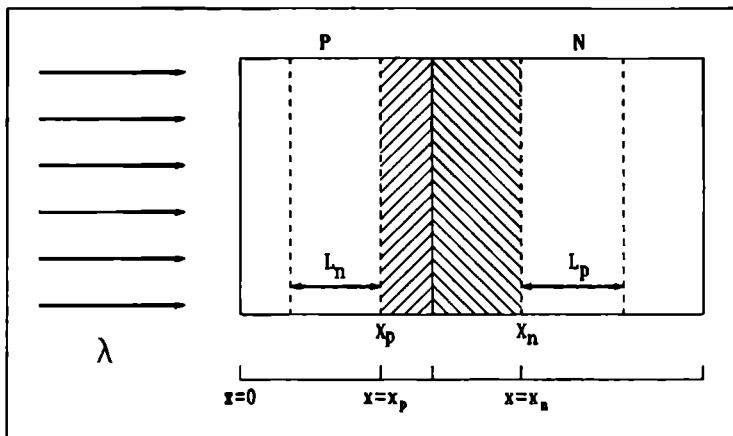


Figure 6.3 Cross section of the p/n-junction of a solar cell. In this figure the depletion widths in the p- and n-region are hatched and the diffusion lengths of the minority carriers are symbolized by the arrows indicated by $L_{n,p}$.

collection efficiency. From this it follows that I_L depends on L_n and L_p . The diffusion lengths $L_{n,p}$ can be defined as $L_{n,p} = \left(\frac{kT\mu_{n,p}\tau_{n,p}}{q} \right)^{1/2}$ [12]. One can conclude from this that the light current increases with increasing lifetimes of the minority charge carriers and increasing minority charge carrier drift mobilities.

From eq. 6.7 and the discussion above it is clear that the lifetimes of the minority charge carriers have to be as large as possible in order to obtain high efficiency solar cells. An increase in the minority charge carrier drift mobility decreases the saturation current and increases the light current. So, the materials used for solar cells should have high carrier drift mobilities. Also it must be remembered that the mobility of the charge carriers in the semiconductor must be high in order to be able to transport current through the device without unacceptable high losses due to the resistance in the semiconductor.

6.4 Characterization and results

In this section the influence of material parameters like the influence of the lifetimes of the minority carriers on the maximum obtainable efficiency will be investigated using a solar cell simulation program called PC-1D [13]. After these simulations, data will be presented of the real characterization of materials and solar cells.

The PC-1D computer simulation program is dedicated to simulate the working (efficiency) of solar cells. All kind of parameters (68 different parameters) can be changed in order to calculate the influence of one of them on the performance of the solar cell. The program is based on formulas for the drift current density of electrons and holes, on formulas for the band edge potentials on both sides of the junction and the Poisson equation. In addition to these basic formulas of course additional equations to determine the carrier mobilities, generation and recombination of carriers, absorption of photons and doping profile are used. All these formulas together with the given parameters, or variation of parameters, are used to proceed a minimalization procedure.

In this section the influence of the lifetimes of the minority carriers, the series resistance, the surface recombination velocity, the layers thicknesses and the mobilities of the material on the cell performance will be shown and compared with the measured values.

Before starting these exercises the maximum obtainable efficiency of the basic solar cell is calculated. This is reached by assuming that the minority carrier lifetimes are each 1 second, which are of course unrealistic high values, and surface and interface recombination rates of zero (in practice also not obtainable). The result for this situation is:

η	V_{OC}	I_{SC}	FF
28.93 %	1.0521 V	30.67 mA/cm ²	0.89

A first point of investigation is the carrier concentration and the mobility of the base and emitter. This is done in order to compare the real values with the ones in the basic solar cell of fig. 6.1. To determine these values special samples were grown on semi-insulating substrates with the same growth conditions as used for the growth of a complete solar cell. The samples were characterized using Hall-Van der Pauw measurements [14]. The results for this situation are:

layer	μ (cm ² /Vs)	n or p (cm ⁻³)
base	4094	3.35×10^{17}
emitter	216	8.45×10^{17}

As can be concluded from this table, the carrier concentrations should be slightly adjusted to meet the values given for the basic solar cell. From PC-1D calculations it follows that the mobilities of the emitter are very high. The same conclusion can be drawn for the n-type material of the base. From the tables of Walukiewicz et al. [15] the compensation ratio of the n-type layers can be determined. The resulting compensation ratio for the emitter is 0.10. When compared with literature [16,17], this value is very low, implying only a small percentage silicium is incorporated on a arsenic side and thereby lowering the mobility of the material. Also the window layer and contact layer were investigated the same way. Both layers were doped high enough, the window layer (Al_{0.45}Ga_{0.55}As): $p=3 \times 10^{18}\text{cm}^{-3}$, $\mu = 57 \text{ cm}^2/\text{Vs}$ and the contact layer $p = 1 \times 10^{19}\text{cm}^{-3}$; $\mu = 102 \text{ cm}^2/\text{Vs}$, in combination with good mobilities so that they will not give a high contribution to the series resistance of the cells. From the electric quality point of view high efficiencies for the cells could not be any problem.

With the PC-1D program the optimum carrier concentration for the base and emitter were calculated, based on the thicknesses for the layers as depicted in fig. 6.1. The optimization procedure has been performed two-dimensionally, in which the p- and n-type doping concentrations have been varied independently. The result of this optimization procedure is that the combination of a base with an concentration $n = 3.35 \times 10^{17} \text{ cm}^{-3}$ and an emitter of $p = 8.45 \times 10^{17} \text{ cm}^{-3}$ gives a maximum efficiency of 28.33 %. This is only a loss of 0.6 % as compared to the basic cell.

The next step was to investigate minority carrier lifetimes in the base and emitter. For that purpose special structures were grown. In order to investigate both the bulk minority charge carrier lifetime and the interface recombination velocity of the base and emitter, Al_xGa_{1-x}As ($x=0.2$) double hetero structures (DH) have been grown [18]. The GaAs layers were as heavily doped as the representative layers in the solar cell. The AlGaAs cladding layers must have the same doping level to prevent that the carriers, which are generated in the GaAs layer, drift into the AlGaAs layer. This is a real problem for the n-type case. It is hard to dope the AlGaAs as high as the GaAs layers because of the presence of the DX-centra in the cladding layers. Therefore only the lifetimes of the p-type and the undoped layers will be presented.

The photoluminescence lifetime of the generated carriers have been deter-

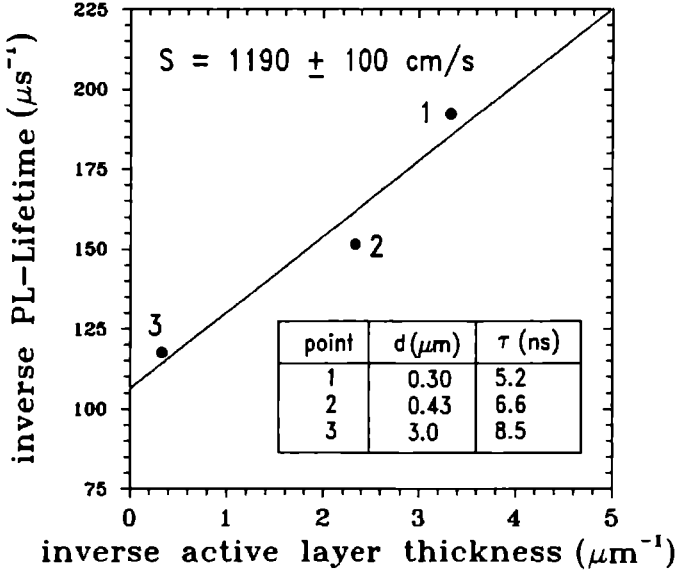


Figure 6.4 Results of the PL decay measurements on the p-type emitter material. Measurements have been performed on three thicknesses.

mined by means of the Time-Correlated Single Photon Counting (TCSPC) technique, which has been described extensively in ref. [19]. The measured effective lifetime (τ_{eff}) is a function of the minority charge carrier lifetime (τ), the surface recombination velocity (S) and the active layer thickness (d):

$$\frac{1}{\tau_{\text{eff}}} = \frac{1}{\tau} + \frac{2S}{d}, \quad (6.8)$$

and where the minority charge carrier (τ) lifetime equals:

$$\frac{1}{\tau} = \frac{1}{\Phi \tau_{\text{rad}}} + \frac{1}{\tau_{\text{SRH}}}, \quad (6.9)$$

with Φ the photon recycling factor (important at higher layer thicknesses), τ_{rad} the theoretical radiative lifetime ($\frac{1}{\tau_{\text{rad}}} = B N_{\text{maj}}$, with B the radiative recombination constant ($\approx 1.4 \times 10^{-10} \text{ cm}^3/\text{s}$) for GaAs and N_{maj} the majority carrier concentration) and τ_{SRH} the Shockley-Read-Hall lifetime, i.e. the

lifetime due to the recombination at deep levels [20]. By plotting the measured decay time versus the thickness of the active layer, as has been done in fig. 6.4, one obtains the interface recombination velocity from the slope of the line through the measured points. The line through the measured points to determine this interface recombination velocity is obtained by fitting according to the least-square technique. The points are corrected for photon recycling. The intercept at the y-axis gives the bulk minority charge carrier lifetime.

As can be deduced from fig. 6.4 the lifetimes of the electrons in the p-type material of the emitter are very good. The theoretical radiative lifetime for $p = 2 \times 10^{18} \text{ cm}^{-3}$ is $\tau = 8.9 \text{ ns}$ (corrected for photon recycling according to Asbeck [22]) and the measured bulk lifetime is determined to be $\tau = 9 \text{ ns}$. The recombination at deep levels is very low ($\tau_{\text{SRH}} \gg 1 \mu\text{s}$) [21] implying good material quality. In fact the lifetime is so high that hardly any Shockley-Read-Hall recombination takes places in this material. From the slope of the line in fig. 6.4 the interface recombination velocity of the GaAs/AlGaAs interface can be determined. The value for this is approximately 1200 cm/sec . Also normally undoped GaAs - $\text{Al}_x\text{Ga}_{1-x}\text{As}$ ($x = 0.2$) double hetero structures were measured. In those samples a Shockley-Read-Hall lifetime of about $7 \mu\text{s}$ was obtained, indicating the very good quality of the material and the absence of deep centers.

The influence of the minority charge carrier lifetimes on the cell performance is calculated. Additionally the effect of the interface recombination velocity (S) is investigated. The results of the calculations are plotted in fig. 6.5. In this figure the absolute efficiency or a normalized efficiency is plotted on the y-axis versus the variable on the x-axis. The normalization is with respect to the maximum obtainable efficiency of the ideal cell.

In fig. 6.5-A the results are plotted for the effect of a variation of the minority charge carrier lifetime in the emitter (p-type material). From this figure it is obvious that a lifetime of 5 ns and larger results in a normalized efficiency of $\geq 96\%$. The measured value of the bulk lifetime for the p-type material was 9 ns , implying a normalized efficiency of 98% . From this figure and our measurements it can be concluded that the minority lifetime of the electrons in the emitter does not hinder good solar cell performance.

In fig. 6.5-B the normalized efficiency is plotted versus the minority charge carrier lifetimes of the holes in the base as calculated by PC-1D. From this it is obvious that a bulk lifetime of $\geq 10 \text{ ns}$ results in a efficiency of $\geq 98\%$. An increase of the lifetime till 100 ns will result in a normalized efficiency of 100% . Unfortunately the minority hole lifetime could not be measured, but considering the good electrically quality of the n-type material and the high

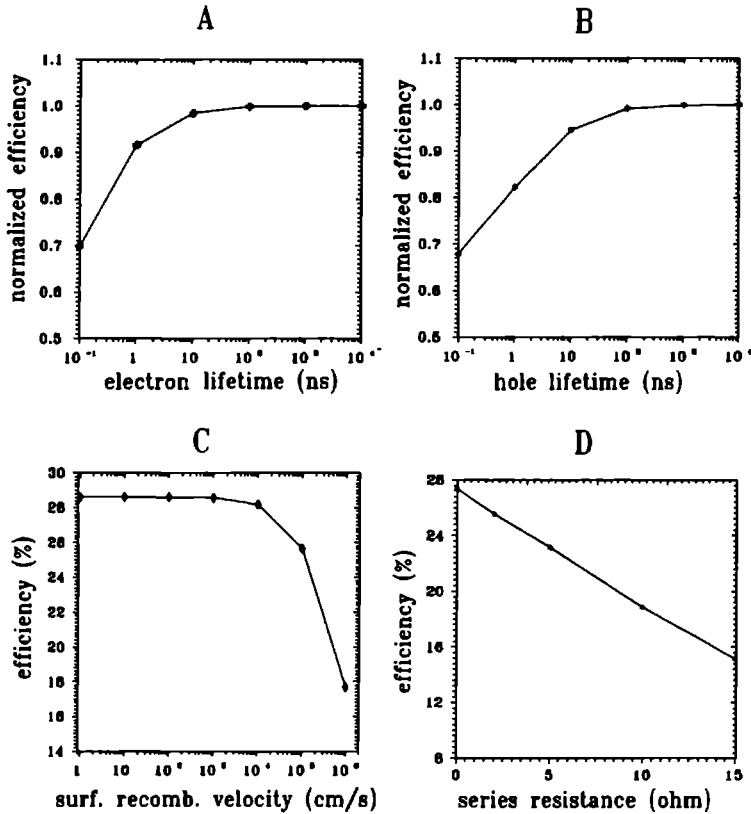


Figure 6.5 Results of the PC-1D calculations.

Fig. 6.5-A: influence of the minority electron lifetime (ns) in p-type GaAs on the normalized efficiency.

Fig. 6.5-B: influence of the minority hole lifetime (ns) in n-type GaAs on the normalized efficiency.

Fig. 6.5-C: influence of the surface recombination velocity (cm/s) on the efficiency (%).

Fig. 6.5-D: influence of the series resistance (Ω) on the efficiency (%).

bulk lifetimes in the normally undoped material, no difficulties are expected with respect to this point.

In fig. 6.5-C the absolute efficiency is given versus the interface recombination velocity. As was already mentioned before, an interface recombination velocity (S) of ≈ 1200 cm/s was measured for our DH structures. Comparing this value with the ones in fig. 6.5-C indicates that the measured value of S has no negative influence on the cell performance at all. A GaAs/air interface has a interface recombination velocity between $10^5 - 10^7$ cm/s [23,24]. So, the absence of an window layer will result in a decrease of the efficiency of the cell from 28.9% to 17.4% for $S = 1 \times 10^6$ cm/s. From this, one can conclude that a suitable window layer is required in order to obtain a good cell performance by lowering the interface recombination velocity. One has to take care that this window layer does not absorb too much light.

Up till now the various material qualities of the used materials have been measured and their influence on the cell performance have been calculated. It is now appropriate to test real solar cells. From I-V measurements at different light intensities one can obtain the series resistance (R_S), the shunt resistance (R_P), the saturation current (I_S) and the diode ideality factor (n).

From I-V measurements of the basic cell the following values can be obtained for 1 sun AM 1.5:

V_{OC}	=	1.01 V	R_S	=	5.48 Ω
J_{SC}	=	24.75 mA/cm ²	R_P	=	$196.7 \times 10^3 \Omega$
FF	=	0.683	n	=	1.18
η	=	17.1 %	J_S	=	53×10^{-15} mA/cm ²

Analyzing these data one comes to the conclusion that the junction quality of the cell is good. This is based on the high open circuit voltage (V_{OC}) and a diode ideality factor close to 1. Additionally the saturation current of the diode is low. These measured values were checked with the PC-1D program to confirm this conclusion. The measured V_{OC} is only slightly lower than the maximum obtainable one of 1.0521 V. The value of the short current density as measured, is remarkably lower than the maximum obtainable value, but this is also due to the non-ideal anti-reflection coating (SiO instead of $MgF_2/ZnS/MgF_2$) and due to shadow losses caused by the topcontacts. These last points are not included in the PC-1D calculations.

The major problem is the relatively low fill factor, 0.683, compared with 0.89 for the ideal case. This already results in a relative loss of 24 %. The low fill factor is thought to be a result of the relative high series resistance

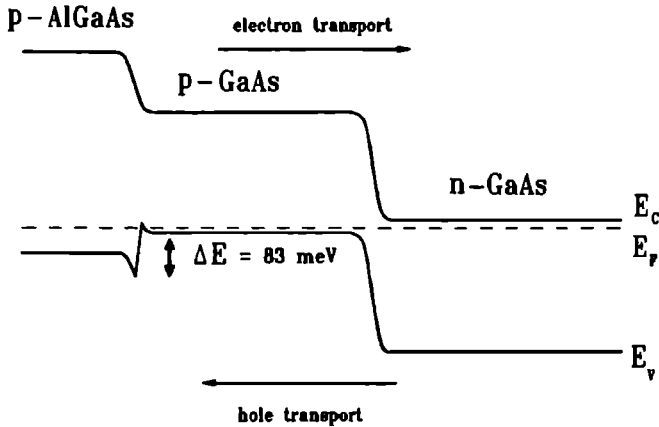


Figure 6.6 Schematic drawing of the band structure of a part of the solar cell in case of a too low doped AlGaAs window layer.

of $5.48 \, \Omega$ in the circuit of the cell. Calculations with PC-1D to investigate the influence of the series resistance on the cell performance are presented in fig. 6.5-D. From this it is obvious that a series resistance of only $5 \, \Omega$ already results in a loss of 12.5% compared to a series resistance of $2 \, \Omega$. Also the influence of the shunt resistance (R_P) on the cell efficiency is calculated. From this it can be concluded that the shunt resistance of our cell is high enough to ensure no negative influence of it on the cell performance.

With the good material properties of the cell and the good diode quality in mind, as described above, only two possibilities are left for the high series resistance of our cells. First of all the doping concentration of the window layer can be too low. In that case the junction between the too low doped window layer and the highly doped contact layer gives a problem. Due to the differences in band-offset and effective mass a barrier exists in the valence band of that junction. In the case of our first cells, the window layer was doped to a concentration of about $p = 5 \times 10^{17} \text{ cm}^{-3}$ which gives, in combination with $p = 2 \times 10^{18} \text{ cm}^{-3}$ for the emitter layer, rise to a barrier of about 83 meV for the holes transport. This situation is depicted in fig. 6.6. Upon increasing the carrier concentration of the AlGaAs window layer to $3 \times 10^{18} \text{ cm}^{-3}$ this barrier vanished, where upon the series resistance dropped from $7.4 \, \Omega$ to $5.5 \, \Omega$. So part of the problem has been solved, but still the fill factor remained

too low.

The second possibility is that the contact resistance of the p-type top contact is still too high. Transmission Line Measurements (TLM) [25] were performed in order to obtain the specific contact resistance (ρ_c) of the top contacts. A value of about $0.01 \Omega\text{cm}^2$ is obtained for ρ_c . This value is only slightly too high and results in a relative loss of about 2 %.

Apart from the well known influence of the series resistance on the fill factor, the small fill factor can also originate from factors due to the processing of the solar cell. We found that defining the cell area by a mesa etching step, instead of cleaving the sample, increases the fill factor with about 10%. This is probably due to the fact that defects, induced by the cleaving of the sample, can act as recombination centres, thereby lowering the cell performance.

The presented analysis of the performance of the basic solar cell has been used to improve this cell design and to optimize the processing procedure. In order to optimize the cell design, we have made the minor adjustments in the carrier concentrations of the basis and emitter as mentioned before. However, the major improvement has come from the incorporation of an $\text{Al}_{0.3}\text{Ga}_{0.7}\text{As}$ back surface field and an $\text{Al}_{0.85}\text{Ga}_{0.15}\text{As}$ window layer instead of the $\text{Al}_{0.45}\text{Ga}_{0.55}\text{As}$ one. These changes together with the improved processing procedure have resulted in our record cell.

The incorporation of a $\text{Al}_{0.3}\text{Ga}_{0.7}\text{As}$ back surface field has resulted in an increase of the fill factor and slight improvement of the open circuit voltage. The incorporated $\text{Al}_{0.85}\text{Ga}_{0.15}\text{As}$ window layer has resulted in a better blue response of the cell, as was measured with quantum efficiency measurements, and in an increase of the fill factor as compared to the window layer with $x_{\text{Al}} = 0.45$. The doping concentrations used for the record cell are:

layer	μ (cm^2/Vs)	n or p (cm^{-3})
base	4424	2.34×10^{17}
emitter	115	3.80×10^{18}
window	102	1.10×10^{18}
cap	65	2.2×10^{19}

The IV curve of this cell was measured using a calibrated GaAs cell (grown at our departement with the same design). The results are:

V_{oc}	=	1.008 V
J_{sc}	=	24.50 mA/cm ²
FF	=	0.831
area	=	0.93 cm ²
η	=	20.5 %

Looking at these figures, one can conclude that these out put parameters can still be improved. Currently we are further optimizing the cell design (adjusting doping levels and layer thicknesses) and anti-reflection coating. Also, we are investigating the influence of the combination of the diode ideality factor and the corresponding saturation current(s) on the fill factor. From the first analysis it appears that these two parameters are important in determining the fill factor. A fit program is in development in order to get insight in this dependency.

6.5 Conclusions

In this chapter a theoretical analysis has been made in order to investigate the physical basis of the solar cell behaviour. It has become clear that the minority charge carrier lifetime is one of the most important parameters in the solar cell performance. An ideal cell construction can be calculated when extreme minority charge carrier lifetimes are used in the fit program. Also the influence of the saturation current of the diode has become more clear and insight is obtained which parameters determine its value.

We measured the minority charge carrier lifetimes, the carrier concentrations and the mobilities in the materials that were used for the solar cell construction. With the solar cell simulation program PC-1D the influence of these parameters on the solar cell efficiency was quantitatively calculated and compared with the theoretical values. These theoretical analysis and practical improvements have resulted in a solar cell of 20.5 % efficiency. Further improvement of this value is possible by carefully changing the cell design and optimizing the processing procedure of the cell.

References

- [1] L.J. Giling, *Energie Spectrum*, juni/augustus 1987, p. 188.
- [2] A. van Geelen, P.R. Hageman, W. Gabriëlse and L.J. Giling, *Proceedings of the tenth Photovoltaic Solar Energy Conference* (1990) p. 541.
- [3] P.R. Hageman, A. van Geelen, W. Gabriëlse, G.J. Bauhuis and L.J. Giling, *J. Crystal Growth* **125** (1992) 336.
- [4] J.M. Olson, S.R. Kurtz, A.E. Kibbler and P. Faine, *Appl. Phys. Letters* **56** (1990) 623.
- [5] X. Tang, Ph. D. Thesis, University of Nijmegen, 1990.
- [6] A.K. Sinka, T.E. Smith and H.J. Levinstein, *I.E.E.E. Transactions on Electr. Devices* **22** (1975) 218.
- [7] J.M. Woodall and H.J. Hovell, *Appl. Phys. Letters* **21** (1972) 379.
- [8] G.W. 't Hooft, M.R. Leys and F. Roozeboom, *Japan. J. Appl. Phys.* **24** (1985) L791.
- [9] R.K. Ahrenkiel, D.J. Dunlavy and B.M. Keyes, *I.E.E.E. Photovoltaic Specialist Conferenc* (1991) Las Vegas p. 9a-1.
- [10] M.A. Green, "Solar cell, technology and systems.", Prentice Hall, New York (1982).
- [11] S.M. Sze, "Semiconductor devices, physics and technology", John Wiley and sons, New York (1985).
- [12] S.M. Sze, "Physics of Semiconductor Devices", John Wiley and sons, New York (1969).
- [13] Programme developed by: Iowa State University Research Foundation, ver.2.11 (1989).
- [14] L.J. van der Pauw, *Philips Research Report* **13** (1958) 1.
- [15] W. Walukiewicz, L. Lagowski and H.C. Gatos, *J. Appl. Phys.* **53** (1982) 769.
- [16] P.R. Hageman, X. Tang, M.H.J.M. de Croon and L.J. Giling, *J. Crystal Growth* **98** (1989) 249.

- [17] X. Tang, H.G.M. Lochs, P.R. Hageman, M.H.J.M. de Croon, L.J. Giling and A.J. Bons, *J. Crystal Growth* **98** (1989) 827.
- [18] R.J.Nelson and R.G. Sobers, *J. Appl. Phys.* **49** (1978) 6103.
- [19] D.V. O'Connor and D. Philips, "Time Corrolated Single Photon Counting" Academic Press London (1984).
- [20] W. Shockley and W.T Read, *Phys. Rev.* **87** (1952) 335.
- [21] The SRH-recombination rate has also been determined in unintentionally doped $\text{Al}_x\text{Ga}_{1-x}\text{As}$ ($x = 0.2$) DH structures. Here, a measured τ_{SRH} of $\approx 7\mu\text{s}$ already indicates a low influence of the recombination at deep centers in the GaAs layer.
- [22] P. Asbeck, *J. Appl. Phys.* **48** (1977) 820.
- [23] E. Gablononitch, C.J. Sandorf, R. Bhat and T. Gmitter, *Appl. Phys. Letters* **51** (1987) 439.
- [24] M. Ettenberg and H, Kressel, *J. Appl. Phys* **47** (1978) 1538.
- [25] M. Shur, "GaAs devices & circuits" Plenum press, New York (1987).

InGaP, a promising material for tandem solar cells

A. van Geelen, P.R. Hageman, W. Gabriëlse
and L.J. Giling

*Proceedings of the tenth E.C. Photovoltaic Solar Energy
Conference, Lisbon (1991) p. 541*

Abstract

$\text{In}_{1-x}\text{Ga}_x\text{P}$ can be used as a material for wide bandgap solar cells. The photovoltaic quality of $\text{In}_{1-x}\text{Ga}_x\text{P}$ is better than that of $\text{Al}_{1-x}\text{Ga}_x\text{As}$, which is used mostly in GaAs based tandem solar cells. This paper describes the MOCVD growth and characterization of $\text{In}_{1-x}\text{Ga}_x\text{P}$ epilayers on GaAs. Perfectly lattice matched $\text{In}_{1-x}\text{Ga}_x\text{P}$ epilayers have been obtained at different growth temperatures. These lattice matched layers exhibited excellent optical and electrical properties. Photoluminescence measurements at 4 K resulted in a FWHM of 9.0 meV, while Hall-Van der Pauw measurements of the undoped layers gave mobilities of $6000 \text{ cm}^2\text{V}^{-1}\text{s}^{-1}$, the best value reported in literature sofar. The lattice matched layers have been doped n- and p-type over a wide carrier concentration range. Preliminary results on $\text{In}_{1-x}\text{Ga}_x\text{P}$ solar cells indicate an efficiency of 4.5 % (AM1.5). Improvement of this efficiency may be attained easily.

7.1 Introduction

Monolithic two junction solar cells based on GaAs and $\text{Al}_x\text{Ga}_{1-x}\text{As}$ have been predicted to reach an efficiency of 30 - 35 % (AM0, one sun). But in spite of this, only recently a GaAs/ $\text{Al}_x\text{Ga}_{1-x}\text{As}$ tandemcell was able to attain an efficiency slightly higher than a single junction GaAs solar cell [1]. Limitation of the efficiency of the tandemcell is generally ascribed to the poor photovoltaic quality of the $\text{Al}_x\text{Ga}_{1-x}\text{As}$. This is thought to originate from the sensitivity of $\text{Al}_x\text{Ga}_{1-x}\text{As}$ for small traces of O_2 and H_2O present during growth in the MOCVD reactor.

$\text{In}_{1-x}\text{Ga}_x\text{P}$ is a III/V material which can cover, dependent on composition, a wide range of bandgap values. When it is chosen to be lattice matched to GaAs it has a bandgap of about the same value as $\text{Al}_{0.4}\text{Ga}_{0.6}\text{As}$: 1.90 eV. However, compared to $\text{Al}_x\text{Ga}_{1-x}\text{As}$ it has a much lower sensitivity for oxygen and water. This sensitivity is of the same order as for GaAs and forms no problem for modern, state of the art reactors. Furthermore the recombination velocity at the $\text{In}_{0.5}\text{Ga}_{0.5}\text{P}/\text{GaAs}$ interface is approximately 30 times lower than at the $\text{Al}_x\text{Ga}_{1-x}\text{As}/\text{GaAs}$ interface [2,3]. So as for the photovoltaic quality, it seems that $\text{In}_{1-x}\text{Ga}_x\text{P}$ is a more suitable material for tandem solar cells than $\text{Al}_x\text{Ga}_{1-x}\text{As}$.

Control of the $\text{In}_{1-x}\text{Ga}_x\text{P}$ epilayer composition is of primary importance because of the intended lattice matching to GaAs. For $\text{In}_{1-x}\text{Ga}_x\text{P}$ this is less easily achieved than for $\text{Al}_x\text{Ga}_{1-x}\text{As}$. The difference in lattice constant between GaP and InP is large compared with that between GaAs and AlAs. Therefore a small change in composition of the $\text{In}_{1-x}\text{Ga}_x\text{P}$ will cause a relatively large change in lattice constant. In practice, both control of composition and lattice matching can be achieved without difficulties [4]. So it appears that $\text{In}_{1-x}\text{Ga}_x\text{P}$ really is a promising material for tandem solar cells. This is supported by the fact that a monolithic InGaP/GaAs tandem solar cell with an η of 27.3% is made by Olson et al. [5].

In this paper we present the first results of our $\text{In}_{1-x}\text{Ga}_x\text{P}$ growth experiments. Because of its importance, control of the layer composition and lattice matching to the GaAs substrate are discussed first. Secondly, the growth rate of $\text{In}_{1-x}\text{Ga}_x\text{P}$, which is important with respect to control of the layer thickness, is given as a function of temperature. Furthermore n-type and p-type doping of $\text{In}_{0.5}\text{Ga}_{0.5}\text{P}$ have been performed. As a result of these investigations $\text{In}_{0.5}\text{Ga}_{0.5}\text{P}$ solar cells on GaAs substrates were made and some preliminary results are presented.

7.2 Experimental procedure

7.2.1 MOCVD growth and characterization

All the $\text{In}_{1-x}\text{Ga}_x\text{P}$ layers were grown in a commercially available, low pressure MOCVD reactor. Trimethylindium (TMI) and trimethylgallium (TMG) were used as sources for the group III components. Arsine and phosphine, both 100 % pure, were the group V precursors. Disilane (Si_2H_6 , 100 ppm in N_2), was used as n-type dopant while diethylzinc (DEZn) was available as p-type dopant. All epilayers were grown on $(100) \xrightarrow{2^\circ} (110)$ oriented GaAs substrates (both doped and semi-insulating). The reactor pressure was kept at 20 mbar in all experiments. Hydrogen, purified by a palladium diffusion cell, was used as carrier gas at flow rates of 5 or 7 slm.

Samples were electrically characterized with C-V profiling and Hall-Van der Pauw measurements. Optical quality of the grown material was determined with photoluminescence measurements, either at 4 K or at room temperature. The composition of the $\text{In}_{1-x}\text{Ga}_x\text{P}$ epilayers and the mismatch between $\text{In}_{1-x}\text{Ga}_x\text{P}$ and GaAs substrate could be calculated from X-ray rocking-curves and electron microprobe measurements (EPXMA). Layer thicknesses were measured on cleaved and etched samples by SEM and optical microscope.

7.2.2 Solar cell processing and efficiency measurement

After the MOCVD growth front (Au/Zn/Au) and back (Au/Ge/Ni) contacts were made by e-beam evaporation. The front contact was defined by a mask and obscured approximately 8% of the cell area. After evaporation the contacts were annealed for $4 \frac{1}{2}$ minutes at 460 °C. The cell's perimeter was defined by cleaving the edges. A selective etchant was used to remove the GaAs contacting layer between the grid fingers. The anti-reflection coating consisted of three layers: MgF_2 , ZnS, MgF_2 , with thicknesses of 20, 520 and 980 Å.

The cell efficiency was measured using a simple xenon lamp and a water filter. The short circuit current was calibrated by using a reference cell. The current-voltage characteristic was measured by a four contact method.

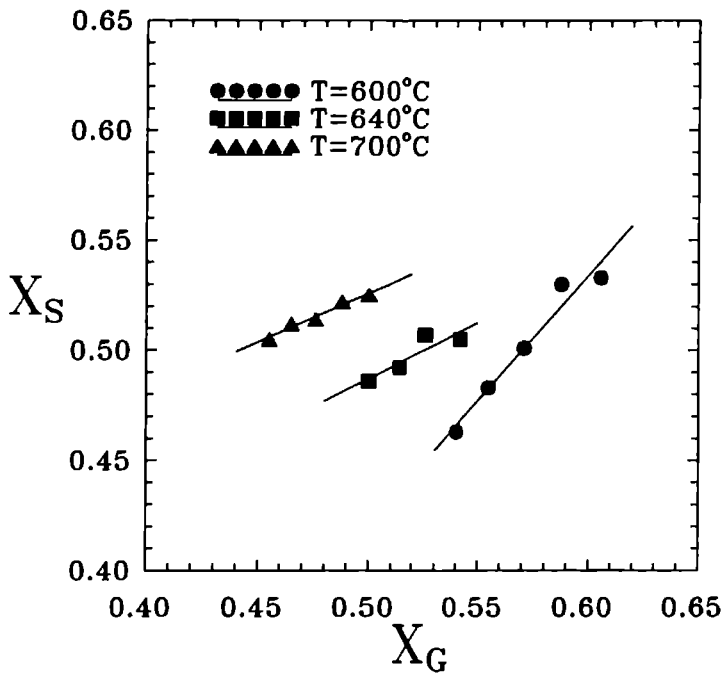


Figure 7.1 Solid phase gallium content (X_S) of the $\text{In}_{1-x}\text{Ga}_x\text{P}$ epilayer as a function of the gas phase composition ($\text{TMG}/(\text{TMG}+\text{TMI})$) at different growth temperatures.

7.3 Results and discussion

7.3.1 Lattice matching

To obtain lattice matched $\text{In}_{1-x}\text{Ga}_x\text{P}$ epilayers on GaAs substrates, x should be 0.516 at room temperature and 0.504 at 900 K.

Experiments were carried out with different gas phase compositions and using different growth temperatures. In fig. 7.1 the fraction gallium in the solid (X_S) is shown as a function of X_G , i.e. the concentration of TMG over the total concentration of III components (TMG + TMI) in the gas phase, at three different growth temperatures. As can be seen in fig. 7.1 lattice matching can be obtained in the whole temperature region used. The gas phase composition

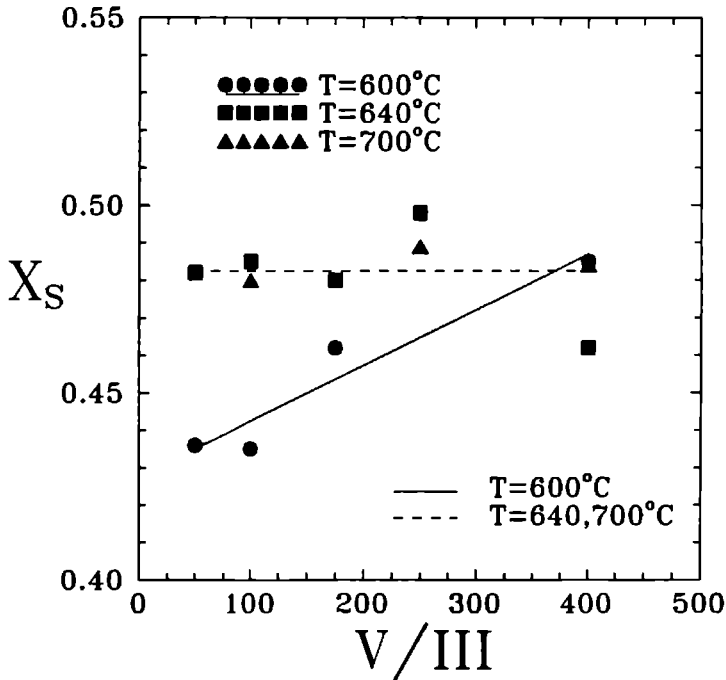


Figure 7.2 Solid phase gallium content (X_S) of the $\text{In}_{1-x}\text{Ga}_x\text{P}$ epilayer as a function of the V/III ratio at different growth temperatures.

necessary to obtain lattice matched epilayers depends however on the growth temperature. At higher growth temperatures less TMG is required.

The solid composition is found to be independent of the V/III ratio (i.e. mole fraction of phosphine over mole fraction TMG and TMI) applied at growth temperatures above 640 °C. At 600 °C instead, the epilayer becomes more gallium rich at higher V/III as is shown in fig. 7.2. This might be due to the fact that TMG decomposes faster in the presence of phosphine or arsine.

Examples of X-ray rocking curves are given in fig. 7.3. Figure 7.3a shows a graph of an $\text{In}_{1-x}\text{Ga}_x\text{P}$ epilayer which is slightly mismatched at room temperature, although it is nearly lattice matched at the growth temperature.

From this rocking curve we calculate a lattice mismatch of -6.5×10^{-4} at room temperature which implies a solid composition $X_{\text{Ga}} = 0.507$. Part b of fig. 7.3 gives a plot of a perfect lattice matched $\text{In}_{1-x}\text{Ga}_x\text{P}$ layer at room

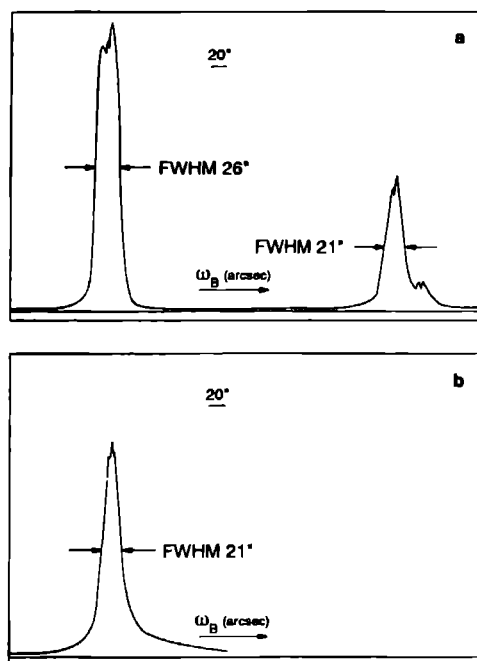


Figure 7.3 X-ray rocking curves for a) slightly mismatched $\text{In}_{1-x}\text{Ga}_x\text{P}$ epilayer and b) perfectly lattice matched epilayer at 300 K.

temperature. The FWHM of 21 arcsec for fig. 7.3a and 21 arcsec or less for fig. 7.3b indicates the good quality of the epilayer. The little satellite peak observed at higher ω in fig. 7.3a (and possibly in fig. 7.3b) is due to a more gallium rich composition of the $\text{In}_{1-x}\text{Ga}_x\text{P}$. This may be caused by a non optimal switching procedure between the GaAs buffer layer and the $\text{In}_{1-x}\text{Ga}_x\text{P}$ epilayer.

7.3.2 Growth rate and incorporation coefficient

The total growth rate and the ratio of the rate of incorporation of gallium and indium species [6] (α) are plotted as a function of reciprocal temperature ($1000/T$ (K^{-1})) in fig. 7.4. For these experiments the concentrations of TMG and TMI were equal and kept constant over the whole temperature region.

The growth rate shows an apparent activation energy of 5.8 kcal/mole in the low temperature region. The same apparent activation energy is found for

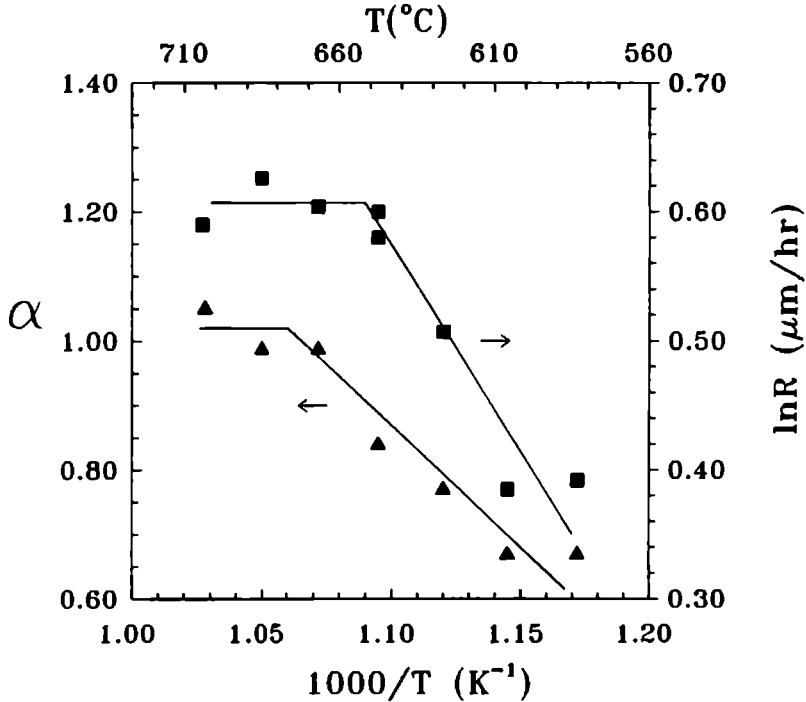


Figure 7.4 Ratio of rates of incorporation of gallium and indium growth species α and growth rate (R) as a function of reciprocal temperature ($1000/T$). α is defined as $r_{\text{TMG}}/r_{\text{TMI}}$. r_{TMG} and r_{TMI} are concentration independent growth rates for GaP and InP.

growth of GaAs under similar conditions. This indicates that this temperature behaviour is determined by the gas phase decomposition of TMG. Under these growth conditions the growth rate is in the transition region between kinetically gas phase limited and diffusion gas phase limited growth.

At growth temperatures higher than 650 °C the growth rate shows nearly no temperature dependence. This is consistent with diffusion limited growth.

The growth rate was found to be independent of the V/III ratio for the growth temperatures used, although the V/III ratio was varied between 50 and 900.

In fig. 7.4 it is seen that at lower temperatures α depends strongly on temperature. This is thought to be caused by the larger activation energy for

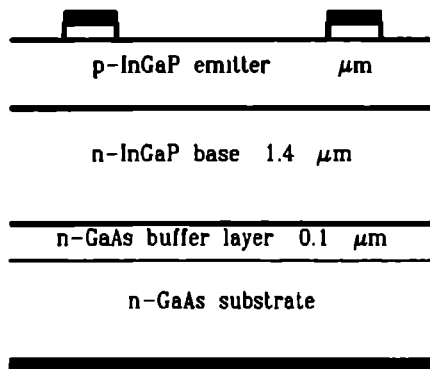


Figure 7.5 Schematic drawing of our $\text{In}_{0.5}\text{Ga}_{0.5}\text{P}$ solar cell.

gas phase decomposition of TMG in comparison with the activation energy of TMI. So at these lower growth temperatures the incorporation ratio and thus the composition of the solid is determined mainly by the TMG decomposition. At higher temperatures both TMG and TMI decompose fast enough so that α levels off. In this case diffusion of growth species towards the surface determines α . In this region α is slightly larger than one, meaning that the overall rate of incorporation of gallium growth species is somewhat larger than that of indium species.

7.3.3 Photoelectrical quality

The photoelectrical quality of lattice matched $\text{In}_{1-x}\text{Ga}_x\text{P}$ as determined by PL is a complex function of growth temperature, V/III ratio and growth rate. In all lattice matched samples reasonable PL intensities and FWHM values were obtained, although some samples did not show any luminescence at room temperature. Our best FWHM at 4K was 9.4 meV (peak energy 1.87 eV), a value which belongs to the best reported in literature.

In all lattice matched samples a PL peak energy shift was observed. The shift indicated a lowering of the normal bandgap of 1.98 eV by 20 to 100 meV (at 4K), depending on the growth conditions. The anomalous change in bandgap is caused by spontaneous (CuPt-type) ordering in the material, as is described by several authors [7,8,9].

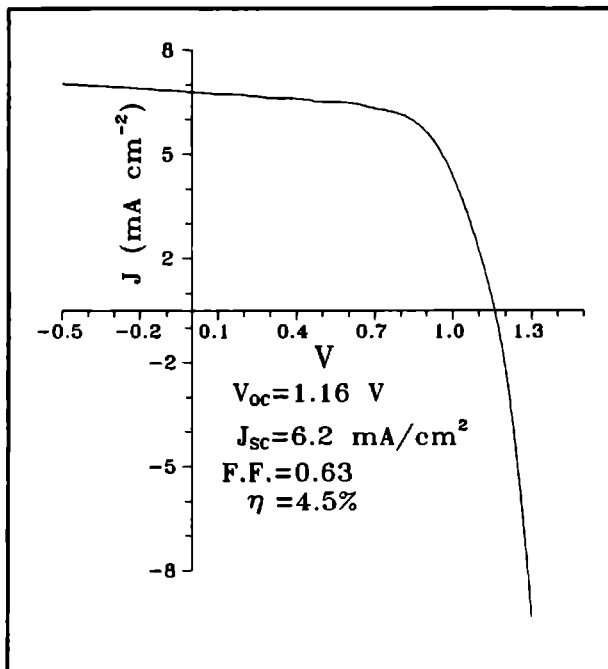


Figure 7.6 I-V characteristic of the solar cell depicted in figure 7.5.

7.3.4 Electrical characterization and doping

Our undoped $\text{In}_{1-x}\text{Ga}_x\text{P}$ layers are typically n-type, with a free carrier concentration of less than 10^{16} cm^{-3} . The mobilities of these undoped layers vary between 3000 and $6000 \text{ cm}^2 \text{ V}^{-1} \text{ s}^{-1}$. To the knowledge of the authors these are the highest values reported in literature.

Doping experiments were performed by changing the input mole fraction of either disilane (n-type) or diethylzinc (p-type). The growth temperature was 600°C . We were able to dope $\text{In}_{0.5}\text{Ga}_{0.5}\text{P}$ n- and p-type over a wide range starting at a few times 10^{16} up to $8 \times 10^{18} \text{ cm}^{-3}$. Mobilities of the intentionally doped layers are very high in respect to the literature values.

7.3.5 Solar cell characteristics

A design of our first $\text{In}_{0.5}\text{Ga}_{0.5}\text{P}$ solar cells is depicted in fig. 7.5. The solar cells were grown at 600 °C on n-type GaAs substrates ($n = 5 \times 10^{17} \text{ cm}^{-3}$). First a thin GaAs buffer layer was grown ($n = 5 \times 10^{17} \text{ cm}^{-3}$). Successively the $\text{In}_{0.5}\text{Ga}_{0.5}\text{P}$ base and emitter were grown and doped respectively $n = 2 \times 10^{17} \text{ cm}^{-3}$ and $p = 1 \times 10^{18} \text{ cm}^{-3}$. The p-type GaAs contacting layer was doped $p = 8 \times 10^{18} \text{ cm}^{-3}$. No passivating layer was applied yet. The solar cells were made intentionally rather thin because of their future use as a top cell in a monolithic tandem solar cell.

Although no effort has been made to optimize this $\text{In}_{0.5}\text{Ga}_{0.5}\text{P}$ solar cell, already an efficiency of 4.5 % is reached (AM 1.5, one sun). From fig. 7.6 it can be seen that the V_{OC} is 1.16 V, the J_{SC} is 6.2 mA cm^{-2} and the FF is 0.63.

The cells still suffer from a rather big series resistance, causing the poor fill factor. Also the current density is not maximal, probably because part of the incoming light is not absorbed in the thin solar cells. The lack of a passivating layer results in a rather high recombination velocity at the emitter/air interface which diminishes the current. The value of the open circuit voltage indicates that the p-n junction is not optimal yet.

Improvements can be carried out easily by establishing the optimal values for layer thicknesses and doping levels. Further benefits are expected from a thin passivating layer of $\text{Al}_x\text{Ga}_{1-x}\text{As}$ or $\text{Al}_x\text{In}_{1-x}\text{P}$ on top of the emitter. Also the switching procedure from GaAs to $\text{In}_{1-x}\text{Ga}_x\text{P}$ can be improved, thereby reducing the number of threading dislocations at the junction.

7.4 Conclusions

The results of our first investigations on the wide bandgap material $\text{In}_{1-x}\text{Ga}_x\text{P}$ are quite encouraging. By MOCVD the material can be grown lattice matched to GaAs over a wide range of temperatures. In the lower temperature region (600°C – 650°C) both incorporation coefficient and growth rate depend on the decomposition rate of TMG.

High quality $\text{In}_{0.5}\text{Ga}_{0.5}\text{P}$ epilayers could be grown with an X-ray rocking curve FWHM of 21 arcsec, 4 K photoluminescence FWHM of 9.0 meV and record mobilities of $6000 \text{ cm}^2 \text{ V}^{-1} \text{ s}^{-1}$ in undoped samples when optimal growth conditions were used. Preliminary efforts to make $\text{In}_{1-x}\text{Ga}_x\text{P}$ solar

cells yielded an efficiency of 4.5%. Improvement of the cell can be obtained easily by finding the optimal values of thickness and doping levels for the different layers. Also a passivating layer may be applied. At this time improvement of the solar cell efficiency seems straightforward and there seems to be no basic limitation towards higher efficiencies.

Acknowledgments

The authors like to thank P.C. van Rijsingen, G.J. Bauhuis, S.M. Olsthoorn and A.L.H. Stolls for their indispensable help.

References

- [1] B.C. Chung, G.F. Virshup and J.G. Werthen, *Appl. Phys. Letters* **52** (1988) 1889.
- [2] G.W. 't Hooft, M.R. Leys and F. Roozeboom, *Japan J. Appl. Phys.* **24** (1985) L791.
- [3] J.M. Olson, R.K. Ahrenkiel, D.J. Dunlavy, Brian Keyes and A.E. Kibbler, *Appl. Phys. Letters* **55** (1989) 1208.
- [4] Shigekazu Minagawa, Hitoshi Nakamura and Hisumi Sano, *J. Crystal Growth* **71** (1985) 377.
- [5] J.M. Olson, S.R. Kurtz, A.E. Kibbler and P. Faine, *Appl. Phys. Letters* **56** (1990) 623.
- [6] W.G.J.H.M. van Sark, G.J.H.M. Janssen, M.H.J.M. de Croon, X. Tang, L.J. Giling, W.M. Arnold Bik, C.P.M. Dunselman, F.J.P.M. Habraken and W.F. van der Weg, *J. Appl. Phys.* **64** (1988) 195.
- [7] Tohru Suzuki, Akiko Gomyo and Sumio Iijima, *J. Crystal Growth* **93** (1988) 396.
- [8] Akiko Gomyo, Tohru Suzuki and Sumio Iijima, *Phys. Rev. Letters* **60** (1988) 2645.
- [9] G.B. Stringfellow, *J. Crystal Growth* **98** (1989) 108.

Optical and electrical quality of InGaP grown on GaAs with Low Pressure Metalorganic Chemical Vapour Deposition.

P.R. Hageman, A. van Geelen, W. Gabriëlse, G.J. Bauhuis
and L.J. Giling

J. Crystal Growth **125** (1992) 336

Abstract

The growth of InGaP has been investigated in a low pressure MOCVD reactor. Experiments have been performed in order to study the influence of several parameters on the growth process, such as the influence of the growth temperature, V/III ratio and total gas flow on the solid composition and on the growth rate. The optical and electrical quality of the grown InGaP layers is discussed in relation to the amount of lattice mismatch of the epilayers. Finally the morphology of the epitaxial InGaP layers is described. A defect, typical for the growth of InGaP on GaAs, is presented. A hypothesis of the origin of this defect is given which results in a method to avoid its formation.

8.1 Introduction

The last few years there has been a great interest in the ternary III/V semiconductor $\text{In}_{1-x}\text{Ga}_x\text{P}$, especially when lattice matched to GaAs due to its potential in opto-electronic devices as lasers and solar cells [1-4]. It can be employed as active layer in laser diodes, in particular in combination with AlInGaP acting as a barrier [2]. In this way it is possible to obtain lasers operating near $0.67\text{ }\mu\text{m}$. Even shorter wavelengths can be realized if quantum well heterostructures consisting of these two semiconductors are used [2,5-7]. A second field of interest for this material is that of high efficiency solar cells. In order to obtain these high efficiencies, it is inevitable to use multi junction solar cells. Recently a tandem solar cell consisting of a GaAs bottom and an InGaP top cell, interconnected with a GaAs tunnel diode, demonstrated an efficiency of 27.3% [3].

The great interest in this material can be explained when its material qualities are compared with the more frequently used ternary alloy AlGaAs. When lattice matched to GaAs, InGaP has a direct bandgap of around 1.9 eV [1,8,9] which is as large as AlGaAs containing around 40 % aluminum. This is about the maximal bandgap without AlGaAs becoming indirect. However, InGaP suffers none of the problems which are connected with AlGaAs. When growing AlGaAs with MOCVD one has to be extremely careful to avoid traces of oxygen and humidity in the reactor [10,11]. These contaminants will lead to high resistivity and bad optical quality of the samples. Contrary to AlGaAs, InGaP is relatively insensitive toward traces of oxygen and water [10]. This makes the growth of InGaP easier than of AlGaAs. As a result of this the GaAs/InGaP interface shows a remarkable low recombination velocity, as low as 1.5 cm/sec [12], which is about 30 times lower than the best values reported for the AlGaAs/GaAs interface (53 cm/sec [13]). Another advantage of InGaP, lattice matched to GaAs, compared to AlGaAs is the fact that it possesses no so called DX centers. So it is no problem to grow highly doped n-type InGaP in contrast to AlGaAs in which a decrease of the free carrier concentration is observed with increasing aluminum content while the dopant input concentration is kept constant [14].

Although it seems that InGaP has only advantages over AlGaAs and no disadvantages, there are still several drawbacks. One of the main problems of this material is composition control. Independent of the growth method used (LPE, VPE, MOCVD, MBE and GSMBE) control of the alloy composition must be within 0.15 % absolute, because of the large differences in lattice constants of InP, GaP and GaAs [15]. In growing AlGaAs this problem does

not occur because of the small difference in lattice constant of AlAs and GaAs. Furthermore the difference in thermal expansion coefficients between GaAs and InGaP [15] can cause additional stress in the grown epilayers upon cooling down from growth to room temperature.

Additionally, when InGaP is grown with MOCVD techniques, the material exhibits a typical behaviour. Depending on growth conditions like the growth temperature, growth rate, V/III ratio and substrate orientation, the bandgap can range between high (≈ 1.9 eV) and low (≈ 1.8 eV) values for a fixed composition, lattice matched to GaAs [16]. The shift in bandgap energy can be as large as 100 meV at room temperature [17,18]. This behaviour of the bandgap energy is thought to originate from a CuPt type of ordering on the group III - sublattice. Ordered material shows low values of the band gap energies and completely disordered material exhibits the highest values [16-21].

In this paper we will present the growth and characterization of high quality InGaP material grown in a low pressure MOCVD reactor. The influence of the growth temperature, V/III ratio, total gas flow and gas phase composition on the quality of the InGaP epilayers is investigated. Electrical and optical qualities of the grown material are examined with C-V, Hall-Van der Pauw and photoluminescence measurements. Our samples exhibit, to our knowledge, the highest mobilities reported in literature so far.

8.2 Experimental procedure

All samples were grown in a commercial available low pressure MOCVD reactor with a horizontale reactor cell [22]. Pure arsine (AsH_3) and phosphine (PH_3) were used as group V species. For the group III species trimethyl gallium (TMG) and trimethyl indium (TMI) were used as precursors. All growth experiments were performed on $(100) \xrightarrow{2^\circ} (110)$ oriented GaAs wafers. The growth runs were performed at a reactor pressure of 20 mbar and at growth temperatures between 580 °C and 700 °C. The total gas flow through the reactor was chosen to be 5 or 7 slm respectively, while the V/III ratio was varied between 50 and 400. The mole fractions TMG and TMI varied between 0.0043 % and 0.0065 % each. The resulting growth rate varied, depending on the growth temperature and total gas flow and amount of group III precursor, between 1 and 2.2 $\mu\text{m/h}$.

The solid composition of the layers was determined using electron microprobe analysis (EPXMA) and X-ray diffraction. Transmission electron microscopy (TEM) and high resolution transmission electron microscopy

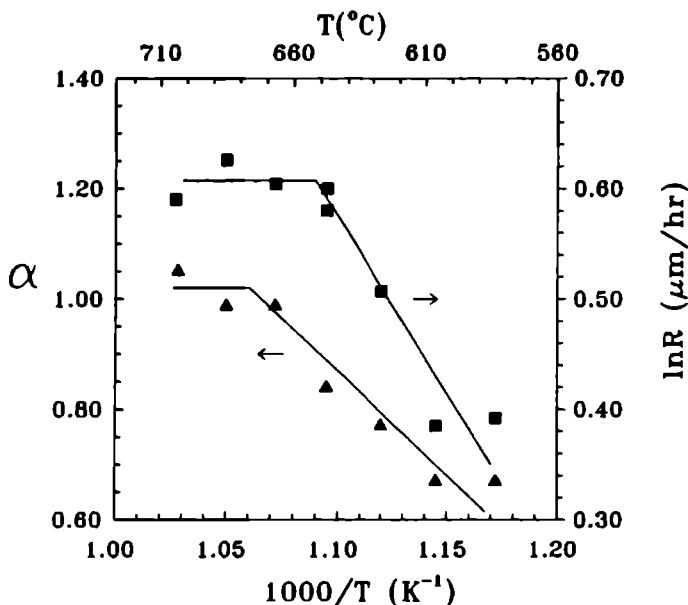


Figure 8.1 Plot of ratio of rates of incorporation of gallium and indium growth species (α) and growth rate (R) versus reciprocal temperature ($1000/T$). α is defined as $\frac{\bar{r}_{\text{TMG}}}{\bar{r}_{\text{TMI}}}$ where \bar{r}_{TMG} is the concentration independent growth rate of GaP and is \bar{r}_{TMI} the concentration independent growth rate of InP as defined in section 8.3.

(HRTEM) were used to investigate dislocations in the InGaP epilayers and to determine the amount of ordering. All samples were electrically characterized by Hall-Van der Pauw measurements performed at room temperature. Temperature dependent Hall-Van der Pauw measurements down to 4.2 K were performed at some selected samples.

The optical material quality of the grown $\text{In}_{1-x}\text{Ga}_x\text{P}$ epilayers was investigated by photoluminescence measurements. These measurements were performed at room temperature and 4.2 K. At the latter temperature, the sample was mounted in a cryostat with the sample in He exchange gas. Optical excitation was provided by the 2.41 eV (514.5 nm) line from an Ar^+ laser with an excitation density of 5.3 W/cm^2 . The luminescence was dispersed by a double monochromator fitted to a cooled photomultiplier tube with a S1 response.

8.3 Results and discussion

8.3.1 Influence of the growth temperature on the solid composition and growth rate of InGaP

Experiments were done in order to study the influence of the growth temperature on the composition of the $\text{In}_{1-x}\text{Ga}_x\text{P}$ epilayers and on the growth rate of this material. In these experiments the growth temperature was chosen between 580 °C and 700 °C while the gas phase composition was kept constant. This implies that the fraction trimethylgallium in the gas phase X_G ($= \frac{[\text{TMG}]}{[\text{TMG}] + [\text{TMI}]}$) and the V/III ratio, i.e. the ratio between the amount of phosphine and the total amount of group III growth components (TMG + TMI), was unchanged. The total amount of group III species in the gasphase was 0.018 %, the V/III ratio was 250.

In fig. 8.1 the growth rate is plotted versus the reciprocal temperature (K^{-1}). From this figure it is clear that at growth temperatures higher than 650 °C the growth rate of $\text{In}_{1-x}\text{Ga}_x\text{P}$ is temperature independent, which implies that the growth rate in this temperature region is gas phase diffusion limited. Because of the high V/III ratio used (250), the group III growth species are the growth rate limiting species. The diffusion of these growth components through the gas phase toward the growing surface is the limiting factor in the growth rate of $\text{In}_{1-x}\text{Ga}_x\text{P}$ at these temperatures. At growth temperatures below 650 °C the growth is temperature dependent with an apparent activation energy, E_{act} , of 6 kcal/mole as can be deduced from fig. 8.1. This value for E_{act} indicates that the growth is determined by gas phase diffusion coupled to gas phase decomposition of, at least one of the group III growth components, i.e. TMG or TMI. However, in growing GaAs in the same reactor at the same temperature and pressure conditions, the same apparent activation energy (4.2 kcal/mole) has been found [22]. This means that in this temperature region probably the decomposition of TMG in the gas phase coupled to the diffusion through the gas phase of Ga growth species is the limiting factor in the growth of $\text{In}_{1-x}\text{Ga}_x\text{P}$. This is consistent with the fact known from literature that the decomposition of TMG is completed at higher temperatures than that of TMI [23-28]. When gas phase decomposition kinetics would solely determine this process an apparent activation energy of about 20 kcal/mole would have been found [29].

In fig. 8.1 also the ratio of the incorporation rates of gallium and indium species, α , is plotted versus the reciprocal temperature. This ratio α is defined as $\frac{\bar{r}_{\text{TMG}}}{\bar{r}_{\text{TMI}}}$. In this expression \bar{r}_{TMG} is the concentration independent growth rate

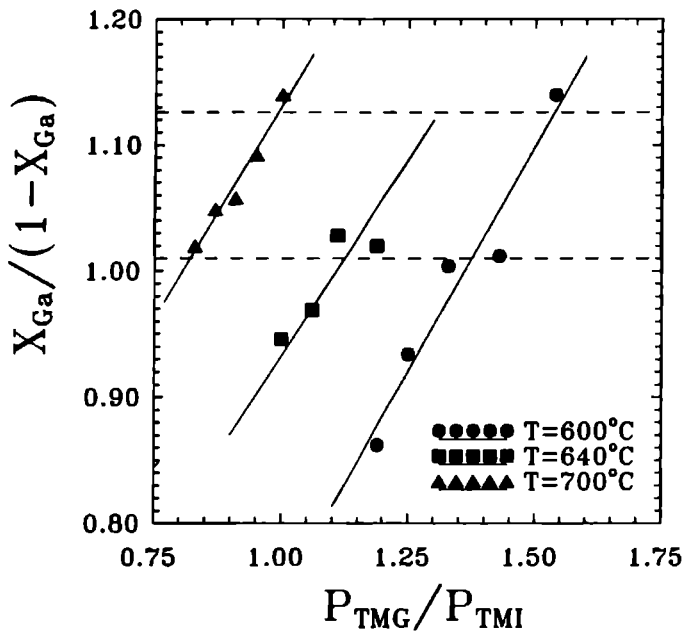


Figure 8.2 Plot of the ratio of the fraction of gallium in the solid (X_{Ga}) to the solid phase fraction of indium ($1-X_{Ga}$) in the $In_{1-x}Ga_xP$ epilayer as a function of the ratio of input mole fractions TMG (P_{TMG}) and TMI (P_{TMI}) at three different growth temperatures. The dashed lines represent the lattice matched region around $\frac{X_{Ga}}{1-X_{Ga}}$.

of GaP and \tilde{r}_{TMI} is the concentration independent growth rate of InP [30]. The observed growth rate is given by:

$$r = C_0 \tilde{r},$$

where C_0 is the input concentration of the group III component. Explicit expressions for \tilde{r} are not really needed here. For the regimes where transport through the gas phase is rate determining or where the chemical kinetics dominate, it is given that [30] for the diffusionally limited process :

$$\tilde{r}(D_0, v_0, h, z, T) = A \frac{D_0}{h} \exp\left(-B \frac{D_0}{v_0 h} \frac{z}{h}\right),$$

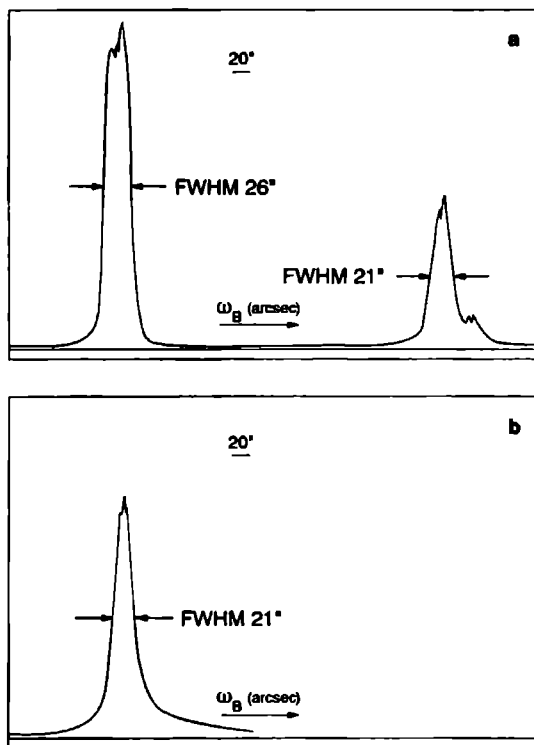


Figure 8.3 X-ray rocking curves for a) a slightly mis-matched epilayer and for b) a perfectly lattice matched epilayer of InGaP on GaAs at T=300 K.

and for the kinetically limited process:

$$\bar{r}(k_0, T) = k_0 \exp\left(-\frac{E_a}{RT}\right),$$

where:

- D_0 = the binary diffusion coefficient of the group III component at room temperature,
- v_0 = the mean horizontal gas flow velocity,
- h = the free height above the susceptor,
- z = the coordinate along the susceptor (heating starts at $z=0$),

- A,B = temperature-dependent dimensionless numbers, which are a weak function of T and the thermal diffusion factor α_T only,
 k_0 = pre-exponential factor of the rate constant,
 E_a = activation energy for chemical reaction or reaction enthalpy for equilibria,
T = growth temperature,
R = gas constant.

A detailed discussion of these equations is given by Van Sark et al. [30]. At temperatures lower than 660 °C, the factor α decreases with decreasing temperatures. The decreasing factor α indicates decreasing (concentration independent) growth rate of GaP. This supports our view that decomposition of TMG is most probably the rate limiting factor of the growth rate at these temperatures.

At higher temperatures, above 660 °C, α levels off to about unity. This result again points to a gas phase diffusion limited growth process at these temperatures. The difference in diffusion coefficient between Ga and In growth species is small ($\approx 15\%$) enough to ensure that it has hardly any noticeable effect on the solid state composition.

In fig. 8.2, the ratio of the fraction gallium in the solid state (X_{Ga}) and the fraction indium in the solid state ($1 - X_{Ga}$) is plotted versus the ratio of the input partial pressure TMG and the input partial pressure TMI for three different growth temperatures. In these experiments the input partial pressure TMI is kept constant and the input partial pressure TMG is varied. At all three growth temperatures this ratio ($X_{Ga}/(1 - X_{Ga})$) varies linearly with the ratio of the input partial pressures (P_{TMG}/P_{TMI}). In all these situations the slope is about 0.7. In case of gas phase diffusion limited growth of a III/V semiconductor with mixing on the group III sub-lattice like InGaP, the amounts of indium and gallium in the solid state should correspond to the partial pressures of TMI and TMG in the gas phase, i.e. the distribution coefficient between the gas phase and the solid state should be about one. The deviation we obtained in our experiments from this theoretical distribution coefficient must be explained by a non linear, but reproducible, behaviour of the electronic TMG massflow controller.

At higher temperatures, more TMI (relative to TMG) is needed in the gas phase in order to grow lattice matched material at a fixed indium content. Most probably this is caused by a larger desorption rate of indium growth species than of gallium growth species from the surface at higher temperatures. This is consistent with the lower value of the InP bond strength as compared

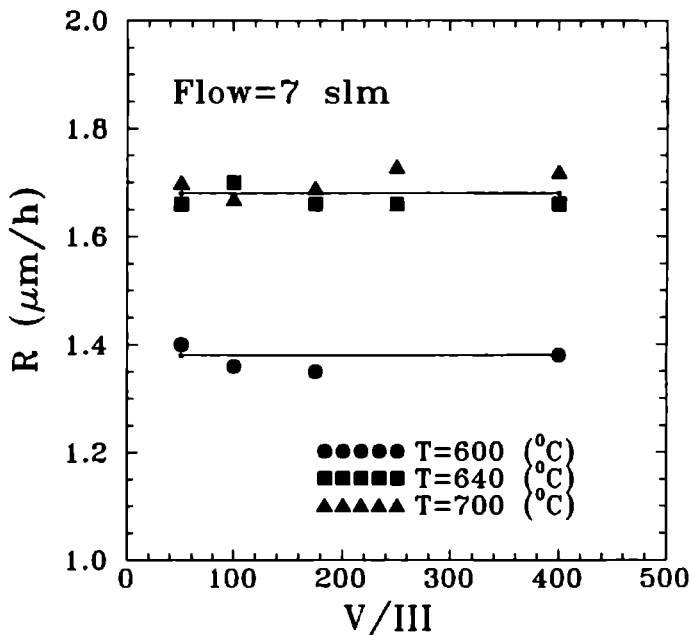


Figure 8.4 Growth rate of the InGaP epilayers as a function of the input V/III ratio for 3 different growth temperatures and for a total flow of 7 slm.

to that of GaP.

The dashed lines in fig. 8.2 represent the boundaries of the region in which the $In_{1-x}Ga_xP$ is still lattice matched to the GaAs substrate. In this paper, we define lattice matching by a lattice mis-match of less than 1×10^{-3} around the exactly lattice matched composition $X_{Ga} = 0.516$ (at room temperature) [15]. It can be seen from this figure that at all three temperatures lattice matched epilayers can be grown by using different gas phase compositions of TMG and TMI. An example of this is given in fig. 8.3. In this figure, two rocking curves are plotted of InGaP epilayers on GaAs substrates. In fig. 8.3a, the epilayer is slightly (tensile) mismatched ($(\frac{\Delta a}{a_0}) = -1 \times 10^{-3}$) and in fig. 8.3b, a perfectly lattice matched epilayer is given. The FWHM of the rocking curve of the perfectly matched epilayer is only 21 arcsec. or less, a good value for this material.

8.3.2 The effect of the V/III ratio and the total gas flow on the growth rate and solid composition

Experiments have been performed in order to investigate the effect of the V/III ratio on the growth rate. In these experiments the amount of III component was kept constant and the concentration of phosphine in the gas phase was varied. The ratio between the concentration of TMG and TMI was chosen in such a way that lattice matched epilayers could be grown at the temperatures used.

For a total gas flow of 7 slm (i.e. the sum of all the precursor flows and carrier gas flow) and at three different growth temperatures, the results are plotted in fig. 8.4. From this figure it is obvious that the V/III ratio within the region investigated has no influence at all on the growth rate. From fig. 8.4 one can conclude that at the two higher temperatures used (640 and 700 °C) the growth rate indeed is purely gas phase diffusion limited because both growth rates are exactly equal while at 600 °C the growth rate is smaller because gas phase kinetics still play a role.

In fig. 8.5 the gallium composition in the InGaP epilayer is plotted versus the V/III ratio for the three different growth temperatures used (600, 640 and 700 °C). At the two highest temperatures, i.e. 640 and 700 °C, the solid composition, as expected, is independent of the V/III ratio. However, at 600 °C the gallium incorporation increases as the V/III ratio increases. It appears that the decomposition of TMG, and thus the gallium incorporation, is stimulated by increasing amounts of phosphine in the gas phase. It is known from literature that the pyrolysis of TMI is enhanced by the presence of phosphine [15,31,32]. Similar observations have been made for the decomposition of TMG in the presence of arsine [26,28]. Now it appears that also the decomposition of TMG is enhanced by the presence of phosphine. The influence of total flow rate on the growth of InGaP was also investigated. It appeared that optimal results in our reactor were obtained for a total flow rate of 7 slm corresponding with a real gas velocity of 228 cm/s in the reactor at the growth temperature.

8.3.3 Electrical and optical quality of the InGaP layers

The electrical quality of the grown samples was evaluated with Hall-Van der Pauw measurements at room temperature using a cloverleaf configuration. All grown samples were n-type, with carrier concentrations ranging from 1 to $10 \times 10^{15} \text{ cm}^{-3}$. The mobility exhibited a much greater spread, mainly

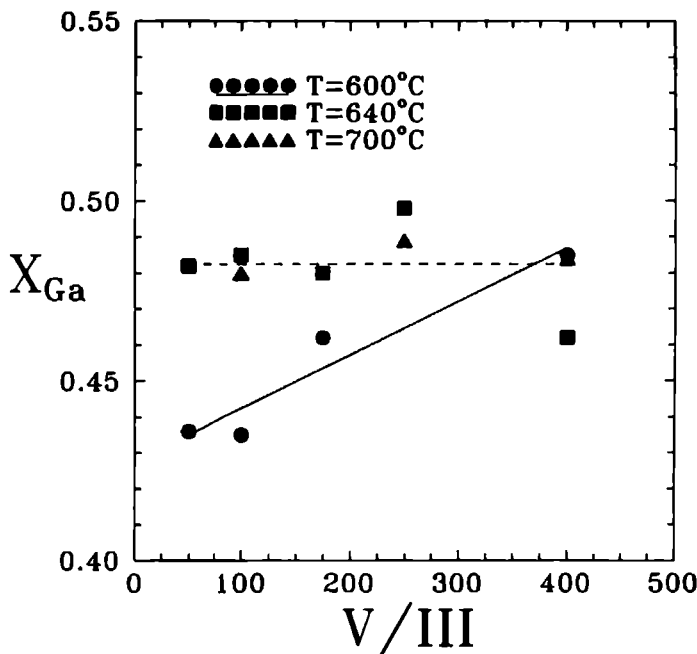


Figure 8.5 Gallium content X_{Ga} of the $In_{1-x}Ga_xP$ epilayer as a function of the V/III ratio grown at different temperatures.

depending on the amount of lattice mismatch. In fig. 8.6 the mobility is plotted versus the solid composition of the epilayers. The dashed lines represent the boundaries of the lattice matched region. From this figure it can be concluded that the highest values for the mobilities are obtained in the lattice matched area. In these samples only elastic strain is present, no misfit dislocations were observed. The mobility values around $6000 \text{ cm}^2/\text{V} \cdot \text{s}$ are to our knowledge the highest values reported in literature. However, some care has to be taken in comparing the values of the mobilities of different samples because the degree of ordering of the material can influence these values drastically [33,34].

To check whether the presence of a 2-DEG could have effected our mobilities values we performed some magneto photoluminescence (MPL) measurements [35] and temperature dependent Hall-Van der Pauw measurements. Both measurements did not give any indication of such a 2-DEG in contrast to some effects reported in literature [1,36]. Instead, the temperature depen-

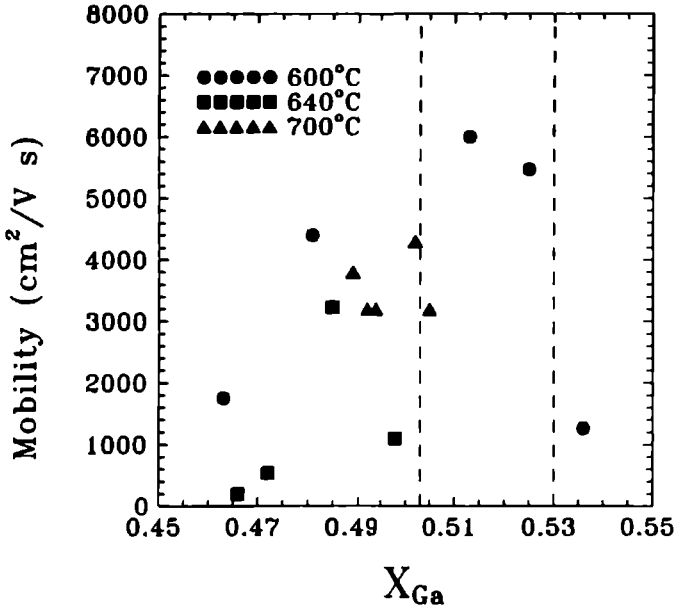


Figure 8.6 Mobility ($\text{cm}^2/\text{V sec}$) versus the solid phase gallium content X_{Ga} of InGaP epilayers grown at different temperatures. The dashed lines represent the lattice matched region.

dent Hall-Van der Pauw measurements gave an indication that in a sample at low temperatures a "hopping" conduction mechanism is present instead of the usual carrier freeze out [37]. This is illustrated in fig. 8.7. In this figure the Hall coefficient (R_H) is plotted versus the reciprocal temperature (K^{-1}). In the lower temperature region the Hall coefficient exhibits a sudden sharp drop. This behaviour is typical for a hopping type of conduction [38].

The data points plotted in fig. 8.6 were obtained from samples with carrier concentrations of 1 to $10 \times 10^{15} \text{ cm}^{-3}$. The corresponding mobilities are relatively high, which ensures, in combination with the carrier concentrations, a low compensation ratio for those samples. This implies that the epilayers, which were all n-type, contain only low concentrations of acceptor atoms. So the effect of the misfit dislocations on the mobility will not be screened by large amounts of compensating acceptors [39]. As in the lattice matched region no misfit dislocations are present, we indeed find an effect of the strain

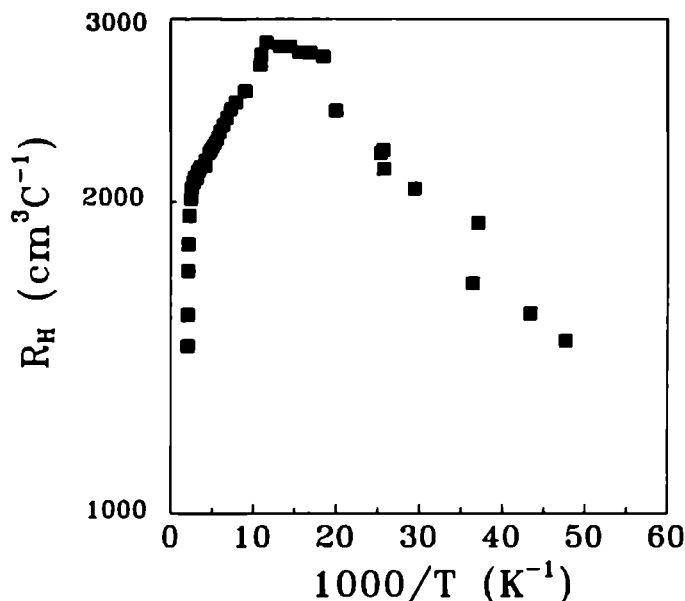


Figure 8.7 Plot of the Hall coefficient (R_H) (cm^3/C) of an InGaP sample versus the reciprocal temperature ($1000/T$ (K^{-1})).

on the electrical properties of the material in this region. Samples grown with a larger mismatch exhibited a dislocation pattern (see section 3.5). The electrical properties of these dislocations are most likely the reason for the lower values of the mobilities. Future experiments with more samples grown lattice matched at different growth temperatures may reveal a significant relation between the growth temperature and mobility.

The optical properties of the samples were measured using photoluminescence techniques at 4.2 K. At this temperature all samples showed luminescence. However, at room temperature some samples did not show any luminescence at all. A typical luminescence spectrum at 4.2 K is given in fig. 8.8B, for a slightly mis-matched epilayer. In this figure only one peak can be observed, which is common for this material. This peak is generally assigned to a band-to-band transition [1]. For a perfectly lattice matched sample, we found a smallest FWHM at 4.2 K of 9.4 meV for this band-to-band transition peak, as can be seen in fig. 8.8A. In literature sometimes, in less pure material, a

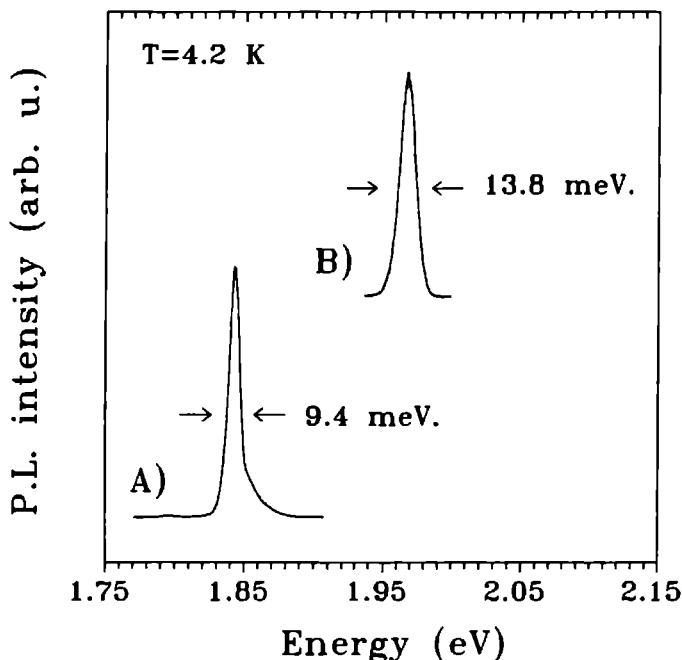


Figure 8.8 Photoluminescence spectra recorded at 4.2 K for A) a slightly mis-matched sample and B) a perfectly lattice matched epilayer InGaP.

second peak in the photoluminescence spectrum is detected which is ascribed to a conduction band to acceptor transition. According to literature probably zinc is this acceptor [5,15]. We did not find any indication of excitonic transitions in our material. Until now, nobody in literature has found luminescence from excitonic transitions in this material. A possible explanation for this absence of excitonic transitions is the local perturbation of the bandedges because of the presence of a microstructure in InGaP and the spatial separation of carriers and ionized dopants [40,41].

In fig. 8.9 the FWHM of the band-to-band transition is plotted versus the solid composition of the material. The experiments were performed at different growth temperatures. The experiments performed at 600 °C give an indication that the lowest FWHM's are obtained for those samples which are lattice matched. This coincides with results in literature [39,42]. From this figure one can also conclude that in general the two higher growth temperatures (640 and

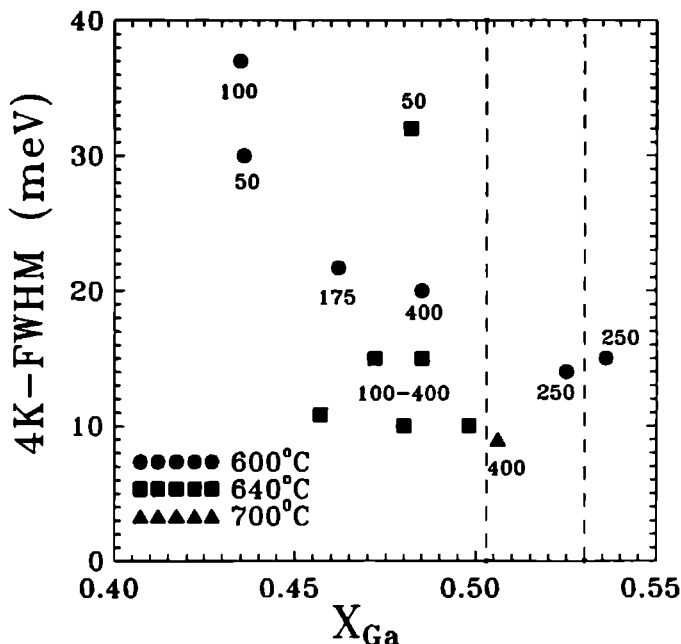


Figure 8.9 FWHM of the photoluminescence peaks recorded at 4.2 K versus the solid phase content gallium X_{Ga} of the InGaP epilayers grown at different temperatures. The numbers in this figure correspond to the V/III ratio used for the growth of each sample. The dashed lines represent the lattice matched region.

700 °C) give better optical results. Although the results of photoluminescence experiments obtained on our samples are good, the scattering of these results is rather large. These variations of the photoluminescence signal originate from local variations of the material caused by the non homogeneous ordering in our samples. This ordering is confined in domains of about 100 Å in diameter which are embedded in a matrix of disordered material. This will be discussed in more detail in the next section.

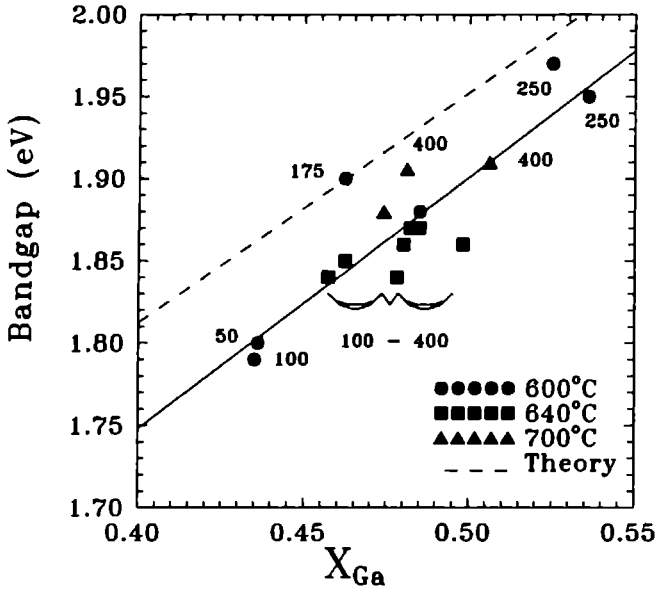


Figure 8.10 Bandgap at 4.2 K as measured with P.L. versus the solid state composition (X_{Ga}) of the InGaP epilayers. The numbers in this figure correspond with the V/III ratio used for the growth of the epilayers. The dashed line shows the theoretical value for the bandgap at 4.2 K without ordering [55]

8.3.4 Ordering of the InGaP epilayers

We investigated some of the grown samples with TEM on the presence of the well known ordered structure. In accordance with literature all these samples possessed a CuPt type of ordering on the $\{111\}$ planes. However, the ordering is only present in two of the four possible $\{111\}$ planes, most probably the $(\bar{1}11)$ and $(1\bar{1}1)$. One of these two planes shows a more intense diffraction spot than the other indicating that in this plane a higher degree of ordering is present. The diffraction pattern of the samples exhibited also so-called streaks in the $\langle 001 \rangle$ directions. The presence of these streaks suggests that the ordered regions are not perfect, i.e. the ordered domains consist of different type of microdomains [43]. All these TEM observations coincide with results published in literature [16,44-48].

HREM investigations of an ordered sample revealed that the ordering starts at the InGaP-GaAs interface, so immediately when InGaP starts to grow. Also the HREM measurements clearly show that ordering occurs on only two of the four possible $\{111\}$ planes. In the ordered domains so-called Anti Phase Boundaries (APB) are observed. These are the result of an imperfect variation of the indium and gallium planes in the lattice. So two neighbour indium or gallium planes form an APB. This is conform the literature results[47].

Ordering is known to affect the bandgap of the material, the bandgap shifts to lower values as compared to disordered material. The influence of ordering on the bandgap was investigated using PL techniques. It was found that the peakpositions at 4.2 K of the ordered samples were about 60 meV lower than the theoretical values expected for the solid composition of the material [21].

We observed a strong influence of T_{growth} and the V/III ratio on the value of the bandgap. At a growth temperature of 600 °C, a maximum was observed in the bandgap at V/III=175 while at 700 °C the samples with the highest V/III ratio (400) showed the highest values for the bandgap. This is shown in fig. 8.10. These results are comparable with the results published in literature [17,44,49,50]

8.3.5 Morphology

The four samples grown in the lattice matched area (as defined before) show a specular surface, although some precautions had to be taken to avoid the growth of a typical defect on the surface. Samples with a tensional misfit larger than $\frac{\Delta a}{a_0} \leq -1.4 \times 10^{-3}$ show a misfit dislocation line pattern only in the $[01\bar{1}]$ direction. The samples grown under compression (larger than $\frac{\Delta a}{a_0} \geq 4 \times 10^{-3}$) show a dislocation cross-hatched pattern which is oriented in the $[011]$ and in the $[01\bar{1}]$ directions. Ozasa et al. [39] performed double-crystal x-ray diffraction measurements on slightly mismatched InGaP epilayers grown on GaAs and also had to conclude from these measurements that the tensile strain in the epilayers is released more easily than the compressive strain. The difference in the misfit dislocation patterns between the tensile and compressive situations can be explained taking into account the a-symmetry of the zincblende structure of III/V compounds [51,52].

8.3.6 Defects

In the beginning of this investigation all InGaP epilayers showed defects all over the surface. The defect density increased going from the middle to the edges of the substrates. The defects all have the same orientation, their length axis is oriented along the [011] axis. The density of the defects increased when the material is grown at higher temperatures. The defect density also increased using lower V/III ratios. We observed these defects in both compressive and tensile strained material as well as in perfectly lattice matched InGaP. So this defect is not caused by stress relaxation as is described in ref. [52]. The defects showed a remarkable resemblance to the so-called "oval defects" described in ref. [53].

In order to investigate the origin of these defects GaAs epilayers were grown in the same cell and on the same susceptor as was used for the growth of the InGaP layers and with the same experimental growth procedure. These experiments resulted in GaAs layers covered with the same type of defects. It has to be noticed that GaAs layers grown with the cell and susceptor used for the growth of GaAs exclusively, showed mirror-like surfaces without any oval-like defects. Microprobe analysis of a cleaved and stained defect on the GaAs layer showed that the nucleus [53] of the defect consist of material with a high indium concentration. This nucleus is right on top of the GaAs substrate. So probably some adsorbed indium from the susceptor or cell evaporates onto the GaAs substrate, leading to a defect. In the defects on the InGaP layers the indium content of the nucleus could not be measured due to the masking effect of large amounts of indium in the InGaP epilayers.

Microprobe analysis of the defects on InGaP layers show that these defects are all gallium rich compared to the epilayer. This is especially true for layers grown at low temperatures (600 °C). This difference in composition of defect and epilayer decreases in going to higher temperatures. At 700 °C, there is no difference in composition between the defect and the epilayer left although the defects are still present. Differences in enthalpies of formation of GaP and InP (24.4 and 21.2 kcal/mole [54]) indicate that the strength of the Ga - P bond is larger than the In - P strength. This is also true for the Ga - As and In - As bonds [54]. So the indium species will diffuse more easily over the surface than the gallium species.

All these observations lead to the conclusion that these defects were caused by an initial adsorption of indium onto the GaAs substrate. This indium originates from previous InGaP growth experiments on the same susceptor. This is supported by the fact that if a susceptor is used on which the previous

InGaP layer was covered with an GaAs caplayer the defect density is very low. Desorption of indium from the susceptor and the following adsorption on the GaAs substrate results in the forming of an indium rich nucleus (InAs ?) on the GaAs substrate, which is incorporated into the GaAs buffer layer. An alternative for this GaAs caplayer is a high temperature treatment of the susceptor with HCl.

The experiments described in the former sections of this paper were all carried out with a "clean" susceptor which resulted in defect free epilayers with specular surfaces.

8.4 Conclusions

InGaP epilayers have been grown on GaAs substrates. The influence of several growth parameters as the growth temperature, V/III ratio and In/Ga ratio in the gas phase has been investigated. It appeared that the growth rate of InGaP is gas phase diffusion determined for growth temperatures of about 650 °C and higher. At temperatures lower than 650 °C the growth rate is determined by kinetics coupled to the diffusion through the gas phase. The growth process exhibits an apparent activation energy of about 5 kcal/mole. The decomposition of TMG is partly responsible for this. Also decomposition of TMG is more effective in the higher temperature region. This, together with the observation that indium growth species will desorb at higher temperatures, leads to the fact that one has to increase the TMI concentration in the gas phase when the growth temperature is raised in order to obtain the same solid composition. At all growth temperatures, perfectly lattice matched InGaP epilayers could be obtained.

The V/III has no influence on the growth rate at the temperatures used, both at a total flow of 5 and of 7 slm. At the two highest growth temperatures used (640 and 700 °C) the solid composition does not depend on the V/III ratio. At 600 °C the solid composition becomes more gallium rich when the V/III ratio is increased.

When the total flow rate through the reactor was increased from 5 to 7 slm, with constant amounts of precursors, the growth rate decreased with about 10%.

The electrical quality of our layers is excellent. The mobilities measured in our samples are high, but are not due to the presence of an 2-DEG at the GaAs-InGaP interface. However, care has to be taken in comparing the

values for the mobilities with values reported in literature because the ordering present in InGaP can influence this figure. In one sample evidence has been found for a hopping type of conduction at low temperatures. Photoluminescence experiments showed that our samples are of good optical quality. These experiments also point to the fact that ordering is common in our samples. This ordering is a function of the growth conditions. Growing at high temperatures at moderate V/III ratios resulted in disordered material. The morphology is specular whenever lattice matched material was grown but exhibited the typical cross hatched pattern when the samples were not perfectly lattice matched. It turned out that the use of a clean susceptor is necessary in order to avoid defects in the InGaP epilayers.

Acknowledgments

The authors are greatly indebted to S.M. Olsthoorn and F. Driessen for performing and discussing the (magneto) photoluminescence measurements and M. Goemans (Philips Components, Nijmegen) for the X-ray measurements. The authors would like to thank Dr. A.-J. Bons for performing the HREM and TEM investigations and the National Centre for High Resolution Electron Microscopy at the University of Delft for use of their microscopes. This work was financed by NOVEM, project No. 41.220-003.1 and No. 41.22-002.10.

References

- [1] C.F. Schaus, W.J. Schaff and J.R. Shealy, *J. Crystal Growth* **77** (1986) 360.
- [2] M. Ikeda, K. Nakano, Y. Mori, K. Kaneko and N. Watanabe, *Appl. Phys. Letters* **48** (1986) 89.
- [3] J.M. Olson, S.R. Kurtz, A.E. Kibbler and P. Faine, *Appl. Phys. Letters* **56** (1990) 623.
- [4] S.H. Groves, Z.L. Liao, S.C. Palmateer and J.N. Walpole, *Appl. Phys. Letters* **56** (1990) 312.
- [5] J.P. André, E. Dupont-Nivet, D. Moroni, J.N. Patillon, M. Erman and T. Ngo, *J. Crystal Growth* **77** (1986) 354.

- [6] A. Valster, C.T.H.F. Liedenbaum, M.N. Finke, A.L.G. Severens, M.J.B. Boermans, D.E.W. Vandenhoudt and C.W.T. Bulle-Lieuwma, *J. Crystal Growth* **107** (1991) 403.
- [7] P. Roentgen, W. Heuberger, G.L. Bona and P. Unger, *J. Crystal Growth* **107** (1991) 724.
- [8] C.C. Hsu, R.M. Cohen and G.B. Stringfellow, *J. Crystal Growth* **62** (1983) 648.
- [9] J.R. Shealy, C.F. Schaus and L.F. Eastman, *Appl. Phys. Letters* **48** (1986) 242.
- [10] T.F. Kuech, D.J. Wolford, E. Veuhoff, V. Deline, P.M. Mooney, R. Potemski and J. Bradley, *J. Appl. Phys.* **62** (1987) 632.
- [11] H. Terao and H. Sunakawa, *J. Crystal Growth* **68** (1984) 157.
- [12] J.M. Olson, R.K. Ahrenkiel, D.J. Dunlavy, B. Keyes and A.E. Kibbler, *Appl. Phys. Letters* **55** (1989) 1208.
- [13] G.W. 't Hooft, M.R. Leys and F. Roozeboom, *Japan. J. Appl. Phys.* **24** (1985) L761.
- [14] P.M. Mooney *J. Appl. Phys.* **67** (1990) R1.
- [15] S. Minagawa, H. Nakamura and H. Sano, *J. Crystal Growth* **71** (1985) 377.
- [16] A. Gomyo, T. Suzuki, K. Kobayashi, S. Kawata and I. Hino, *Appl. Phys. Letters* **50** (1987) 673.
- [17] M.C. Delong, P.C. Taylor and J.M. Olson, *Appl. Phys. Letters* **57** (1990) 620.
- [18] M.C. Delong, P.C. Taylor and J.M. Olson, *J. Vac. Science Technol. B* **8** (1990) 948.
- [19] K. Meehan, F.P. Dabkowski, P. Gavrilovic, J.E. Williams and W. Stutius, *Appl. Phys. Letters* **54** (1989) 2136.
- [20] W.E. Plano, D.W. Nam, J.S. Major, Jr., K.C. Hsieh, and N. Holonyak, Jr., *Appl. Phys. Letters* **53** (1988) 2537.

- [21] J.E. Bernard, S.-H. Wei, D.M. Wood and A. Zunger, Appl. Phys. Letters **52** (1988) 311.
- [22] P.R. Hageman, M.H.J.M. de Croon, J.N.H. Reek and L.J. Giling, J. Crystal Growth **116** (1992) 169.
- [23] M. Suzuki and M. Sato, J. Electrochem. Soc. **132** (1985) 1684.
- [24] N.I. Buchan, C.A. Larsen and G.B. Stringfellow, J. Crystal Growth **92** (1988) 605.
- [25] N.I. Buchan, C.A. Larsen and G.B. Stringfellow, J. Crystal Growth **92** (1988) 591.
- [26] C.A. Larsen, N.I. Buchan and G.B. Stringfellow, Appl. Phys. Letters **52** (1988) 480.
- [27] W. Richter, P. Kurpas, R. Lückcrath, M. Motzkus and M. Waschbüsch, J. Crystal Growth **107** (1991) 13.
- [28] C.A. Larsen, S.H. Li, N.I. Buchan, G.B. Stringfellow and D.W. Brown, J. Crystal Growth **102** (1990) 126.
- [29] D.H. Reep and S.K. Ghandhi, J. Electrochem. Soc., **130** (1983) 675.
- [30] W.G.J.M. van Sark, G. Janssen, M.H.J.M. de Croon, X.Tang and L.J. Giling, J. Appl. Phys. **64** (1988) 195.
- [31] B.R. Butler and J.P. Stagg, J. Crystal Growth **94** (1989) 481.
- [32] N.I. Buchan, C.A. Larsen and G.B. Stringfellow, Appl. Phys. Letters **51** (1987) 1024.
- [33] M.K. Lee, R.H. Horng and L.C. Haung, Appl. Phys. Letters **59** (1991) 3261.
- [34] D.J. Friedman, A.E. Kibbler and J.M. Olson, Appl. Phys. Letters **59** (1991) 2998.
- [35] F.A.J.M. Driessen, S.M. Olsthoorn, H. Pen and L.J. Giling, Application of a new non-destructive method for determination of a (quasi) 2-DEG in undoped MOVPE grown GaAs – Al_{1-x}Ga_xAs, poster presented at EM-MOVPE IV, Nijmegen, june 1991.

- [36] H. Hotta, I. Hino and T. Suzuki, *J. Crystal Growth* **93** (1988) 618.
- [37] G.J. Bauhuis, to be published
- [38] B.I. Shklovskii and A.L. Efros, *Electronic properties of doped semiconductors*, (Springer Verlag, Heidelberg 1984), chp. 4.
- [39] K. Ozasa, M. Yuri, S. Tanaka and H. Matsunami, *J. Appl. Phys.* **68** (1990) 107.
- [40] J.E. Fouquet, V.M. Robbins, J. Rosner and O. Blum, *Appl. Phys. Letters* **57** (1990) 1566.
- [41] M.C. Delong, W.D. Olson, I. Viohl, P.C. Taylor and J.M. Olson, *Japan. J. Appl. Phys.* **70** (1991) 2780.
- [42] M. Hoshino, K. Kuninori, K. Kodama and M. Ozeki, *J. Crystal Growth* **96**, (1989) 188.
- [43] O. Ueda, M. Hoshino, K. Kodama, Y. Yamada and M. Ozeki, *J. Crystal Growth* **99** (1990) 560.
- [44] M. Kondow, H. Kakibayashi and S. Minagawa, *J. Crystal Growth* **88** (1988) 291.
- [45] T. Suzuki, A. Gomyo and S. Iijima, *J. Crystal Growth* **99** (1990) 60.
- [46] P. Bellon, J.P. Chevalier, G.P. Martin, E. Dupont-Nivet, C. Thiebaut and J.P. André, *Appl. Phys. Letters* **52** (1988) 567.
- [47] T. Suzuki, A. Gomyo and S. Iijima, *J. Crystal Growth* **93** (1988) 396.
- [48] F.P. Dabkowski, P. Gavrilovic, K. Meehan, W. Stutius and J.E. Williams, *Appl. Phys. Letters* **52** (1988) 2142.
- [49] S.R. Kurz, J.M. Olson and A. Kibbler, *Appl. Phys. Letters* **57** (1990), 1922.
- [50] A. Gomyo, K. Kobayashi, S. Kawata, I. Hino and T. Suzuki, *J. Crystal Growth* **77** (1986) 367.
- [51] P.J. van der Wel, J. te Nijenhuis, E.R.H. van Eck and L.J. Giling, *Semicond. Sci. and Technol.*, **7** (1992) A63.

- [52] J. te Nijenhuis, P.J. van der Wel, E.R.H. van Eck and L.J. Giling, to be published.
- [53] J. van de Ven, J.L. Weyer, H. Iking and L.J. Giling, *J. Electrochem. Soc.* **134** (1987) 989.
- [54] J.C. Philips, *Bonds and Bands in Semiconductors*, (Academic Press, New York, 1973), ch. 8.
- [55] G.B. Stringfellow, *J. Appl. Phys.* **53** (1982) 6849.

Summary

This thesis describes the metalorganic chemical vapour deposition (MOCVD) growth and doping of III/V semiconductors, viz. GaAs, $\text{Al}_x\text{Ga}_{1-x}\text{As}$ and $\text{In}_{1-x}\text{Ga}_x\text{P}$. The dopants studied in this thesis are silane (SiH_4), disilane (Si_2H_6) and diethylzinc (DEZn). Additionally, the development and optimalization of GaAs solar cells is presented.

In chapter 2 the silicon doping of GaAs as a function of the growth temperature is discussed. In this study two different silicon precursors are investigated, silane and disilane, at one atmosphere total reactor pressure. An analysis of the rate determining step in the incorporation process is given based on the presence of a chemical boundary layer. From this analysis it can be concluded that the doping of GaAs with silicon is a kinetically determined process with a strong temperature dependence, independent of the used silicon precursor. This temperature behaviour is attributed to the decomposition of SiH_4 into SiH_2 when performed with SiH_4 . The doping process with Si_2H_6 at one atmosphere reactor pressure is a similar process with the same temperature dependence.

A more detailed analysis of the silicon incorporation process with silane at one atmosphere reactor pressure in MOCVD grown GaAs is presented in chapter 3. This incorporation process is studied as a function of the substrate orientation and input mole fraction silane. The carrier concentration increases linearly with the input mole fraction silane, with an incorporation efficiency in the order $(100) \xrightarrow{2^\circ} (110) > (111)\text{Ga} > (110)$. The trend in the compensation ratios of the grown epilayers could be explained by taking into account the differences in surfaces at the growth conditions of the different substrate orientations used. At high silane input mole fractions ($> 1 \times 10^{-6}$) silicon precipitates are found in the grown layers as is predicted by equilibrium calculations. This chapter supports the conclusions from chapter 2 that the rate limiting step in the silicon incorporation process in GaAs from silane is the decomposition of SiH_4 into SiH_2 .

Chapter 4 describes the investigations on the pressure and temperature dependence of silicon doping of GaAs with the use of disilane. It was found that the rate limiting step in this process changes when the total reactor pressure was changed. At 20 mbar total reactor pressure, the incorporation from silicon is determined by the decomposition of Si_2H_6 coupled to the diffusion through the gas phase. At 100 mbar reactor pressure this incorporation appears to be completely gas phase diffusion limited, and shows consequently

no temperature dependence. At atmospheric pressure the doping process is determined by the decomposition of SiH_4 instead of Si_2H_6 . So, only at 100 mbar total pressure the doping of GaAs with disilane is temperature independent, at the two other investigated pressures the silicon incorporation is strongly temperature dependent.

After the thorough study and analysis of the silicon doping process with silane and disilane, in chapter 5 the p-type doping of GaAs and $\text{Al}_{1-x}\text{Ga}_x\text{As}$ with diethylzinc is discussed. The experiments are performed at different total reactor pressures and growth temperatures in two different reactors. The obtained results are remarkably comparable. The zinc incorporation follows a linear behaviour in a log-log plot of the hole concentration versus the input mole fraction DEZn with a slope of 1. The zinc incorporation decreased with an increase of the growth temperature. This temperature dependence follows an Arrhenius kind of behaviour, independent of the fraction aluminium in the $\text{Al}_{1-x}\text{Ga}_x\text{As}$ alloy ($0 < x < 0.45$). A model is suggested which explains all experimental results, including the depletion behaviour of the zinc incorporation. This theoretical description of the process is based on the assumption that the zinc incorporation is precluded by an adsorption/desorption equilibrium at a step.

Chapter 6 describes the theoretical and practical analysis and development of the GaAs solar cells grown and processed in our laboratory. This process started with the growth of a basic solar cell, which served as a starting point for further development and improvement. To understand the performance of a solar cell, a theoretical description of the physical behaviour is given. In order to improve the performance of the basic solar cell, the material is completely characterized. With the obtained material parameters, computer simulations have been performed to calculate what has to be improved in order to obtain higher efficiencies. This has led to some minor changes of the cell design in combination with improvements to the solar cell processing. This has resulted in a GaAs solar cell of 20.5% efficiency at AM 1.5, 1 sun.

In chapters 7 and 8 the growth of a different III/V semiconductor is discussed, viz. $\text{In}_{1-x}\text{Ga}_x\text{P}$ lattice matched to GaAs. The major problem with this III/V compound is the precise control of the growth. It is necessary to grow as exact lattice matched (to GaAs) as possible. Larger deviations from the lattice matched composition will cause misfit dislocations in the epilayers. This will diminish the quality of the material. Besides the growth of this material at different growth temperatures and at different growth conditions, attention is paid to the so-called "100 meV problem" of the $\text{In}_{1-x}\text{Ga}_x\text{P}$ material. This problem is caused by ordering of the indium and gallium atoms on

the group III sub-lattice. In these two chapters it is shown that good material, lattice matched to GaAs, has been grown and has been thoroughly characterized. Electrical measurements of some of the samples showed that a hopping conduction mechanism is present at low temperatures, probably caused by ordering in the samples.

Samenvatting

In dit proefschrift wordt de groei en dotering van de III/V halfgeleiders GaAs, $\text{Al}_x\text{Ga}_{1-x}\text{As}$ and $\text{In}_{1-x}\text{Ga}_x\text{P}$ met behulp van de Metaalorganische Chemische Gasfase Depositie techniek (Eng: Metalorganic Chemical Vapour Deposition) beschreven. De gebruikte verbindingen voor het doteren zijn: silaan (SiH_4), disilaan (Si_2H_6) en di-ethielzink (DEZn). Vervolgens wordt de ontwikkeling en optimalisatie van GaAs zonnecellen gepresenteerd.

In hoofdstuk 2 wordt het doteren van GaAs met silaan als een functie van de groeitemperatuur bediscussieerd. In deze studie worden twee verschillende siliciumverbindingen gebruikt, nl. silaan en disilaan, bij een reactordruk van één atmosfeer. Een analyse, gebaseerd op de aanwezigheid van een z.g. chemische grenslaag (Eng.: Chemical Boundary Layer), van de snelheidsbepalende stap in de siliciuminbouw wordt gegeven. Uit deze analyse volgt dat de dotering van GaAs een kinetische bepaald proces is met een sterke temperatuursafhankelijkheid, welke onafhankelijk blijkt te zijn van de gebruikte siliciumverbinding. In het geval van het gebruik van silaan wordt dit temperatuursgedrag toegeschreven aan de thermische ontleding in de gasfase van SiH_4 tot SiH_2 . Wanneer gebruik gemaakt wordt van Si_2H_6 bij één atmosfeer reactordruk, vertoont het doteringsproces een identiek karakter en temperatuursafhankelijkheid.

Een gedetailleerdere analyse van het silicium inbouwproces gebruikmakend van silaan in een atmosferische MOCVD reactor, is in hoofdstuk 3 beschreven. Het inbouwproces is bestudeerd als functie van de substraatorientatie en de aan de gasfase toegevoegde molfractie silaan. De ladingsdragersconcentratie neemt lineair toe met de toegevoegde hoeveelheid silaan, waarbij de inbouwefficiëntie toeneemt in de volgorde $(100) \xrightarrow{2^\circ} (110) > (111)\text{Ga} > (110)$ van de substraatorientaties. De vertoonde trend in de compensatie-verhoudingen van de epitaxiale lagen kon verklaard worden door de verschillende oppervlakten van de gebruikte substraatorientaties te beschouwen en onderling te vergelijken. Silicium precipitaten zijn gevonden in de gegroeide lagen bij grote toegevoegde hoeveelheden silaan ($> 1 \times 10^{-6}$). Dit verschijnsel is ook voorspeld door evenwichtsberekeningen. Dit hoofdstuk ondersteunt de in hoofdstuk 2 getrokken conclusies over de snelheidsbepalende stap in het inbouwproces van silicium in GaAs, uitgaande van silaan. Deze snelheidsbepalende stap blijkt de decompositie van SiH_4 tot SiH_2 te zijn.

Hoofdstuk 4 beschrijft het onderzoek naar de temperatuurs- en drukafhankelijkheid van de siliciuminbouw in GaAs, gebruikmakend van di-

silaan. Het bleek dat in dit proces de snelheidsbepalende stap veranderde wanneer de totaal druk in de reactor werd veranderd. Bij een reactordruk van 20 mbar, wordt de siliciuminbouw bepaald door de thermische decompositie van Si_2H_6 , gekoppeld aan de diffusie door de gasfase. Bij een totaal druk van 100 mbar is de inbouw compleet bepaald door de gasfase-diffusie, wat tot gevolg heeft dat de inbouw bij deze druk geen temperatuursafhankelijkheid vertoont. Bij atmosferische drukken wordt dit proces bepaald door de decompositie van SiH_4 in plaats van Si_2H_6 . Het valt dus te concluderen dat alleen bij een totaal druk van 100 mbar in de reactor de inbouw van silicium uit disilaan temperatuursonafhankelijk is. Bij de twee andere onderzochte totaal drukken is er wel degelijk een temperatuursafhankelijkheid.

Na deze grondige studie en analyse van het doteringsproces met silicium, is in hoofdstuk 5 de p-type dotering van GaAs en $\text{Al}_{1-x}\text{Ga}_x\text{As}$ m.b.v. di-ethielzink bediscussieerd. De experimenten zijn in twee verschillende reactoren uitgevoerd bij verschillende totaal drukken en groeitemperaturen. De resultaten van de verschillende reactoren komen opmerkelijk met elkaar overeen. De zinkinbouw vertoont een lineair gedrag wanneer in een log-log plot de toegevoegde hoeveelheid DEZn is uitgezet tegen de ladingsdragersconcentratie. De zinkinbouw vermindert naarmate de groeitemperatuur toeneemt. Deze temperatuursafhankelijkheid volgt een Arrhenius gedrag. Dit gedrag is onafhankelijk van de hoeveelheid aluminium in de $\text{Al}_{1-x}\text{Ga}_x\text{As}$ verbinding ($0 < x < 0.45$). Er wordt een model voorgesteld welke de experimentele resultaten verklaart, ook het depletiegedrag van de zinkinbouw. Deze theoretische beschrijving van het inbouwproces is gebaseerd op de aanname dat de zinkinbouw vooraf gegaan wordt door een adsorptie/desorptie-evenwicht aan een stap op het oppervlak.

Hoofdstuk 6 behandelt de theoretische analyse van de ontwikkeling van de GaAs zonnecellen, welke gegroeid zijn in ons laboratorium. Dit verbeteringsproces is gestart met een basiszonnecel. Vanuit deze situatie hebben de verbeteringen en ontwikkelingen plaats gevonden. Om de werking van een zonnecel beter te begrijpen wordt eerst een theoretische beschrijving van de fysische achtergronden gegeven. Ter verbetering van de prestaties van de basiscel is een complete materiaal analyse gedaan. Met de op deze manier verkregen materiaalgegevens is met behulp van een simulatieprogramma uitgerekend wat aan dit celontwerp en deze materiaalkwaliteit verbeterd kon worden. Deze simulaties hebben geleid tot kleine aanpassingen aan het celontwerp en aan wat veranderingen in de productie (de handelingen na het eigenlijke groeien, zoals het aanbrengen van de contacten en de anti-reflectie-laag) van de cel. Dit alles heeft geresulteerd in een GaAs zonnecel met een efficiëntie van 20.5 %

bij een AM 1.5 spectrum van 1 zon.

In de hoofdstukken 7 en 8 wordt de groei van een geheel andere III/V halfgeleider behandeld, nl. $\text{In}_{1-x}\text{Ga}_x\text{P}$. Dit materiaal wordt gegroeid op GaAs zonder misaanpassingen. Het grootste probleem van de groei van dit materiaal is de nauwkeurige controle van de samenstelling van het gegroeide halfgeleider materiaal. Alleen hele kleine afwijkingen van de juiste samenstelling kunnen getolereerd worden, omdat anders de misaanpassing te groot wordt. Naast de groei van dit materiaal onder verschillende groeiomstandigheden, is ook aandacht geschonken aan het zogenaamde "100 meV probleem" van het $\text{In}_{1-x}\text{Ga}_x\text{P}$. Dit probleem wordt veroorzaakt door ordening van de indium en gallium atomen op het groep III subrooster. In deze twee hoofdstukken wordt aangetoond dat goed materiaal, met een kleine of geen misaanpassing, gegroeid kan worden op GaAs. Dit materiaal is grondig gekarakteriseerd. Elektrische metingen van sommige lagen InGaP op GaAs vertoonden een zogenaamde "hopping" geleidingsmechanisme bij lage temperaturen. Dit wordt waarschijnlijk veroorzaakt door de ordening in de lagen.

Curriculum Vitae

Paulus Robertus Hageman

Geboren op 23 november 1961 te Doetinchem.

- 1973-1980 : VWO, Gemeentelijke Scholengemeenschap "Doetinchem" te Doetinchem.
- 1980-1987 : Studie Scheikunde aan de Katholieke Universiteit Nijmegen.
Kandidaatsexamen: 24 september 1984
Doctoraal examen: 31 augustus 1987
Hoofdvakken: anorganische chemie, vaste stof chemie
- 1987-1991: Als assistent in opleiding werkzaam op de afdeling Vaste Stof Fysica III van de Faculteit Natuurwetenschappen van de Katholieke Universiteit te Nijmegen.
- 1991-heden: werkzaam als medewerker op de afdeling afdeling Vaste Stof Fysica III van de Faculteit Natuurwetenschappen van de Katholieke Universiteit te Nijmegen.

ISBN: 90 - 9005929 - 6